INVESTIGATING GROUNDWATER AND SURFACE WATER EXCHANGE IN THE UMGENI CATCHMENT, KWAZULU-NATAL, SOUTH AFRICA.

By

THOBEKA S MPUNGOSE

Submitted in fulfilment of the requirements of

Master of Science

in Hydrology

Centre of Water Resources Research

School of Agriculture, Earth, and Environmental Sciences

University of KwaZulu-Natal

Pietermaritzburg

South Africa

18 July 2024

Supervisor: Prof. S Kebede-Gurmessa

PREFACE

The research contained in this dissertation/thesis was completed by the candidate while based in the Discipline of Hydrology, School of Agricultural, Earth and Environmental Sciences of the College of Agriculture, Engineering and Science, University of KwaZulu-Natal, Pietermaritzburg, South Africa. The research was financially supported by the Water Research Commission (WRC).

The contents of this work have not been submitted in any form to another university, and except where the work of others is acknowledged in the text, the results reported are due to investigations by the candidate.

_____

Signed: Supervisor

Date: 18 July 2024

DECLARATION PLAGIARISM

I, Thobeka Mpungose, declare that:

(a) The research reported in this dissertation, except where otherwise indicated or acknowledged, is my original work;

(b) This dissertation has not been submitted in full or in part for any degree or examination to any other university;

(c) This dissertation does not contain other persons' data, pictures, graphs or other information, unless specifically acknowledged as being sourced from other persons;

(d) This dissertation does not contain other persons' writing unless specifically acknowledged as being sourced from other researchers. Where other written sources have been quoted, then:

i) their words have been re-written but the general information attributed to them has been referenced;

ii) where their exact words have been used, their writing has been placed inside quotation marks, and referenced;

(e) where I have used material for which publications followed, I have indicated in detail my role in the work;

(f) This dissertation is primarily a collection of material prepared by myself, published as journal articles or presented as a poster and oral presentations at conferences. In some cases, additional material has been included;

(g) This dissertation does not contain text, graphics or tables copied and pasted from the Internet, unless specifically acknowledged, and the source being detailed in the dissertation and in the References sections.

Student signature: 

Date: 18 July 2023

Supervisor signature: 

Date: 18 July 2023

ABSTRACT

The understanding of the role of groundwater in river basin hydrology and its contribution to the water resources base is limited. Past studies have focused on quantifying and modelling surface water. Recent South African policies emphasise the need for conjunctive use of water resources, including adding groundwater into the national water security mix and water balance accounting. Groundwater and stream networks fed by groundwaters are proven to be resilient against global climate change. The current study aims to shed light on groundwater recharge processes and its connection to the stream network in the Umgeni Catchment of KwaZulu-Natal province in South Africa. The groundwater recharge-flow-discharge processes are examined across altitudinal gradients and scales with specific emphasis on the role of wetlands, lithology, geomorphology, dykes, land use and land cover in controlling the connection between groundwater and surface water. Proven isotope tracers (Oxygen-18 (^{18}O) and Deuterium (^{2}H) and Radon (^{222}Rn)), piezometry, electrical conductivity and baseflow separation were employed to investigate groundwater recharge processes and the connection between groundwater and surface waters. About 220 rainwater samples have been collected on a daily to monthly basis between March 2022 and January 2024 at three locations (Durban, Pietermaritzburg and Howick). In addition, we collected 180 samples, including streams (105), springs (18), wetlands (15) and boreholes (43), representing both the wet and dry seasons. The results showed that rainfall predominantly recharges the groundwaters. ^{222}Rn data from the stream network revealed that the headwater streams of the Umgeni catchment are dominated by groundwater inflow, while the stream network downstream shows little sign of groundwater inflow. The findings highlight the critical role of rainfall in recharging groundwater and the strong influence of geology on groundwater contributions to surface waters in the Umgeni Catchment. The identification of groundwater-dominated headwaters and surface water-dependent downstream areas underscores the need for region-specific water management strategies. Protecting recharge zones, implementing sustainable groundwater abstraction, and integrating groundwater-surface water management will be essential for ensuring long-term water security.

Keywords: *Rainfall isotopes, local meteoric water line, ^{222}Rn, Groundwater and surface water interactions, groundwater recharge mechanisms, Umgeni Catchment.*

ACKNOWLEDGEMENTS

First and foremost, I would like to thank God for His unending grace and guidance throughout this journey. As it is written in Proverbs 16:9, "In their hearts, humans plan their course, but the Lord establishes their steps."

I am deeply grateful to the Water Research Commission for funding this project. The discussions and conclusions presented in this paper are solely those of the author and do not necessarily reflect the views of the WRC.

I am thankful to the ICFR, WestfaliaFruit Farm, Virginia Airport, and Ashok Rampersad, along with all other parties that allowed or facilitated access for sampling.

I sincerely thank my supervisor, Prof. Seifu Kebede, for his support, insightful guidance and understanding throughout this research. His expertise, patience and encouragement have been invaluable, fostering an environment where I could grow and thrive as a researcher.

I would also like to express my heartfelt thanks to Dr. Daniel Kibirige for his significant contributions, especially during the early stages of this work. His assistance with writing, critical feedback, and belief in my abilities have been crucial to my progress.

I thank Vivek Naiken for his assistance. His step-by-step guidance has been beneficial, from identifying sampling sites to conducting lab work.

I extend my appreciation to Mutondi Tshikororo and Thabang Phori for their support and teamwork. We have always believed that two minds are better than one. I am grateful for their insights and collaborative spirit. I wish them all the best in their academic journey.

I thank my family and friends for their unwavering love and support. This journey would not have been possible without their encouragement and understanding.

To the CWRR team, thank you for your continuous support and encouragement.

Finally, to everyone who may not have been mentioned but has contributed in any way. Your support is appreciated.

TABLE OF CONTENTS

LIST OF TABLES

LIST OF FIGURES

ABBREVIATIONS, ACRONYMS AND UNITS

ALMWL	Africa Local Meteoric Water Line
A	Area
^{39}Ar	Argon
BFI	Baseflow index
Bq/m^3	Becquerels per cubic meter
Bq/L	Becquerels per litre
Cd	Cadmium
CLMWL	Cape Town Local Meteoric Water Line
CO2	Carbon dioxide
^{14}C	Carborn-14
cm	centimetre
Cr	Chromium
F	Constant factor
Cu	Copper
°	Degree
δ	Delta
DWS	Department of Water and Sanitation
^{2}H	Deuterium
D-excess	Deuterium excess
EC	Electrical conductivity
EPA	Environmental Protection Agency
Etc.	et cetera
GMWL	Global Meteoric Water Line
GW and SW	groundwater and surface water
$\delta^{2}H$	Hydrogen isotope composition
km	Kilometre
85Kr	Krypton
KZN	KwaZulu-Natal
LIMS	Laboratory Information Management System
LULC	Land use and land cover
Pb	Lead

ℓ	litres
ℓ/s	litres per second
LMWL	Local Meteoric Water Line
MWL	Meteoric Water Line
m	Metre
masl	metres above sea level
µS/cm	Micro siemens per centimetre
µg/L	Micrograms per litre
µm	Micrometre
ml	Millilitre
mm	Millimetres
MBR	Mountain Block Recharge
MFR	Mountain-front recharge
NGA	National Groundwater Archive
N	Number of Days
n	Number of samples
^{16}O	Oxygen 16
^{17}O	Oxygen 17
^{18}O	Oxygen 18
$\delta^{18}O$	Oxygen Isotope composition
ppm	Parts per million
‰	per mill
%	Percent
pCi/L	Picocuries per litre
PtLMWL	Pietermaritzburg Local Meteoric Water Line
±	Plus or minus
PLMWL	Pretoria Local Meteoric Water Line
PCA	Principal component analysis
^{1}H	Protium
^{222}Rn	Radon
SABS	South African Bureau of Standards
km^2	Square kilometre
TLMWL	Thohoyandou Local Metworic Water Line

TDS	Total dissolved solutes
UKZN	University of KwaZulu-Natal
Vsmow	Vienna Standard Mean Ocean Water
WRC	Water Research Commission
WHO	World Health Organization
Zn	Zinc

1. INTRODUCTION

Rainfall, surface water and groundwater originate within a closed system of water occurring on Earth (Cavazza and Pagliara, 2009). Rainfall is a significant source of freshwater in most systems, sustaining surface waters and recharging underlying aquifers (Leaney and Herczeg, 1995; Durowoju *et al.*, 2019; Cheng *et al.*, 2021). The surface waters (streams, lakes and wetlands) are sustained by large amounts of rainfall overland flow (20-50% in humid areas and 50-90% in arid regions) originating in the mountainous areas (Viviroli and Weingartner, 2004). Depending on the subsurface hydrogeological structures, the runoff generated from mountains flows through the stream network and recharges adjacent lowland aquifers as focused recharge (Cheng *et al.*, 2021). Concurrently, the aquifers also discharge into surface water bodies, especially in arid and semi-arid regions during dry periods or drought seasons (Wang *et al.*, 2018).

Globally, there is increasing demand for freshwater, one-third of freshwater withdrawals worldwide are through groundwater (Wang *et al.*, 2018). About 1.5 billion people rely on groundwater as a primary source for domestic use and sanitation practices in communities, with additional abstractions necessary for sustaining agricultural and industrial economies (Wang *et al.*, 2018; Cheng *et al.*, 2021; Gibrilla *et al.*, 2022). Groundwater systems encounter stress in recharge, discharge mechanisms and hydrogeological processes happening underground (Schaller and Fan, 2009). The outcomes affect the water supply, river flow, and dependent ecological environments (Wang *et al.*, 2018). A study by Wilson and Guan (2004) reported that understanding catchment scale groundwater flows in connection with surface water can aid in the legitimate application of conceptual and numerical models to predict and manage water resources at various catchment scales.

Groundwater recharge, discharge and flow processes affect catchment water resource management (Madlala *et al.*, 2021; Valett and Reinhold, 2022). The exchanges between groundwater and surface water (GW and SW) in recharge and discharge determine water availability in springs, seeps, baseflow, rivers, lakes and aquifers (Cantor *et al.*, 2018). Decreased groundwater recharge with excessive abstractions impacts groundwater-dependent ecosystems by decreasing water table and baseflow (Cantor *et al.*, 2018). Therefore, groundwater recharge alters the catchment water balance, quality and availability (Madlala *et al.*, 2021).

Groundwater movement serves as a pathway for chemical and heat exchanges (Valett and Reinhold, 2022). Therefore, with increasing water demands, understanding and characterising the interactions between GW and SW is becoming a critical tool for managing and protecting water resources (Wilson *et al.*, 2022). Despite the considerable progress made in studying the GW and SW interactions globally (Scanlon *et al.*, 2007; Stellato *et al.*, 2008; Barthel and Banzhaf, 2016; Xu *et al.*, 2017), our understanding of the role of groundwater in river basin hydrology and its contribution to the water resources base is limited in South Africa (West *et al.*, 2022). Past studies have focused on GW and SW as distinct entities (Kebede *et al.*, 2021). Thus, hindering progress in understanding and characterising the GW and SW relations.

Previous studies (Geppert *et al.*, 2022; Modie *et al.*, 2022; West *et al.*, 2022; Petersen *et al.*, 2023) suggested that analysis of water isotopes can bridge the gaps in assessing the relevance of precipitation varying patterns, moisture sources, groundwater recharge and flow complexities, as well as their interactions with surface waters. In addition to the authors mentioned above, Abiye et al. (2015) emphasised that measurements of deuterium (^{2}H) and oxygen-18 (^{18}O) in a water sample can be used to investigate groundwater recharge mechanisms, using the relative deviation from the Global Meteoric Water Line (GMWL) as well as the Local Meteoric Water Line (LMWL).

There have been notable efforts to lay the groundwork for understanding the GW and SW interactions. In South Africa, studies have attempted the basis of understanding GW and SW interactions such as establishing LMWLs, use of isotope effects and deuterium excess (d-excess) (Braun *et al.*, 2017; Leketa *et al.*, 2018; Durowoju *et al.*, 2019; Welgus and Abiye, 2022). The studies mark a crucial initial step towards unravelling the complexities of characterising the GW and SW interactions.

1.1 Research Problem and Significance

Umgeni Catchment is one of the KwaZulu-Natal (KZN) provinces where groundwater is used to support domestic and agricultural activities. The day-to-day dependence of many people necessitates frequent monitoring to understand the state of groundwater at a local scale. Understanding the hydrogeological aspects of groundwater and its connection to surface waters can assist in the management and sustainable use of water resources.

The primary innovation of this study is to investigate the recharge and discharge processes in the Umgeni Catchment and unravel the geologic and human-induced catchment features that alter the groundwater movement across the catchment. The project employed integrated

approaches, including piezometric reanalysis, aquifer characterisation, tracer hydrology, and water chemistry surveys. The results to be generated may inform catchment water managers where to invest in groundwater recharge zone protection, which will advance groundwater protection from depletion and contamination, as well as the investment in ecological infrastructure protection.

1.2 Research Questions

The following research questions will be investigated:

i) What is the role of groundwater flows in maintaining the surface waters (wetlands and rivers)?
ii) What dominant geological and human-induced processes govern the connection between groundwater and surface waters in the Umgeni catchment?

1.3 Research Aims and Objectives

The study aims to shed light on the groundwater flow processes and its connection with the surface waters of the Umgeni Catchment of KZN province in South Africa.

The specific objectives are:

- To characterise isotope signals in rainfall, surface waters and groundwater to understand their interactions.
- To investigate factors that control the connection between GW and SWs.
- To develop a conceptual model of GW and SW interactions.

1.4 Organisation of Thesis

This thesis is divided into five chapters. Chapter One (**INTRODUCTION**) provides background information on the significance of studying GW and SW exchanges globally, in South Africa, and in the Umgeni Catchment. It articulates the research problem and existing limitations in understanding the GW and SW interactions.

The second chapter (**LITERATURE REVIEW**) presents the relevant existing literature that focuses on investigating groundwater recharge, flows and discharge. The section provides the concepts, mechanisms, processes and methodologies that have been previously assessed to investigate GW and SW interactions. The chapter concludes with a literature synthesis, highlighting the gaps identified in previous studies.

Chapter Three (**METHODOLOGY**) describes and characterises the Umgeni Catchment. The chapter focuses on the factors currently presumed to control GW and SW interactions and

outlines the sampling sites and methods employed to investigate these interactions. Chapters Four and Five (**RESULTS** and **DISCUSSION**) present the results and discussion of the study's findings. Thus, Chapter Six (**CONCLUSIONS AND RECOMMENDATIONS**) provides the conceptual model, discusses study limitations, and offers recommendations for future research.

.

2. LITERATURE REVIEW

This chapter presents an in-depth review of relevant existing knowledge in Umgeni, South Africa, and globally. The literature survey assesses existing knowledge on methodology and published and unpublished literature on hydrological knowledge. This includes:

- An analysis of the basis of using isotopes in hydrology, including concepts of isotope effects, d-excess and
- The use of isotopes in groundwater investigation/studies
- Understanding of the groundwater recharge, flows and discharge processes.
- Review of GW and SW interactions Globally, in South Africa and at Umgeni catchment.

2.1 Basis of Applying Stable Isotopes in Hydrology

Water has two major elements: hydrogen and oxygen (Harris *et al.*, 2010). Hydrogen has two naturally occurring stable isotopes (^{1}H – protium and ^{2}H – deuterium), and oxygen has three stable isotopes known as Oxygen-16 (^{16}O) Oxygen-17 (^{17}O), Oxygen-18 (^{18}O) (Mook and Rozanski, 2000). Isotopes naturally exist within water molecules, exhibiting different combinations of hydrogen and oxygen atoms, resulting in variations that can be classified as either light or heavy. The diagram below (**Error! Reference source not found.**) illustrates the different combinations of hydrogen and oxygen isotopes.

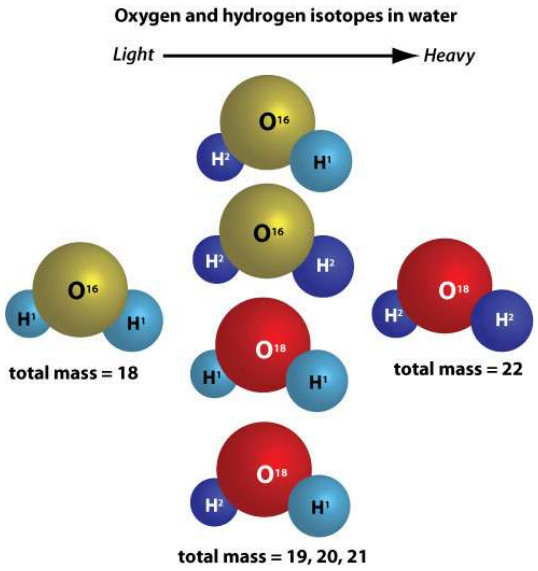

Figure 2.1 Varying ratios of oxygen and hydrogen in water (Anderson, 2015).

Various processes, including chemical reactions, physical reactions, exchange, and diffusion, occur at different rates, leading to distinct isotope ratios (Diamond, 2022). During hydrological processes such as precipitation and evaporation, lighter isotopes evaporate rapidly and condense more readily than heavier isotopes (Mook and Rozanski, 2000). The ratio of light to heavy isotopes in water changes in a predictable form during these processes, allowing isotopes to be used as tracers of the hydrologic cycle (Mook and Rozanski, 2000; Harris *et al.*, 2010). Stable isotopes in meteoric waters have been used as tracers and important tools in studies focusing on groundwater recharge and flow, pollution sources, validation of transport models, evaluation of artificial recharge practices, water balance of lakes as well as GW and SW interactions (Liu *et al.*, 2010; Abiye *et al.*, 2013; Durowoju *et al.*, 2019). Typically, the analysis of isotope ratios of precipitation is a prerequisite to the climatological assessments, given that precipitation is a significant input to the hydrological systems (Liu *et al.*, 2010).

2.1.1 Isotope effects

The rainfall isotope compositions vary with time and location (Allen *et al.*, 2022). The reason driving the isotope variability is called the isotope effect, which includes natural factors such as the climatic conditions (temperature, humidity and rainfall amount) and physical characteristics (altitude, distance from the ocean and rainfall moisture sources) (Harris *et al.*, 2010; Durowoju *et al.*, 2019; Leketa and Abiye, 2020). The **Figure 2.2** illustrates the meteoric water line and the isotopic composition of different water bodies. Such plots serve as the basis for interpreting hydrological processes at various scales.

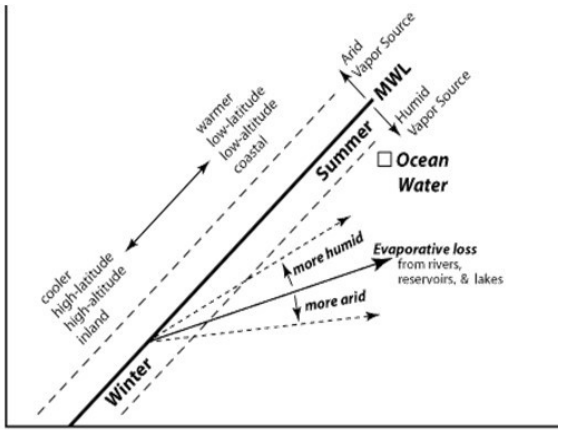

Figure 2.2 Isotope variations due to climate and environmental conditions (Zega *et al.*, 2020).

2.1.1.1 Altitude effect

The distribution of isotope compositions in precipitation mirrors the topography of continents (Araguas *et al.*, 1998). According to Diamond (2022), the altitude effect results from more significant fractionation brought by orographic lifting and the progressive decrease in temperature moving inland. The altitude effect can only be derived by collecting rainfall in at least two stations at different elevations. Thus, the altitude effect is given as a decrease in the isotope composition of $\delta^{18}O$ and $\delta^{2}H$ per 100 m. Poage and Chamberlain (2001) compiled 68 studies from various regions worldwide. The change in the $\delta^{18}O$ and $\delta^{2}H$ of precipitation along the altitudinal transect (lapse rates) were found to be ~0.28‰/100m and ~2.2‰/100m respectively, for most regions except for extreme latitudes where the lapse rates were higher. The study revealed that regions characterised by high topographic relief result in a strong altitude lapse rate. In addition, Diamond (2022) provided examples of the altitude effect worldwide, shown in **Table 2.1**. Notably, in regions with a strong altitude effect, the precipitation in high elevations exhibits a depletion in heavy isotopes (Gonfiantini *et al.*, 2001; Poage and Chamberlain, 2001; Harris *et al.*, 2010).

Table 2.1 Examples of altitude effect from around the world (Diamond, 2022)

Location	Country	$\delta^{18}O$ Gradient (Δ‰/100m)	Altitude masl	Reference
Mount Cameroon	Cameroon	-0.16	0-4000	Gonfiantini et al., 2001
Eastern Andes	Bolivia	-0.24	200-5200	Gonfiantini et al., 2001
Herault	France	-0.27	500-1800	Ladouche et al., 2009
Whole Island	Taiwan	-0.20	0-2500	Peng et al., 2010
Fuego Volcano	Guatemala	-0.67	800-1200	Mulligan et al., 2011
Table Mountain	South Africa	-0.075	100-1100	Diamond & Harris, 2019
Mount Shasta	California, USA	-0.21	1000-3100	Peters et al., 2018

2.1.1.2 Seasonality effect

The seasonality effect is governed by several factors related to the hydrological cycle and atmospheric processes during different seasons (Allen *et al.*, 2022). Dry seasons are associated with colder temperatures, reducing evaporation rates from different open water bodies. Therefore, condensation of dry season precipitation encounters less isotopic fractionation, resulting in less preferential enrichment of lighter isotopes in the vapour phase.

In contrast, the wet season exhibits high temperatures, resulting in excessive evaporation and enriched heavy isotopes (Liu *et al.*, 2010).

2.1.1.3 Rainfall amount effect

The rainfall amount effect phenomenon is governed by the processes in rainfall formation, such as condensation and rainout (Leketa and Abiye, 2020). The condensation process allows water vapour in the atmosphere to transit from the gaseous phase and forms cloud droplets (Liu *et al.*, 2010; Allen *et al.*, 2022). During the process, the lighter isotopes preferentially leave from the water vapour, enriching the remaining vapour in heavier isotopes. The other process, known as rainout, explains how precipitation develops within a cloud through continuous collisions of droplets, which merge to form raindrops (Allen *et al.*, 2022). The process enhances the depletion of lighter isotopes in the remaining cloud droplets. Therefore, the large raindrops become enriched in heavy isotopes (Liu *et al.*, 2010; Durowoju *et al.*, 2019; Leketa and Abiye, 2020). The figure below (**Figure 2.3**) shows that small raindrops are more enriched than large raindrops. Thus, adding groundwater isotopic composition would allow to determine whether the groundwater is recharged by light or heavy rain in that region.

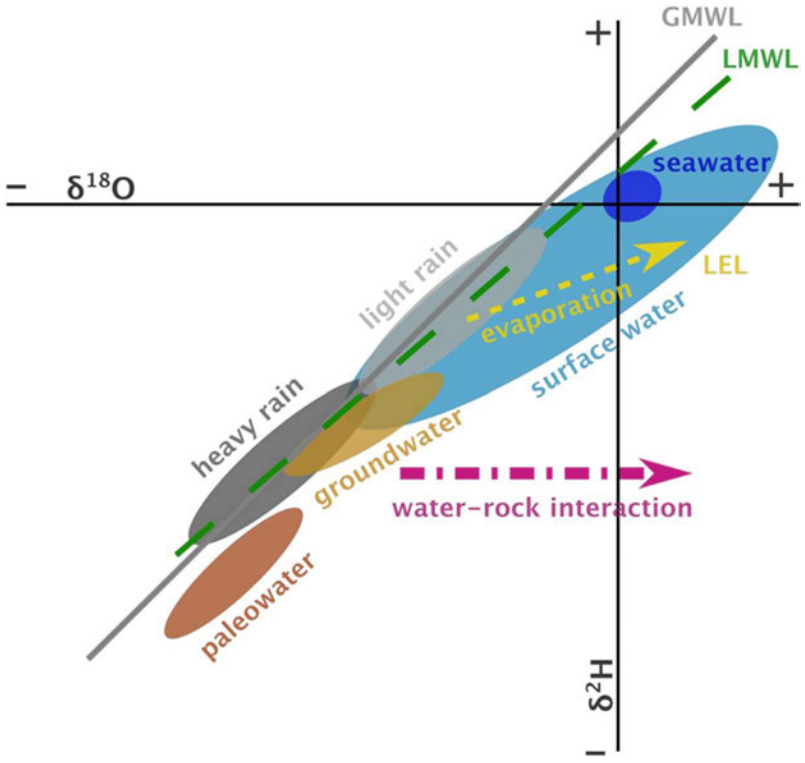

Figure 2.3 Conceptual representation of isotope compositions of heavy and light rainfalls in reference to the GMWL and LMWLs (Diamond, 2022).

2.1.1.4 Continental effect

The apparent depletion of precipitation with increasing distance from the coast is called the continental effect (Araguas *et al.*, 1998). When moving inland, the cooling of moisture in the atmosphere enhances the condensation of heavy molecules; the longer residence time of water vapour over land allows for more extensive isotopic fractionation processes. Therefore, sequential condensation and fractionation occur in air masses rising from the sea to inland regions, resulting in depleted precipitation (Gonfiantini *et al.*, 2001). Meanwhile, the coastal regions are near the source of moisture (ocean). Ocean water undergoes less isotopic fractionation than terrestrial sources, producing more enriched isotopic signatures (Geppert *et al.*, 2022).

2.1.2 Meteoric water lines

The second basis for interpreting the rainfall isotope signatures is using a regression line called the meteoric water line, constructed from the plot of the water isotopes in an X-Y bivariate plot (Craig, 1961). Meteoric water lines (MWL) are typically generated using rainfall samples (Diamond, 2022). A study conducted by Craig in 1961 was the first to reveal the significant correlation between ^{2}H and ^{18}O signatures in precipitation across the globe. The study presented the line of best fit referred to as the GMWL, defined by the equation: $\delta^{2}H = 8 * \delta^{18}O + 10.8$. In each location, the collected precipitation samples over a long period will form a regression line referred to as LMWL (Harris *et al.*, 2010; Durowoju *et al.*, 2019; Leketa and Abiye, 2020; Diamond, 2022).

The **Figure 2.4** shows that precipitation signatures worldwide lie close to the GMWL, although there is variability among regions having slightly different LMWLs (Diamond, 2022). The LMWL provides a good representation of the local hydrological cycle, producing a limited and more specific range of local isotope compositions than the GMWL (Diamond, 2022). LMWLs usually have slopes less than 8, ranging between 5 and 7. Thus, when LMWLs from different climate regions are plotted, they tend to be semi-parallel and stack adjacent, forming the GMWL (Mook and Rozanski, 2000; Diamond, 2022).

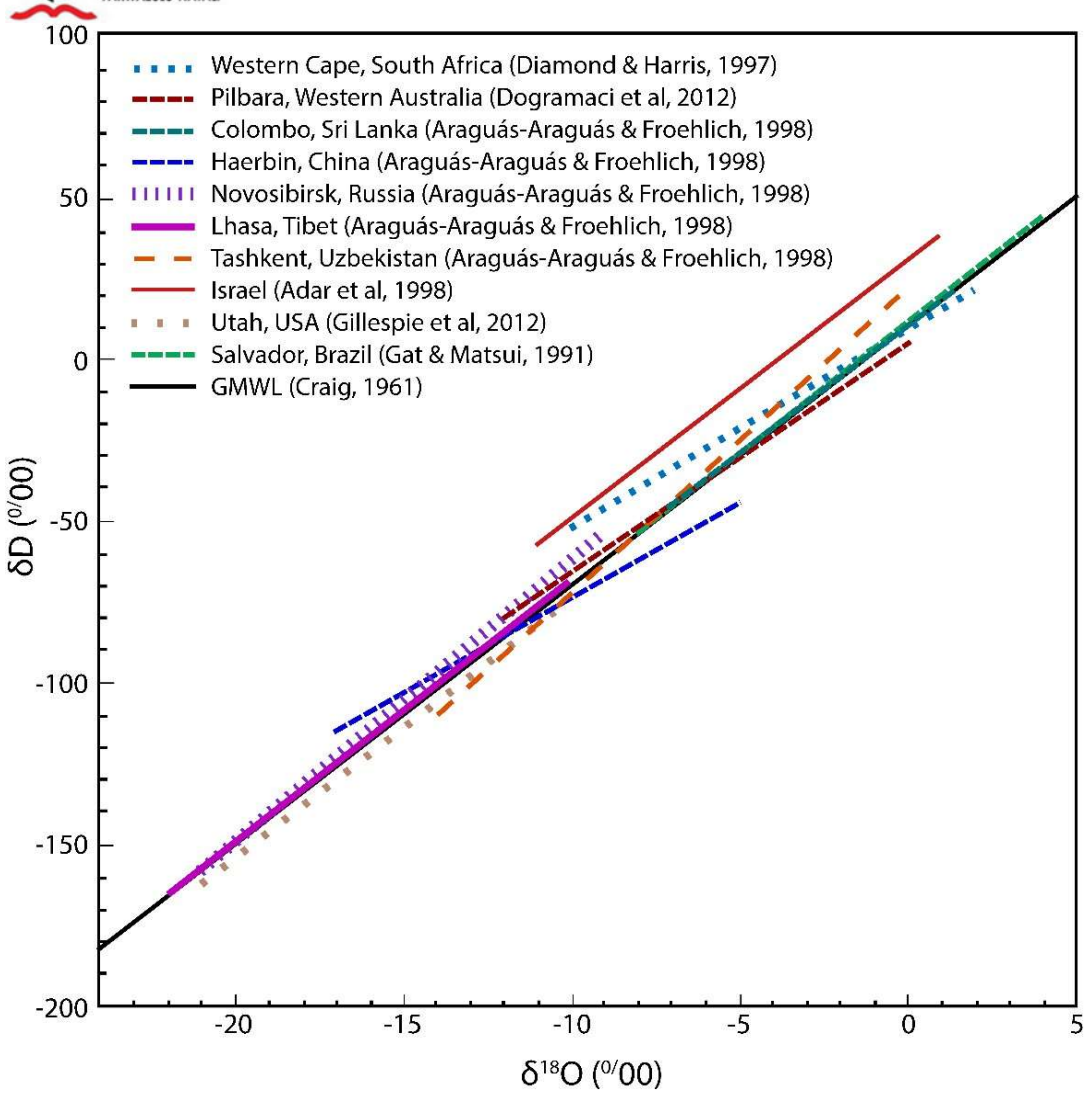

Figure 2.4 LMWLs from different regions worldwide and the GMWL (Diamond, 2022).

Globally, previous studies (Barrie *et al.*, 2022; Modie *et al.*, 2022; Welgus and Abiye, 2022; Tadesse *et al.*, 2023) have demonstrated that comparing the isotope compositions of groundwater, surface water and LMWL facilitates the investigation of various processes, such as secondary evaporation, recharge, flow, discharge mechanisms and mixing processes. However, studies examining the stable isotope composition of precipitation in South Africa are limited (Abiye *et al.*, 2013; Leketa and Abiye, 2020). Only a few studies are available that developed South African LMWLs (Harris *et al.*, 2010; Braun *et al.*, 2017; Leketa *et al.*, 2018; Durowoju *et al.*, 2019; Leketa and Abiye, 2020; Ramudzuli, 2021). These studies serve as a critical foundation for current research by providing basic understanding, temporal trends, spatial variations, and methodological insights and aiding in identifying research gaps.

A study conducted by Harris et al. (2010) examined the δ^2H and $\delta^{18}O$ signatures from rainfall collected over 13 years (1996 to 2008). The study was conducted at the University of Cape Town in the Western Cape Province. Different time scales were employed for sampling rainfall (monthly and daily). Two storms were selected for sampling in less than hourly intervals and at less than 30 minutes for one rainfall event. The established Cape Town LMWL was $\delta^2H = 6.4l * \delta^{18}O + 8.66$. Followed by a study that was conducted by Braun et al. (2017), which examined the δ^2H and $\delta^{18}O$ signatures from rainfall collected daily over four years (2009 to 2012). The study was conducted at Mossel Bay in the Western Cape Province. The established LMWL was $\delta^2H = 7.35 * \delta^{18}O + 11.2$.

Leketa et al. (2020) investigated the isotopic composition of rainfall at Johannesburg in the Gauteng province. The rainfall samples were collected daily for two years (2016 to 2018). The established LMWL was $\delta^2H= 6.78* \delta^{18}O + 10$. Lastly, Durowuju et al. (2019) generated an LMWL for the Thohoyandou catchment in Limpopo province. The rain samples were collected monthly for one year (May 2016 – April 2017). The established LMWL was $\delta^2H = 7.56 * \delta^{18}O + 10.64$.

2.1.3 Deuterium excess

The other basis for interpreting isotope compositions is the d-excess. According to Allen et al. (2022), d-excess ($d = \delta^2H - 8*\delta^{18}O$) is a measure of deviation, in δ^2H units, from the global meteoric water line, which passes through the origin and is defined relative to Vienna Standard Mean Ocean Water (VSMOW) along the equilibrium fractionation slope (slope = 8). Various studies have employed this method in South Africa (West et al., 2014; Leketa and Abiye, 2020). For example, a study by Leketa and Abiye (2020) stated that the d-excess of vapour near the sea surface is negatively correlated with relative humidity. Meanwhile, it is positively correlated with sea surface temperature. The addition of vapour from continental reservoirs to the moisture trajectory from the ocean causes an increase in the d-excess of precipitation; when re-evaporation occurs, the d-excess in rainfall decreases (Leketa and Abiye, 2020).

2.2 Using Isotopes of Water in Groundwater Investigations

A recent study reported that approximately 1.5 billion people rely on groundwater as a primary source for domestic use worldwide (Cheng *et al.*, 2021). The study emphasised that insufficient surface water in arid and semi-arid areas affects the high demand in groundwaters associated with food security, human health and ecosystem management challenges (Liao *et al.*, 2018; Cheng *et al.*, 2021).The growing demand for groundwater has led to the

characterisation of groundwater being one of the key tools for protecting water resources (Wilson *et al.*, 2022). Different techniques have been employed to investigate the isotopic composition of groundwaters, such as environmental tracers including isotopes, noble gases and fluorescent dyes (Chamine *et al.*, 2015; Wilson *et al.*, 2022). Environmental isotopes are used to gain an overview of the groundwater flow dynamics, mixing and recharge conditions by applying the relative deviation from the GMWL and the LMWL (Abiye *et al.*, 2015).

Furthermore, environmental tracers can characterise surface water systems such as springs, streams, lakes and wetlands by determining flow paths and recharge areas (Wilson *et al.*, 2022). According to Wilson et al. 2022, the major challenges associated with tracer studies are time (time-consuming or intensive time required), travel costs and the inability to access certain sampling sites. However, multiple tracer collections at one sampling point could be helpful. The conservative nature of stable isotopes allows us to determine the history of water before recharge and makes it possible to identify the mixing of distinct water resources (Leketa *et al.*, 2018). The groundwater recharge characterisation compares the groundwater signature with precipitation (Leketa and Abiye, 2020). The enrichment of groundwater would indicate direct recharge either from open surface water bodies or the occurrence of hot springs. Meanwhile, depleted groundwater is usually linked to diffuse recharge from infiltration of precipitation.

2.3 Groundwater Recharge, Flows and Discharge

Groundwater recharge amount and its dynamics are key parameters in assessing groundwater resources and their protection. Globally, a few groundwater recharge studies have been conducted over the last decades, revealing the spatial variation in recharge and understanding the main drivers of recharge and the mechanism through which rainfall recharges groundwater.

Several domains have been used to systematise understanding of groundwater recharge. One such approach is classifying the dominant groundwater recharge of a given catchment as focused or diffuse. It can be noted that the type of recharge can be in response to the environmental setting. Diffuse (direct) recharge occurs when precipitation or irrigation replenishes groundwater over large, uniform areas, with water infiltrating the soil and gradually moving downward (Scanlon *et al.*, 2005). In contrast, focused (localized) recharge happens in specific areas like streams, lakes, or depressions, where water accumulates and infiltrates more quickly into the ground (Scanlon *et al.*, 2005). In addition, other research

highlights the importance of rainfall intensity in groundwater recharge, such as tropical storms (Cheng *et al.*, 2021).

Groundwater recharge water is naturally transported through an unsaturated profile that allows water to be stored during rainfall events and then water eventually moves down, recharging the aquifer. In the meantime, the infiltrated rainfall can be extracted by vegetation in the following dry days. According to Cheng et al. (2021), groundwater recharge in semi-arid and arid areas depends on high-intensity rainfalls and the rainy season. During the wet season, heavy rainfall events allow for high water storage in the soil profile, higher than the potential evapotranspiration over a period, allowing relative amounts to reach the groundwater.

Groundwater flow has been investigated since 1963 as local, intermediate and regional. According to Markovich et al. (2019), the local or shallow flow is the groundwater discharging to the nearest stream within the same sub-watershed where it recharged. A slight difference is observed in intermediate flows; here, groundwater exits the sub-watershed after being recharged by subsurface water and discharges to a lower-altitude stream bearing higher order than the source of recharge sub-watershed.

The discharge of shallow and intermediate flow paths to the surface system occurs within the mountain block, called mountain aquifer recharge (Schaller and Fan, 2009; Cheng *et al.*, 2021). In contrast, the deep or regional flows follow a series of paths to exit the mountain block in the subsurface, becoming or contributing to mountain block recharge (MBR). Therefore, deep groundwater flow is equivalent to MBR. Recently, an increasing focus has been on the importance and understanding of lateral groundwater recharge to valley aquifers, such as MBR or mountain-front recharge (MFR). A study conducted by Markovich et al. (2019) highlighted that MBR is a predominant component of recharge, recharging the aquifers in the valleys with an estimate of 60% (Uhlenbrook *et al.*, 2002; Wilson and Guan, 2004; Markovich *et al.*, 2019). The study emphasised that MBR-related studies are limited, and the lack of hydrogeological, climatic and other related data availability remains the key challenge in characterising and quantifying MBR and the MFR (Markovich *et al.*, 2019).

There is also growing interest in the studies on the climate resilience of groundwater flows. For example, shallow flows are documented to be more vulnerable to short-term climatic variations and susceptible to contamination threats because of their proximity to the land surface. Conversely, regional flows have long residence times and are isolated from short-

term climate fluctuations (Gleeson and Manning, 2008; Schaller and Fan, 2009; Markovich *et al.*, 2019). In addition, there is limited coverage of different groundwater flows in the hydrological models (Condon *et al.*, 2020). The hydrological models tend to route all waters in the catchment to streams even though substantial amounts of water can be discharged elsewhere through deep regional flows (Markovich *et al.*, 2019; Kebede *et al.*, 2021).

Groundwater discharge areas include but are not limited to streams, lakes, wetlands, coastal zones or when a pumping well is installed (Vandas *et al.*, 2002). Groundwater may sustain the baseflow of the surface waters and is a primary source of many wetlands, vegetation, springs and hyporheic zones (Sophocleous, 2002b; Vandas *et al.*, 2002; Uhl *et al.*, 2022). The emphasis on understanding groundwater discharge has recently grown because past studies (Madlala *et al.*, 2021; Glanville *et al.*, 2023) have revealed that groundwater supports ecosystem health (natural water purification) and services in several places. For instance, the groundwater-saturated subsurface constitutes the largest continental biome. Thus, groundwater discharge records can be used to estimate how often a flood of a certain magnitude is likely to occur (Vandas *et al.*, 2002).

2.4 Groundwater and Surface Water Interactions

The interactions between GW and SW result from the exchanges where surface water seeps through the sediments into groundwater or when groundwater discharges into surface waters (Sechu *et al.*, 2022). In South Africa, past studies have looked at GW and SW as different entities, whereas even the small-scale exchanges within these two hydrological components impact the water quality and quantity (Xu *et al.*, 2017; Kebede *et al.*, 2021). Research studies that have been conducted on the GW and SW interactions focused on areas such as source identification (Gibrilla *et al.*, 2022; Adyasari *et al.*, 2023), hydrologic dynamics of interchanges (Banks *et al.*, 2009; West *et al.*, 2022), and exchange characteristics of water quality and quantity (Scanlon *et al.*, 2007; Stellato *et al.*, 2008; Barthel and Banzhaf, 2016; Xu *et al.*, 2017; Liao *et al.*, 2018; Kebede *et al.*, 2021).

The relationship between the streams and their groundwaters determines whether the stream can be classified as gaining or losing (McNamara and Frye, 2012). Vandas et al. (2002) elaborated on the interactions happening differently. The study reported that streams might gain from the inflow of groundwater through the streambed, but the streams can lose water as outflow through the streambed and certain locations may allow both ways to occur. Others may be disconnected and let none happen. Streams gaining and losing nature may be

influenced by various factors such as climate and human activities (McNamara and Frye, 2012). Winter (1999) demonstrated the different stream and aquifer interactions, as shown in the figure below (**Figure 2.5**).

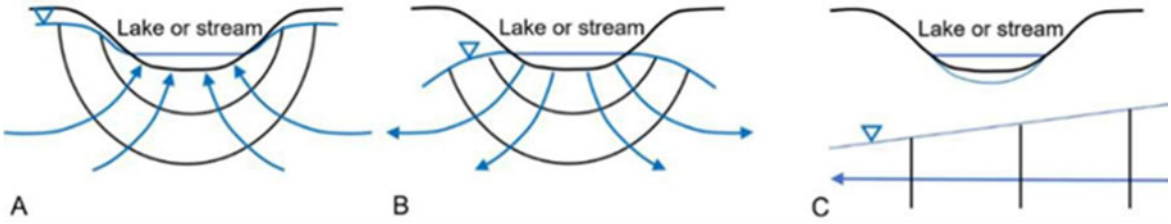

Figure 2.5 Different ways of stream-aquifer interactions, (A) gaining stream, (B) losing stream and (C) disconnected stream (Winter, 1999; Welgus and Abiye, 2022).

2.4.1 Methodologies for assessing groundwater and surface water interactions

Measuring the exchanges between GW and SW is an important component of integrated catchment water management. Such measurements can be applied in the aquifer, surface waters, or transition zone. According to Cai et al. (2020), methodologies accompanied by different techniques have been developed and assessed to investigate the relations between GW and SW. The method's appropriateness depends on the study's scale, which ranges from point to basin scale. These methods include stable isotopes of water, radon, baseflow separation, piezometric and pumping tests.

2.4.1.1 Stable isotopes of water (^{2}H and ^{18}O)

The differing ratios in the signatures of ^{2}H and ^{18}O in waters allow them to be used as tracers in hydrological studies (Kalbus *et al.*, 2006). Nine isotopically different water molecules occur in nature. However, only three have easily detectable concentrations ($^{2}H^{16}O$, $^{2}H^{18}O$, $^{1}H^{2}H^{16}O$). The isotopic concentrations are expressed in delta (δ) values and are compared to the internationally accepted standard (VSMOW) (Mook and Rozanski, 2000). For instance, the analysis of isotope compositions of different waters, such as groundwater, rainfall and surface water, can be used to investigate groundwater recharge, flow paths, mixing processes and the effects of processes such as evaporation and precipitation (Kebede *et al.*, 2021). Focused recharge from enriched surface waters would be resembled by groundwaters being highly enriched in $\delta^{2}H$ and $\delta^{18}O$. Meanwhile, diffuse recharge would lead to depleted groundwater loosely resembling rainfall (Dlamini and Demlie, 2020).

2.4.1.2 Radioactive isotopes (Radon)

The studies that assess the hydrological processes using environmental tracers include the application of radioactive isotopes such as Carbon-14 (^{14}C), krypton (^{85}Kr), Argon (^{39}Ar) and Radon (^{222}Rn) (Kalbus *et al.*, 2006; Cook, 2020; Strydom *et al.*, 2021). Radioactive isotopes are elements with an unstable nucleus that emits alpha, beta and/or gamma rays (Abumurad and Tamimi, 2001; Cook, 2020). The radioactive isotopes have been used to indicate groundwater flow rates, residence times and discharge. For instance, the predictable decay of ^{222}Rn in groundwaters makes it an ideal tracer for GW and SW interactions (Cook, 2020).

The Uranium concentrations depend on the geographical locations where elevated concentrations can be hazardous from a chemical perspective when accumulating in aquifers (Bezuidenhout, 2021). The table below (**Table 2.2**) presents the Uranium concentrations in the rocks in South Africa. The natural Uranium decays through a series chain of progeny to reach the stable end-product lead. Through the long chain of the progeny of Uranium, Radium is formed as a radionuclide that further decays to ^{222}Rn (Eilers *et al.*, 2015; Bezuidenhout, 2021; Strydom *et al.*, 2021). ^{222}Rn quickly degasses to the atmosphere if exposed to high temperatures and turbulence, making it more abundant in groundwaters than in surface waters, especially because there is less contact of radium-bearing minerals with streams (Adyasari *et al.*, 2023).

The use of ^{222}Rn has gained interest worldwide and in South Africa. Notable studies conducted worldwide include studies conducted in Ethiopia (Kebede and Zewdu, 2019; Kebede *et al.*, 2021; Tadesse *et al.*, 2023), Southern Australia (Cartwright *et al.*, 2014), Central Italy (Stellato *et al.*, 2008) and China (Wang, 2002). In South Africa, progress has been made in using ^{222}Rn as a hydrological tracer. A study conducted by Sukanya et al. (2022) assessed the use of ^{222}Rn as a tracer in hydrogeological and geological investigations in South Africa. The study evaluated different ^{222}Rn applications, such as using ^{222}Rn to trace groundwater discharge, estimate the baseflow contribution to streams and locate geological structures. The study concluded that the ^{222}Rn's short half-life (~3.82 days), chemically inert nature, and significant enrichment in aquifers compared to surface waters make ^{222}Rn an ideal tracer of GW and SW interactions.

Another study conducted by Eilers et al. (2015) examined the ^{222}Rn concentrations in the Karoo groundwater in South Africa. It was found that there is an expected increase in ^{222}Rn concentrations associated with the formation of fractures. The study highlighted the risks of

inhaling or digesting high concentrations of ^{222}Rn, including lung, stomach and digestive organ cancer. This is supported by another study conducted by Bezuidenhout (2021) to estimate the indoor ^{222}Rn concentrations in South Africa. The study discovered that the southwestern and northeastern regions have a high ^{222}Rn risk. Thus, it is important to monitor the ^{222}Rn concentrations to protect human health frequently (WHO, 2011; Eilers *et al.*, 2015; Madzunya *et al.*, 2020; Bezuidenhout, 2021). In South Africa, the target gross beta activity in water quality is (0-1.38 Bq/L) issued by the South Africa Department of Water Affairs and Forestry (London *et al.*, 2005; Madzunya *et al.*, 2020). Furthermore, the World Health Organisation has set guidelines for safe water to be 0.5 Bq/L for gross alpha activities and 1 Bq/l for gross beta activities (WHO, 2011; Madzunya *et al.*, 2020)

Table 2.2 Varying concentrations of Uranium in different lithological groups, subgroups and types of rocks in South Africa (Bezuidenhout, 2021).

Rock Types and Subgroups	Uranium (ppm)	Rock Types, and Subgroups	Uranium (ppm)
Amphibolite	3.5	Mafic Volcanic Rocks	4.0
Andesites	1.6	Low-Grade Metavolcanic and Metasedimentary Rock	2.4
Anorthosite	0.2		
Arenite	2.0		
Basaltic Andesite	1.3	Magnetite	11.2
Basalts	0.5	Marine Sediment	1.5
Biotite	7.9	Melanorite	0.1
Breccia	2.4	Melilitite	2.8
Calc-Silicate Rocks	0.1	Microgranite	3.6
Carbonatite	23.0	Migmatite	0.9
Charnockite	1.8	Monzodiorite	8.1
Chert	0.1	Monzogranite	4.4
Dacite	2.6	Monzonite	8.6
Diamictite	4.0	Quartz-Monzonite	12.8
Diorite	0.8	Mudstone	4.9
Quartz Diorite	6.9	Nephelinite	0.4
Dolerite	0.4	Norite	0.3
Dolomite	2.0	Miscellaneous	3.0
Dunite	0.0	Pegmatite	3.4
Eclogite	3.0	Peridotite	0.0
Enderbite	0.4	Phoscorite	11.2
Felsite	8.4	Phyllite	1.9
Fenite	0.0	Picrite	0.8
Foyaite	33.7	Pyroxenite	0.3
Gabbronorite	0.3	Quartzite	0.0
Gabbro	4.2	Rhyolite	4.0
Glimmerite	0.4	Sandstone	1.8
Gneiss	1.2	Schist	2.6
Granite-Gneiss	6.0	Shale	4.6
Granite	6.0	Siltstone	5.7
Granodiorite	5.6	Slate	2.7
Biotite- Granodiorite	7.9	Syenite	7.2
Granophyre	3.6	Quartz-Syenite	12.0
Granulite	0.1	Tholeiite	1.4
Gravels	4.0	Tinguaite	22.4
Greywackes	2.0	Tonalite	0.5
Harzburgite	0.1	Trachyandesite	3.1
Hornblendite	4.4	Trachyte	11.6
Hornfels	3.6	Trondhjemite	1.2
Ijolite	3.0	Volcanic Rock	2.2
Jaspilite	4.0	Wacke	4.0
Leucogranite	4.3	Websterite	0.4

2.4.1.3 Piezometry

The piezometer method provides point measurements of the hydraulic head or pressure in aquifers, which is more appropriate for small/local scale applications (Kalbus *et al.*, 2006). Observations show that piezometric levels near the stream are higher in gaining streams. This suggests that, in these regions, groundwater is flowing from the stream into the surrounding aquifer, contributing to groundwater recharge. Conversely, in losing streams, piezometric levels near the stream are lower, indicating that groundwater is flowing from the aquifer into the stream (Kebede *et al.*, 2021). Furthermore, monitoring fluctuations in piezometric levels over time can reveal seasonal groundwater variations, helping to distinguish the groundwater response during periods of high or low precipitation, as well as during exceptional weather events (Kebede *et al.*, 2021).

2.4.1.4 Pumping test

Pumping test measurements are conducted by pumping water from a well at a constant rate and observing how the aquifer responds over time (Van Tonder *et al.*, 2002). The responses from the aquifer can be recorded as drawdown, change in water level of the pumped well and other nearby observation wells (Van Tonder *et al.*, 2002; McDonald *et al.*, 2013). The changes in groundwater water levels and nearby streams during pumping could give insight into the hydraulic connection between GW and SW (McDonald *et al.*, 2013; Barthel and Banzhaf, 2016; Kebede *et al.*, 2021). Pumping tests are often used to determine the hydraulic properties of aquifers (transmissivity, storage etc.).

2.4.1.5 Temperature

Temperature variations between GW and SW have been used to delineate groundwater recharge-discharge zones (Toran; Kalbus *et al.*, 2006) and determine groundwater contribution to streamflow (Anderson, 2005). Thus, it has been found that temperature is a quick, easy, robust and inexpensive parameter to be measured at a catchment or regional scale (Rorabaugh *et al.*, 1956; Kalbus *et al.*, 2006).

2.4.1.6 Electrical conductivity

Salinity, total dissolved solutes (TDS) and EC are proven tracers for evaluating exchanges between GW and SW (Tredoux and Talma, 2006). EC concentrations reflect the concentration of dissolved ions, which tends to be high in groundwater due to its interaction with subsurface geological formations (Liu and Yamanaka, 2012). Conversely, surface waters exhibit unique EC concentrations influenced by the weathering of rocks and anthropogenic

activities. Therefore, monitoring EC fluctuations in both surface waters and groundwater at various points enables the identification of potential interaction zones and the extent of mixing can be quantified (Kebede *et al.*, 2005; Tredoux and Talma, 2006; Liu and Yamanaka, 2012; Mabokela, 2021).

2.4.1.7 Baseflow separation

After a rainfall event, the observed streamflow consists of three different flows: quick flow, interflow and baseflow. Baseflow is categorised as the longest-responding and lasting, proving the primary source to be groundwater aquifers (Sloto and Crouse, 1996; Indarto *et al.*, 2016; Duncan, 2019). Monitoring the time series of baseflow is a valuable tool for understanding the groundwater status, instream ecology and seasonal flows. This can assist in understanding short-term runoff behaviour (Brodie, 2005; Duncan, 2019). The baseflow proportion of the total streamflow has an index illustrating the catchments' ability to store and release water during different seasons, especially the dry season (Brodie, 2005). The Base Flow Index (BFI) gives the ratio of baseflow to total flow calculated from a hydrograph smoothing and separation procedure using daily discharges (Indarto *et al.*, 2016; Welgus and Abiye, 2022).

There are several methods developed to separate baseflow from total stream flow, which include baseflow recession analysis, baseflow during an event and continuous baseflow separation techniques (Duncan, 2019). The approaches can be applied at broader spatial and temporal scales (Duncan, 2019). For example, the continuous baseflow separation techniques can estimate baseflow on a daily or even hourly basis from long-term datasets, allowing to assess the trends and impacts of climate change (Indarto *et al.*, 2016). Different continuous separation techniques have been used in previous studies (Madlala, 2015; Welgus and Abiye, 2022), which include fixed interval, sliding interval, local minimum (Sloto and Crouse, 1996) and other different versions derived from the local minimum method (Indarto *et al.*, 2016; Duncan, 2019; Welgus and Abiye, 2022).

2.4.2 Factors that control groundwater and surface water interactions

Geological and environmental conditions are widely believed to control GW and SW interactions in the catchment, such as geology, topography, land use and land cover, faults and lineaments, as well as dykes. According to Levy and Xu (2012), GW and SW interactions can be complicated as they may be affected by several factors, including but not limited to

geometries, the location of the surface water bodies with their relative aquifers and anthropogenic activities.

2.4.2.1 Topography

Topography has an influence on the groundwater movement (direction and rate of groundwater flow) (Brannen *et al.*, 2015). Groundwater preferentially moves from regions of high elevation to lower elevation because changing elevation creates variations in the hydraulic head, which is the major driver of groundwater flows (groundwater moves from a higher hydraulic head to a lower hydraulic head) (Winter, 1999). As a result, the highlands tend to be recharge areas, and the discharge zones are the lowlands (Winter, 1999; Sophocleous, 2002a).

From an aerial point of view, when uniform precipitation and infiltration rates occur over an undulating surface, groundwater flow will be directed by the water-table surface that is subject to resemble the land surface (Sophocleous, 2002a). In mountainous regions, groundwater may flow rapidly downslope and there is a high potential for GW and SW exchanges as groundwater can discharge to the surface as springs that can be joined to streams. Conversely, in the valleys, surface waters can recharge groundwater as they encounter steady flows (Levy and Xu, 2012).

2.4.2.2 Geology

Geological formations control the movement and storage of groundwater, creating pathways for groundwater to interact with streams, lakes, wetlands and support the emergence of springs. The type of rock and soil formation present in a catchment determines the permeability and porosity of the subsurface.

According to Levy and Xu (2012), the GW and SW interactions can be complicated as they may be affected by several factors, including but not limited to the geometries, the location of the surface water bodies with their relative aquifers and the anthropogenic activities. This is supported by a recent study conducted by Cai et al. (2020), where the interactions between GW and SWs were proven to be controlled by topography, geology, landform conditions and human activities.

2.4.2.3 Land use and land cover

The changes in land uses and land cover have an impact on groundwater dynamics and may pose significant threats to the ecosystem. Welgus and Abiye (2022) conducted a recent study

investigating the anthropogenic activities associated with a structurally complex geological setting effect on the nature of exchanges between groundwater and surface water. Various methodologies were integrated, which include hydrochemical statical techniques, stable isotopes of water, groundwater level mapping, baseflow separation and microorganisms. Principal component analysis (PCA) indicated a link between the natural hydrochemical processes and anthropogenic activities affecting groundwater composition. Thus, land uses were the major source of stream contamination.

2.4.2.4 Faults and lineaments

Faults and lineaments enhance the interactions between GW and SW by acting as pathways for groundwater flow. A recent study by Modie et al. (2022) used stable isotopes and hydrochemical parameters to investigate the exchanges between groundwater and surface water in the Notwane River catchment. The Notwane basin forms part of the Ramotswa Transboundary Dolomitic Aquifer (RTBDA) in the Limpopo catchment shared between Botswana and South Africa. The analysis indicated an interaction of groundwater and surface water where active groundwater recharge zones in the Notwane River were identified. The identified sites were dominated by faults and karsts, which were responsible for high direct aquifer recharge, especially during certain above-normal rainfall events in the catchment.

2.4.2.5 Dykes

A study conducted in the Karoo basin revealed the role of dykes in groundwater movement (Woodford and Chevallier, 2002). The Karoo dolerites were revealed as interconnected dykes and sills acting as a shallow stockwork-like reservoir. From the observations made in the Karoo catchment, the dolerite dykes were presented to be vertical to a sub-vertical discontinuity that is in transgressive contact with country rocks. Dykes naturally occur as thin, linear zones of higher permeability acting as conduits for groundwater flow in aquifers. Furthermore, the dykes may act as semi to impermeable barriers blocking groundwater movement. In conclusion, more than 80% of drilled boreholes in the Northern KwaZulu-Natal yielding > 0.13 ℓ/s are directly or indirectly supported by dolerite intrusions.

2.4.3 Groundwater recharge, flow, discharge and interactions with surface water in South Africa

South Africa is part of the main Karoo Basin, covering 500,000 km^2 (Woodford and Chevallier, 2002; Khan and Davidson, 2016). The Karoo Basin presents a complex hydrogeological landscape with varying aquifer systems. In South Africa, the shallow

aquifers have been researched and assessed for groundwater resources. However, the deep formations remain under-exploited (Khan and Davidson, 2016).

Documented studies focusing on multi-scale groundwater flows in South Africa are limited. However, some studies have used isotope tracers, groundwater models and hydrochemistry to investigate groundwater flow dynamics and aquifer characteristics (Dlamini and Demlie, 2020; Leketa and Abiye, 2020). A study used $\delta^{2}H$-$\delta^{18}O$ to investigate the groundwater flows in a fractured aquifer in Mpumalanga province; the study revealed certain sites to have similar isotopic signatures among waters, indicating interactions where groundwater discharged into rivers or contributed to baseflow sustaining the rivers (Dlamini and Demlie, 2020). The measured hydraulic head data was used to construct a groundwater level contour map where the regional groundwater flow was observed to follow the topographic gradient, moving from a southeast to a northwest direction of the catchment.

Durowuju et al. (2019) revealed that most South African systems rely on precipitation as a primary source of recharge. This is as highlighted by Leketa et al. (2018), the study revealed that diffuse recharge was dominant in one of the South African regions (Johannesburg). Again, Dlamini and Demlie (2020) revealed that local rainfall recharge is predominant (Mpumalanga), presented by depleted groundwaters resembling rainfalls. Thus, it is important to understand the recharge processes, identify recharge zones and strictly protect the sites.

The flow exchange between groundwater and surface water affects the stream's chemical and biological attributes (Madlala, 2015; Valett and Reinhold, 2022). Unfortunately, studies examining groundwater and surface water integration in South Africa are lacking because groundwater and surface water have been isolated (Madlala, 2015). However, in a research paper by Levy and Xu (2012), the progress in groundwater management and the acknowledgement of GW and SW interactions from the South African perspective were reviewed. Eventually, the implementation of the New Water Act 36 of 1998, which requires integrated water resources management, influenced considerations of GW and SW interactions, knowledge understanding and dissemination among the hydrology and hydrogeology disciplines (Condon *et al.*, 2020; Kebede *et al.*, 2021).

The Umgeni Catchment has been partially investigated for environmental isotopes, Uranium concentrations, hydrogeology, geology, hydrochemistry, groundwater levels and recharge through other studies that were focused on the KwaZulu-Natal province (Botha and Botha,

2002; Manickum *et al.*, 2014; Bordy *et al.*, 2017; Ndlovu, 2018; Ndlovu and Demlie, 2018). No documented studies have focused on investigating GW and SW interactions in the Umgeni Catchment. However, a study by Mtshali et al. (2021) recently used environmental isotopes, baseflow separation, hydrochemistry and piezometry. The study only covered the lower section of the catchment and other areas outside the catchment boundaries (eThekwini Metropolitan area).

The studies that were conducted covered the catchment from various perspectives, including water availability and quality. Kusangaya et al. (2018) reported that the Umgeni Catchment is water-stressed, and the basin has recently experienced significant droughts. The study reflected on the drought from 2015 to 2016, which was the worst drought since 1904. The study emphasised the significance of the effects of extreme events on the economy and the risks they pose to human lives. Therefore, it was concluded that it is important to develop studies that evaluate the water resources in the Umgeni Catchment to aid in adaptation and mitigation of the changes brought about by past events. Thus, to make viable future hydrological projections accompanied by climate change impact studies.

2.5 Literature Evaluation

This section synthesises the existing literature on groundwater recharge, discharge, flows and its connection with the surface waters. The literature review has presented several studies examining the role of groundwater in basin hydrology at various scales. Through conceptualising how groundwater is being recharged, how it joins the surface waters, where it joins and what controls its connection to surface waters. Gaps in understanding, characterisation, and methodologies were identified to investigate groundwater and its interactions with surface water.

The mechanisms of groundwater recharge from mountainous to lowland valleys are still poorly understood in South Africa, yet they hold increasing importance in the context of climate change. There are projected climate changes, including changes in precipitation patterns and rising temperatures, significantly impacting groundwater resources in arid regions (South Africa). The literature presented that the aquifers within semi-arid climate conditions recharge more from stream networks as a focused recharge (Leketa *et al.*, 2018). Nevertheless, the regions dominated by dolerite intrusions and granite-supporting fractured rocks were associated with high diffuse recharge (Modie *et al.*, 2022). The changing rainfall patterns can affect both focused and diffuse recharge. For instance, increased rainfall can alter

surface runoff generation processes, leading to less water available for infiltration and groundwater recharge.

Similarly, studies evaluating groundwater flows are limited, but there is growing interest in South African groundwater flow-related studies. The hydrogeology literature has focused on demonstrating the presence of local and intermediate flows, which are well incorporated into the hydrological models to a certain extent. The deep groundwater flows are still poorly understood, and the hydrological models disregard their contribution to the balance of catchment water resources. This oversight can lead to an incomplete understanding of the catchment's hydrological dynamics and an underestimation of groundwater contributions to the overall catchment water balance.

The hydrological models often fail to account for spatial variability, where groundwater flow paths and recharge rates can differ significantly across geological formations and topographies within the catchment. They also overlook temporal variability, as seasonal changes and long-term climate variations influence groundwater recharge and flow, which are not always captured in static models. Human activities such as groundwater extraction, land use changes and artificial recharge methods like dam releases can significantly alter natural groundwater flow patterns. Deep aquifers' contribution is crucial in sustaining baseflows during dry periods. Thus, the current work will conduct a systematic nested isotope survey to determine where, when and how regional aquifers contribute to stream flows.

The reviewed literature reveals that studies conducted in South Africa to characterise the stable isotope compositions in rainfalls have primarily relied on a single rainfall station, short period and monthly data intervals. Daily data is largely missing, and there is limited coverage across the altitudinal transect. Considering the lack of data, ongoing or future research studies must employ the data collection task on several catchments. Continuous data collection for more extended periods is recommended, where many rainfall samplers will be installed across altitude transects, targeting the daily rainfalls.

Other limitations of past studies include considering groundwater and surface water as separate entities. Research in South Africa has traditionally focused on groundwater or surface water independently. However, recent studies, such as the one by Condon et al. (2020), have begun acknowledging the progress in assessing the interactions between GW and SW. The Investigations into these interactions in South Africa have integrated various

methods, including stable isotopes of water (^{2}H and ^{18}O), Radon (^{222}Rn), hydrochemistry, baseflow separation, piezometric measurements, and pumping tests.

Despite these advancements, there remains a need for comprehensive catchment-scale assessments of GW and SW interactions. The current study addresses this gap by integrating these methodologies to develop the first catchment-scale assessment of GW and SW interactions in the Umgeni Catchment. This approach will map out the magnitude and direction of water exchanges between groundwater and surface water systems. Additionally, it will provide insights into spatial and temporal variations in these interactions, influenced by factors such as geological formations, seasonal changes, and human activities like land use modifications.

The current work aims to enhance the understanding of the interconnection between groundwater and surface water by developing a comprehensive conceptual model. This model will assist in mapping catchment protection areas for groundwater recharge and water quality preservation. By providing detailed insights into the magnitude and direction of water exchanges within the Umgeni Catchment, this study will generate information for effective water resource management. The findings will support the development of strategies to protect and manage water resources, ensuring sustainable usage and maintaining water quality in the changing environmental conditions.

3. METHODOLOGY

3.1 Introduction

The methodology component of this paper stems from an assessment of literature gaps in the previous chapter. The overall aim is to shed light on the groundwater flow processes and their connection with the surface waters of the Umgeni Catchment of KwaZulu-Natal province, South Africa and develop a conceptual GW and SW interaction model. This chapter details the general methodology based on the framework illustrated below (**Error! Reference source not found.**).

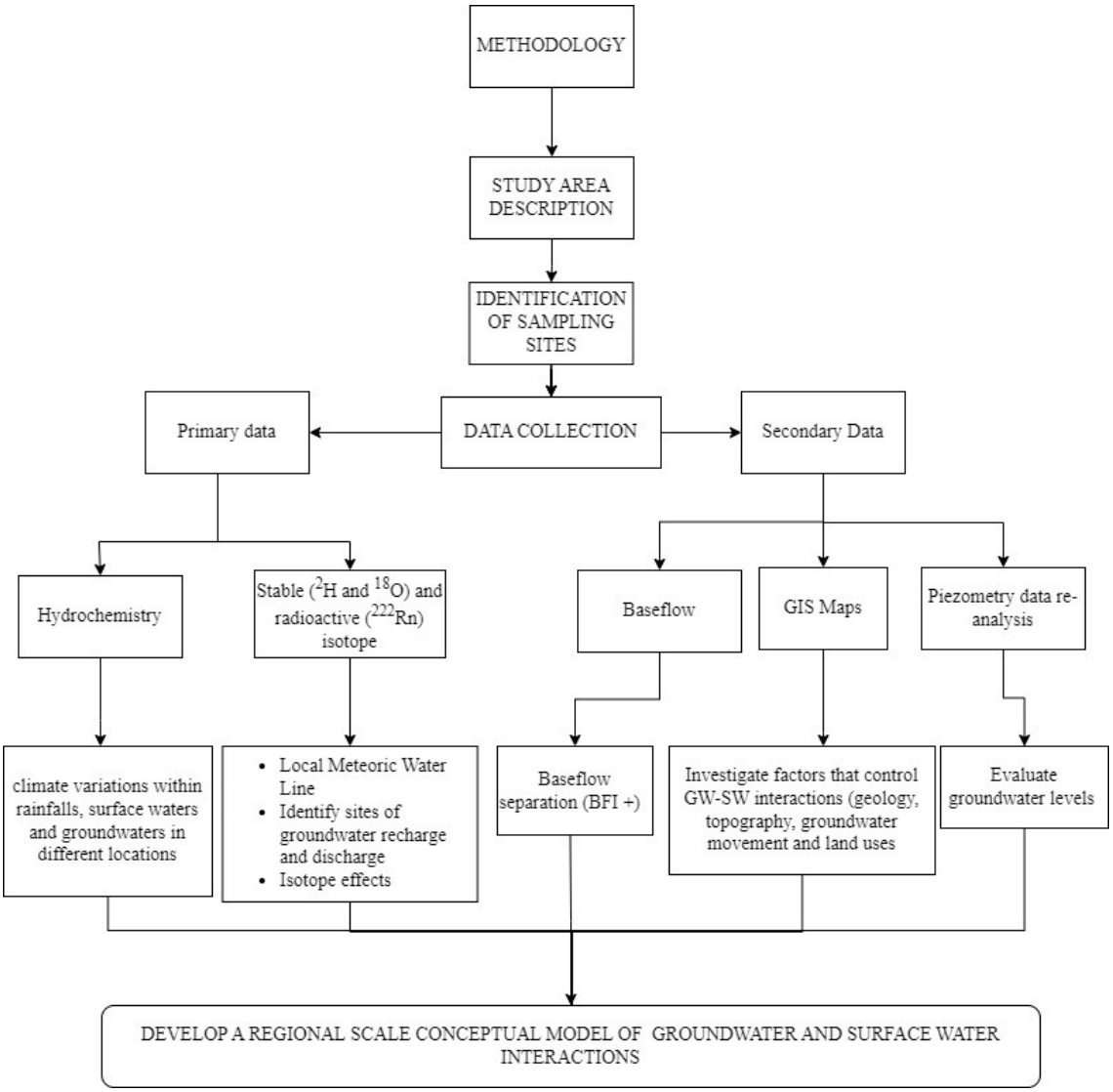

Figure 3.1 Outline of the methodology chapter.

3.2 Study Area Description

The Umgeni Catchment is between 30° and 31° East and has a latitude of 29° South in KwaZulu-Natal province, South Africa (Lorimer, 2012; Namugize *et al.*, 2018). The catchment covers an area of approximately 4481 km^2, as presented in the figure below (**Error! Reference source not found.**). The Umgeni Catchment constitutes approximately 0.33% of South Africa's surface area. However, it supplies water to nearly 15% of the entire population of the country, including the two largest cities: Pietermaritzburg, with ±220 000 people and Durban, with ±600 000 (Kusangaya *et al.*, 2016; Kusangaya *et al.*, 2018).

Considering the water-stressed nature of the Umgeni catchment, it is therefore important to address the uncertainty in understanding groundwater recharge mechanisms, especially with the projected increase in the occurrence of extreme hydrological events that include highly variable rainfall patterns escalating the severe droughts experienced and increased flood risks (Kusangaya *et al.*, 2016; Kusangaya *et al.*, 2018), land use changes or expansions (Ngcobo and Jewitt, 2017), overly abstractions of groundwater and contamination threat (Mothusi, 2014; Rangeti and Dzwairo, 2021), rapid population increase and migration (Namugize et al., 2018), unauthorised mining and water supply issues happening in the catchment (Umgeni-Water, 2020).

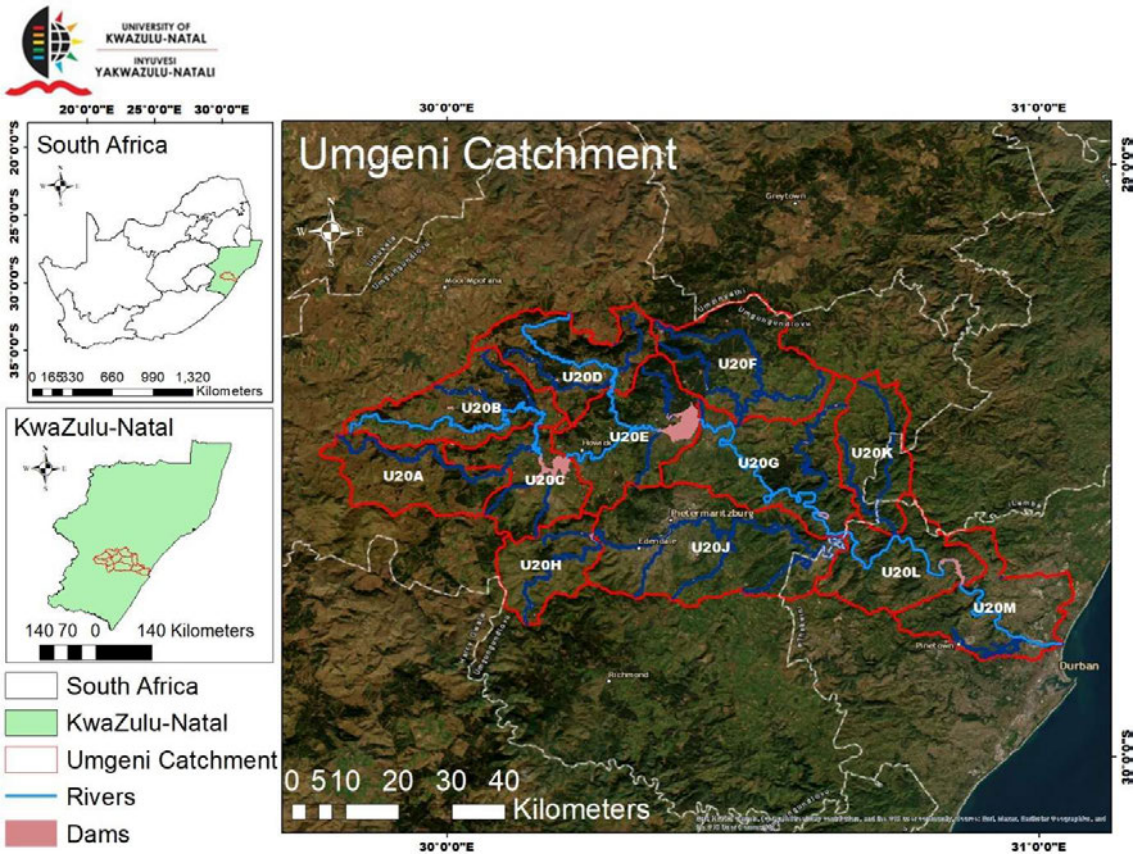

Figure 3.2 The location of the Umgeni Catchment, including the drainage regions, major tributaries, and four major dams.

3.2.1 Climate

The catchment falls within the summer rainfall regions of South Africa, experiencing a warm subtropical climate, and high rainfalls occur from October to March (Kusangaya *et al.*, 2016; Makaya *et al.*, 2019). Markable variations are observed in the distribution of precipitation throughout the catchment, with the mean annual precipitation (MAP) estimated to range between 700-1550 mm (Lorimer, 2012; Kusangaya *et al.*, 2016; Ngcobo and Jewitt, 2017; Kusangaya *et al.*, 2018; Namugize *et al.*, 2018). The high rainfall regions are in the western part of the catchment, experiencing about 1550 mm, followed by estimates of 1000 mm on the coast, and lastly, the drier middle reaches experience nearly 700 mm yearly (Kusangaya *et al.*, 2016).

3.2.2 Geology

The catchment has diverse geology, including sedimentary and basement rocks, as shown in **Figure 3.3**. The Karoo Supergroup that dominates South Africa is well represented in the Umgeni Catchment as the Dwyka Group, Ecca Group and Beaufort Group (Hicks, 2010;

Ndlovu, 2018). The Dwyka Formation within the Umgeni Catchment lies unconformably on the Natal Group. The formation comprises different old rocks from the permo-carboniferious glaciation, forming about 450 m thick succession of massive diamictites, mudstones, siltstone and sandstone (Thomas and Marshall, 1990; Herbert and Compton, 2007). The Natal Group comprises feldspathic and micaceous sandstone with subordinate quartz arenite, granulestone, mudrock and conglomerate. In the Umgeni Catchment, in the North of Durban, the Natal Group lies in two parallel belts divided by outcropping of basement rocks such as the Oribi Gorge Suite, Mapumulo and Maputaland Group (King, 1997). The first western belt lies horizontally along the Valley of a Thousand Hills area, and the other eastern belt has a slight eastward dip. The Natal Group acts as a barrier segmenting the catchment, influencing the groundwater movement (King, 1997; Botha and Botha, 2002; Demlie and Titus, 2015)

The Ecca group comprises the Vryheid, Pietermaritzburg and Volksrust Formations with shale, sandstone, siltstone and coal seams found in the Vryheid Formation (Botha and Botha, 2002). These arenaceous rocks dominate the underlying geology of the Umgeni and are crisscrossed by dolerite intrusions at various angles. The Balfour is known for its mudstones and subordinate sandstones from the ancient floodplains, often rich in fossils. The Tarkastad Subgroup has similar sedimentary rocks with fine to medium grained sandstone (Botha and Botha, 2002).

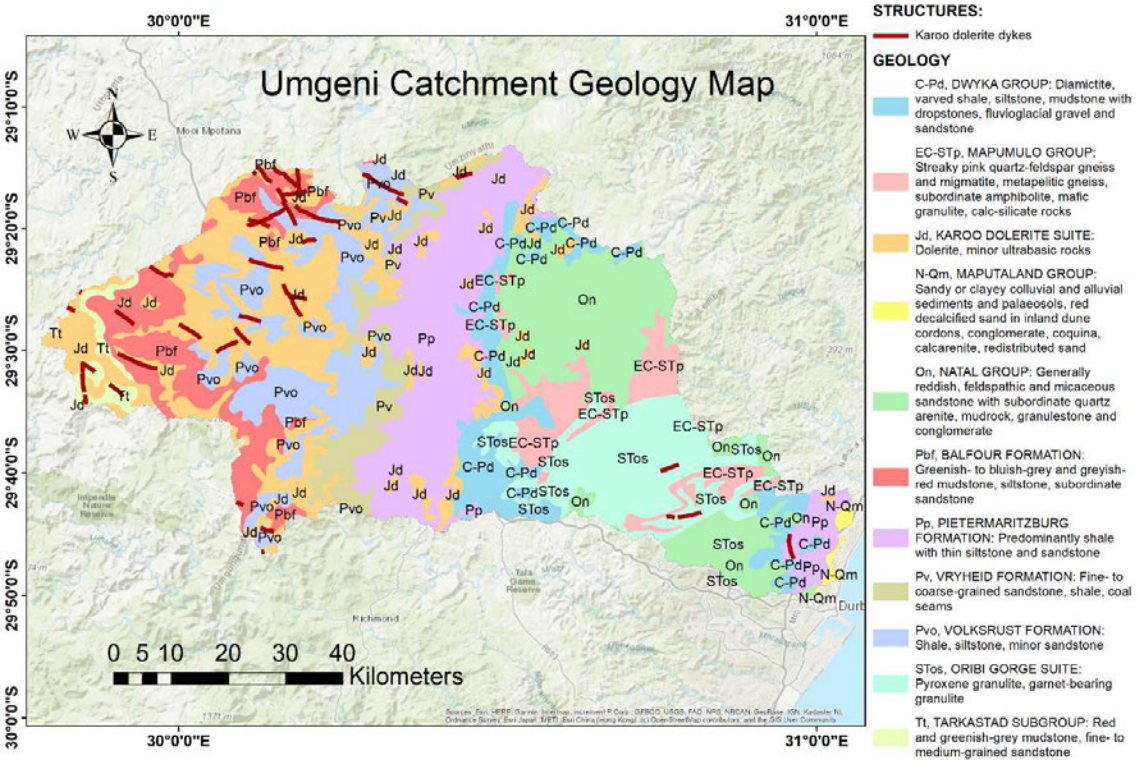

Figure 3.3 The geological map of the Umgeni River Catchment (Source: Council for Geosciences).

3.2.3 Hydrogeology

Umgeni Water (2019) reported that Umgeni Basin is in the KZN Coastal Foreland and Northwestern Middle Veld Groundwater Regions. The region is dominated by intergranular and fracture rock aquifers categorised to have low to medium development potential. A good to fair correlation exists between boreholes supporting yields in the moderate (greater than 0.5 ℓ/s to less than 3.0 ℓ/s) and high (greater than 3.0 ℓ/s) classification ranges and structural features represented by faults and remotely sensed lineaments. The table below (**Table 3.1**) presents the median yield of boreholes in different lithologies.

Table 3.1 Borehole yields in different lithologies in the Umgeni Catchment (Umgeni-Water, 2020)

Underlying lithology	Average median yield	Notes
Natal Group Sandstone	0.33 ℓ/s	Categorised to have the highest-yielding boreholes, 8% has the potential to yield about 4.5 ℓ/s.
Mudstone/shale of the Ecca Group	0.4 ℓ/s	Dominates inland at the head of Umgeni River, around Pietermaritzburg and Howick
Tillite of the Dwyka Formation	0.14 ℓ/s	Forty percent of dry boreholes are tapping this lithology
Granite/gneisses of the Natal Metamorphic Province (NMP)	0.18 ℓ/s	Only found in the lower part of the catchment around the Nagle and Inanda dams.

The most widespread demand for groundwater resources in the Umgeni Catchment is a result of its use as a source of potable water for communities in rural areas (WRC, 2002; Hughes *et al.*, 2018; Umgeni-Water, 2020). Other demands of a more concentrated nature are represented by its supplementation of rainfall and traditional surface water supplies for irrigation (Umgeni-Water, 2020). The **Figure 3.4** shows the current groundwater abstractions sourced from the Department of Water and Sanitation (DWS). Analysis of baseflow-derived stream runoff values per quaternary catchment in the Umgeni catchment suggests that groundwater recharge from rainfall varies from 3% to 7% of the mean annual precipitation (WRC, 2002). Furthermore, **Figure 3.5** also shows the directions of baseflow.

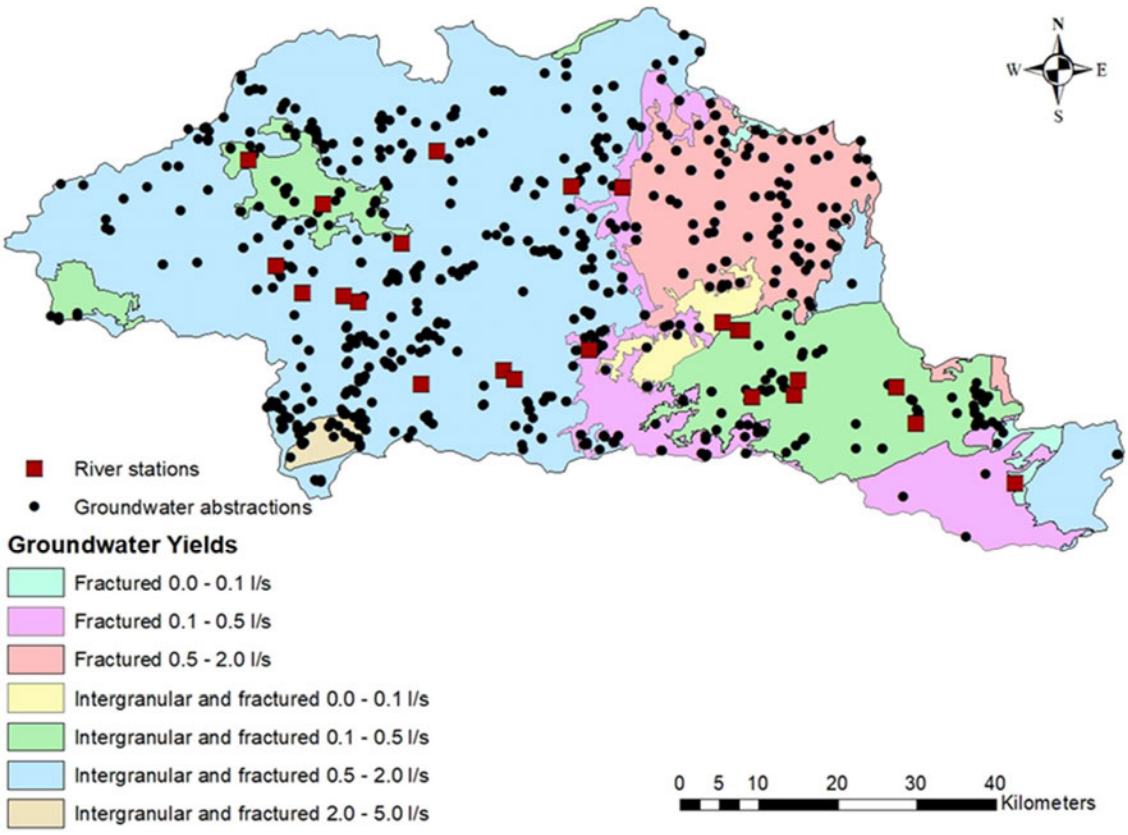

Figure 3.4 Groundwater abstractions and the transmissivity of rocks underlying the Umgeni Catchment (Source: DWS).

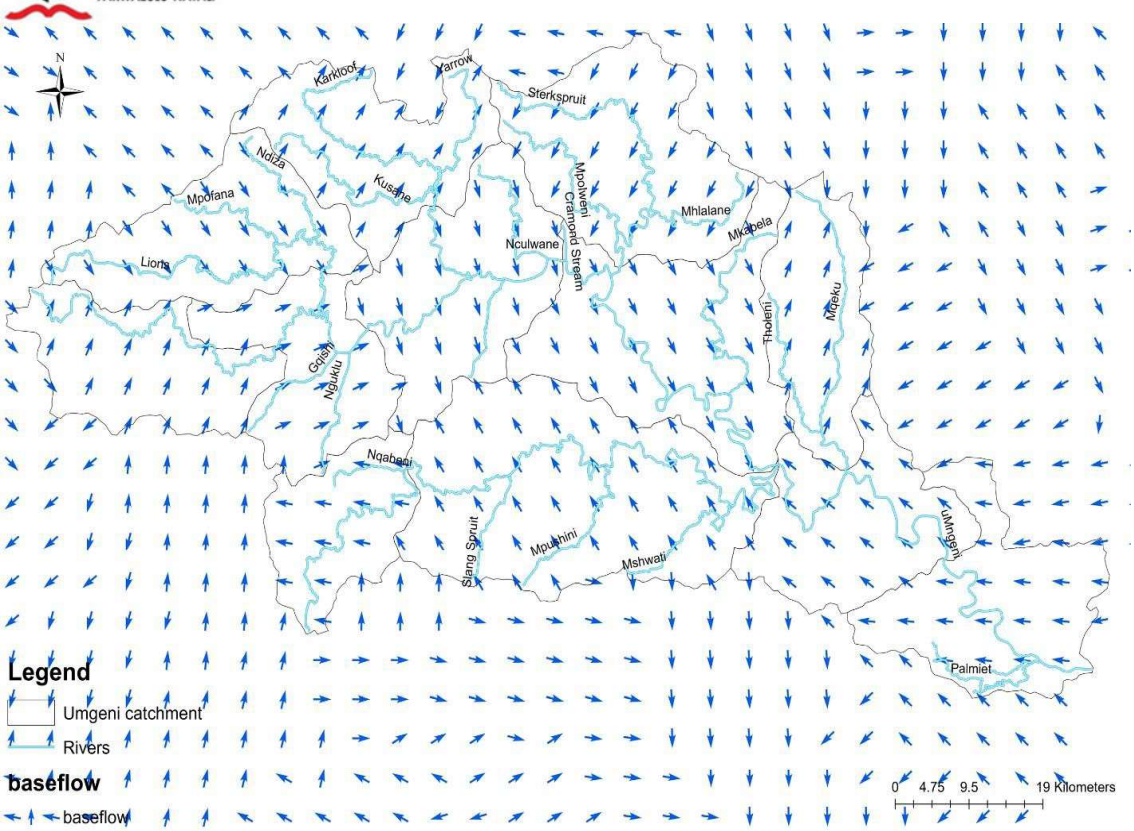

Figure 3.5 Baseflow direction, the angle represents where baseflow is moving, with each symbol representing a tile of 5 kilometres (Source: Water Resources of South Africa, 2005).

3.2.4 Topography

According to Namugize (2018), the altitude across the Umgeni catchment is estimated to vary from 2013 to 0 meters above sea level (masl), starting from the mountainous or highlands of the catchment in the west to the Indian Ocean in the East. In addition, the **Figure 3.6** shows elevation distribution (2067-0 masl), along with a topographic profile of the Umgeni catchment, illustrating the gradual descent from the river's source in the highlands to its outlet at the Indian Ocean.

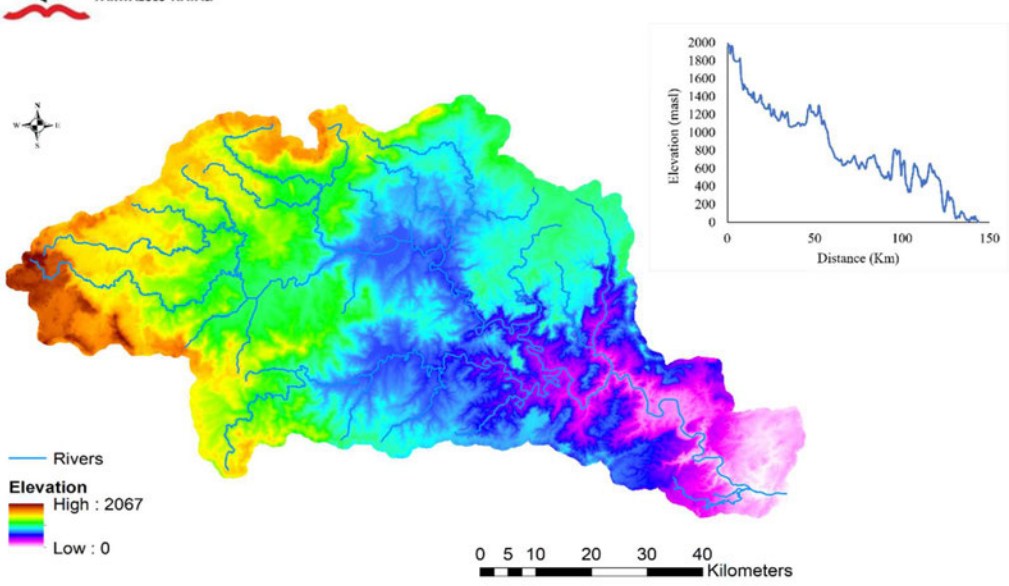

Figure 3.6 Bare ground elevation of the Umgeni catchment and Topographic map of the Umgeni River Catchment, Elevation (masl) vs. Distance (km) (Source: SRTM_90).

3.2.5 Land cover and land use

The Umgeni River transits through various eco-regions, including mountains, savannah, the valley bushveld, sandy lowland, and coastal mangroves (Dickens, 2002). The catchment is dominated by urban and rural settlements, agriculture, forestry, grasslands and natural vegetation (Karar *et al.*, 1999; Kusangaya *et al.*, 2016). A study by Moodley et al. (2023) highlighted stable spatial land use and land cover patterns between 1990 and 2018. The upper reaches are dominated by cultivated land, forestry, and grassland, while the middle and lower reaches are primarily urbanized, with vegetation classes interspersed. Additionally, the WRC (2002) report noted a decrease in grasslands, replaced by indigenous trees and shrub thornveld in rural areas like the Valley of a Thousand Hills. Thus, grasslands also declined due to agricultural and urban expansion, while indigenous forests, wetlands, and degraded areas showed minimal changes. Thus, the **Figure 3.7** shows LULC distribution of the Umgeni catchment.

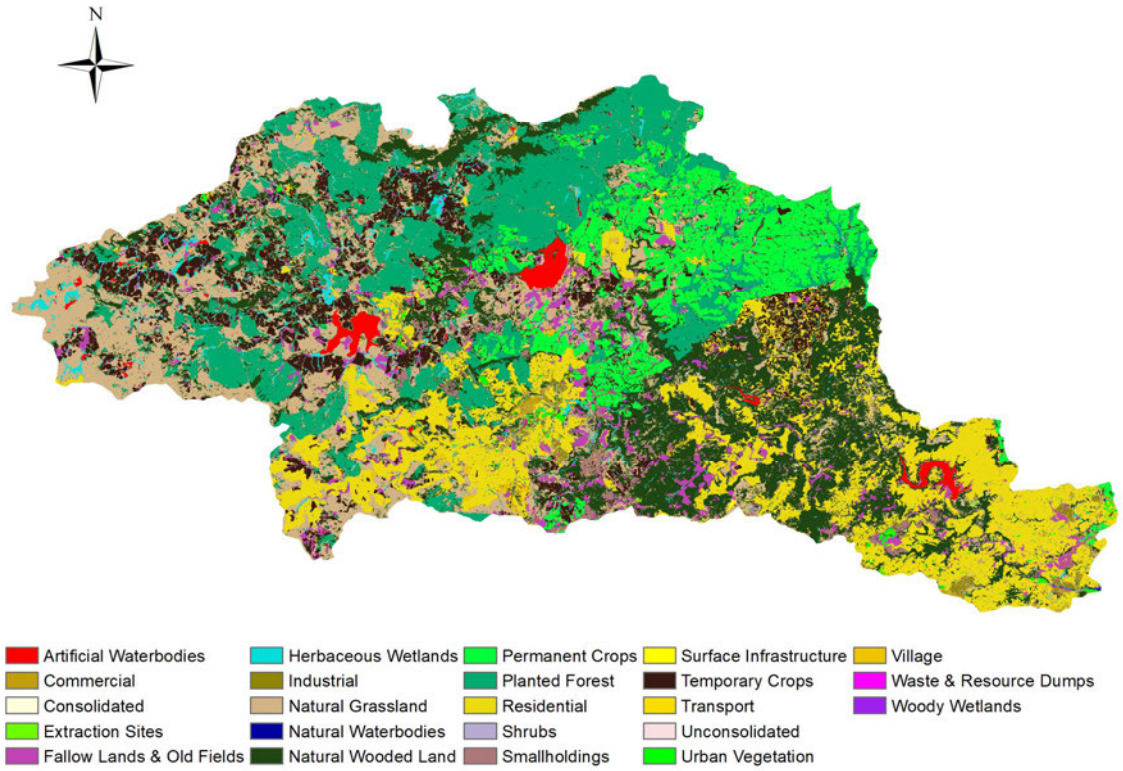

Figure 3.7 Various land uses in the Umgeni River catchment (Source: SANLC 2018).

The Umgeni River has four cardinal tributaries: the Lions River, the Karkloof River, the Impolweni River, and the Umsunduzi River (Chiluwe, 2014). Four major dams (Midmar, Albert Falls, Nagle and Inanda) are part of engineering-designed systems in the basin regulating the flows (Karar *et al.*, 1999; Lorimer, 2012; Chiluwe, 2014; Kusangaya *et al.*, 2016; Kusangaya *et al.*, 2018). The significant dams supply water to Pietermaritzburg and the city of Durban, and the rest of the farm dams (approximately 300 m) located in the upper to the middle reaches supply water for irrigation (Kusangaya *et al.*, 2016). The dams are used for water supply and leisure, significantly contributing to the country's economy (Kusangaya *et al.*, 2018; Namugize *et al.*, 2018). However, they are likely to be affected by climate change (Kusangaya *et al.*, 2018). Thus, there is increasing pressure on water resources induced by sand extractions in drainages outside protected areas reported in the KwaZulu-Natal province, which may be associated with bank erosions leading to flooding (Tian *et al.*, 2015; Lorentz *et al.*, 2020). The figure (**Figure 3.8**) presents the active and abandoned mines in the Umgeni catchment.

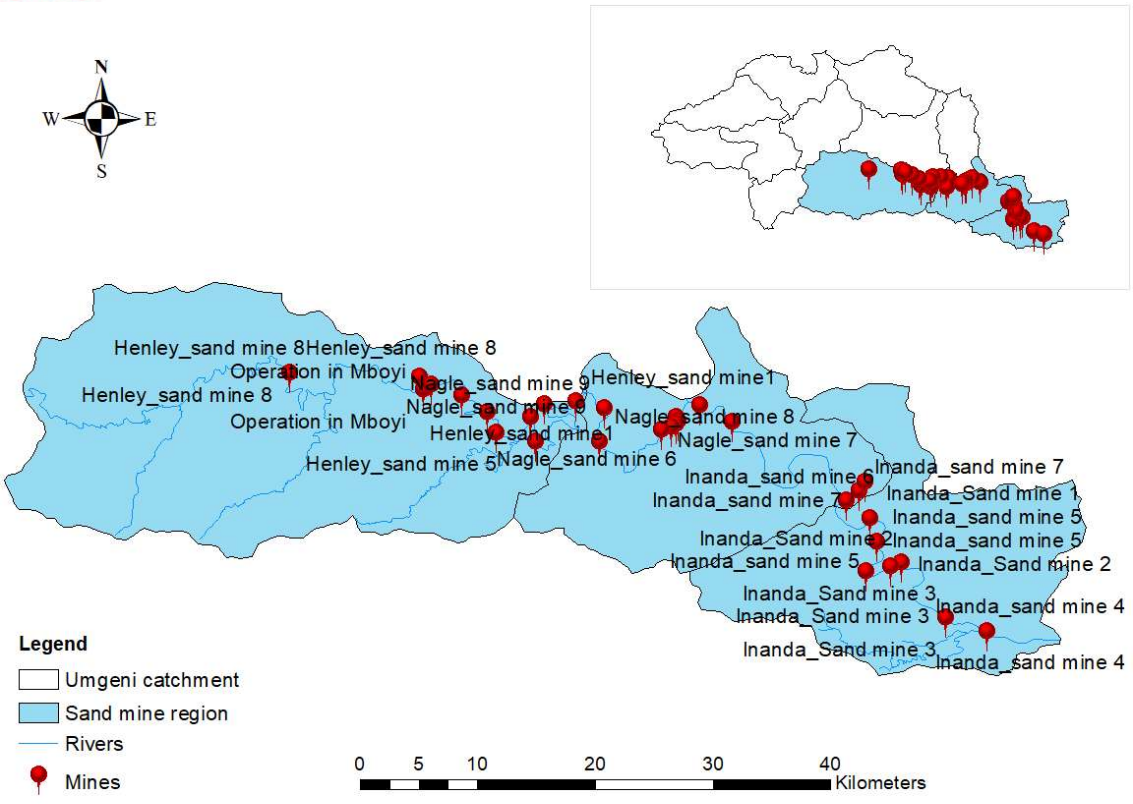

Figure 3.8 Mine locations at the Umgeni Catchment (Umgeni Water).

3.3 Field Sampling

3.3.1 Rainwater sample collection

The collection of rainwater samples began following the successful installation of rainfall samplers. The first sampler was installed in March 2022 on the University of KwaZulu-Natal, Pietermaritzburg campus (30.4027, -29.6278; 680 masl). Rainwater is sampled daily, serving as a point for long-term rainfall monitoring in the study. Continuous sampling ensures a consistent dataset for trend identification and comparative analysis. The station is targeted to assess trends in isotopic signals influenced by rainfall amount, seasonality, and temperature effects. The station is in the middle valleys of the Umgeni catchment, which will allow for an investigation of the influence of elevation on rainfall isotopic comparison with the other stations located in Howick and Durban (**Figure 3.9**).

The second sampler is positioned in the upper reaches of the Umgeni catchment, located within a farm (WestFalia Fruit Farm) in Howick (30.2735, -29.4556; 1000 masl). This station

provides a reference point for monitoring the highland rainfall patterns and isotopic composition. The third sampler is in an airport (Virginia) in Durban (31.055, -29.772, 14 masl). This station is situated at a lower elevation than Howick and Pietermaritzburg. The station's proximity to the sea (Indian Ocean) offers valuable insights into the isotopic rainfall compositions in the catchment's lowland areas. The spatial coverage (~500 masl difference in altitude) is vital for understanding the isotopic variations within the catchment, including altitude and rainfall effects and varying moisture sources.

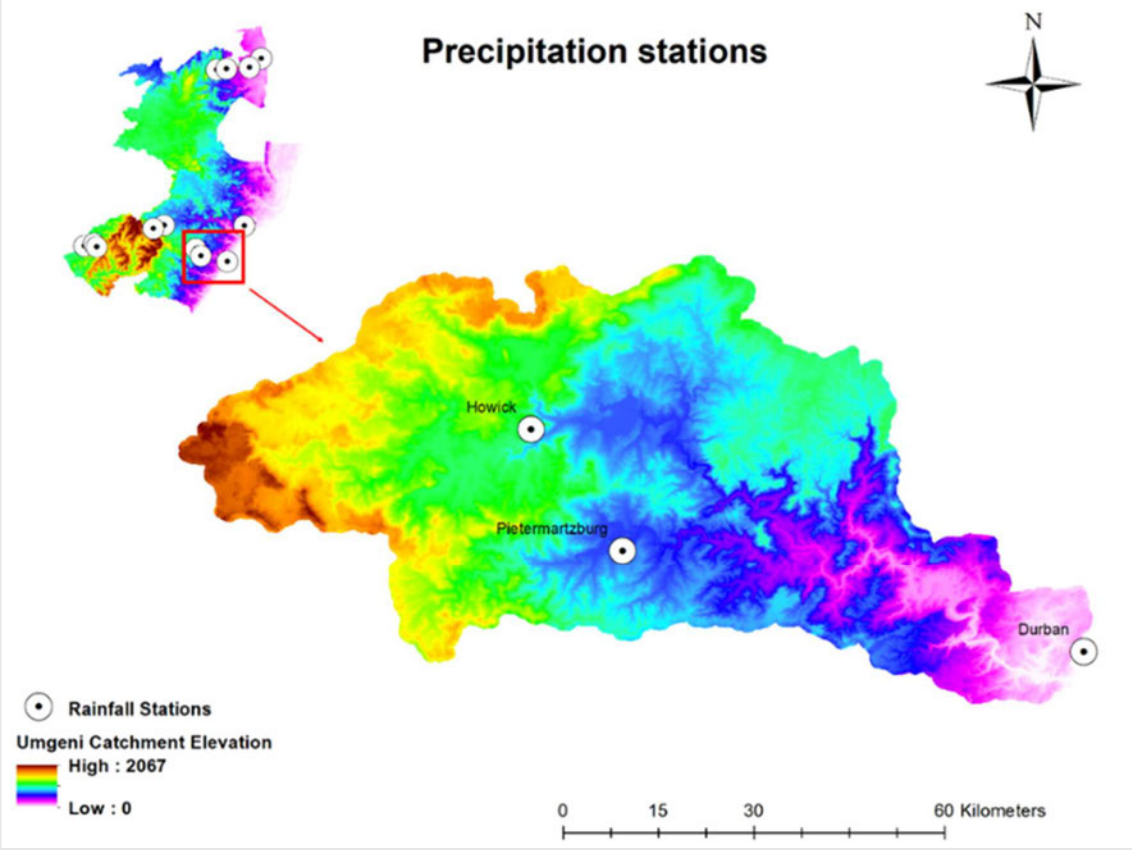

Figure 3.9 Location of Rain Samplers across the Umgeni Catchment.

Rainfall samples were collected using a precipitation water sampler manufactured by PALMEX, Zagreb, Croatia. The sampler is specially designed to minimise any residual evaporation and fractionation. The sampler is feasible for monthly sampling as it avoids re-evaporation and fractionation that can alter the isotopic compositions. The rainfall sampler is placed at approximately 5 m above the ground. The top of the collector has a 23 cm diameter funnel and a metal component to protect against bees or birds. The water is transferred from the funnel through a plastic siphon tube to a 3ℓ plastic water bottle. Each bottle fill is approximately 200 mm (**Figure 3.10**). Consequently, in the event of successive heavy rainfall

occurrences leading to a cumulative collection exceeding 200 mm, the rain collector will reach its capacity, necessitating the immediate collection of the sample before the onset of another rainfall event. A total of 217 rainfall samples from Pietermaritzburg (198), Howick (10) and Durban (9) were collected to be analysed for their isotope compositions (δ^2H-δ^{18}O).

Figure 3.10 Side view of the rainfall station, showing funnel attached to metal protector, plastic siphon tube and plastic bottle.

3.3.2 Groundwater and surface water sampling

The Umgeni, Karkloof, and Lions Rivers were chosen as primary sampling sites to comprehensively represent the highlands, middle valleys and lowlands within the Umgeni Catchment. These rivers were selected due to their significance in the catchment's varying features, which have been proven to alter the interconnections between GW and SW. Thus, the sampling sites were strategically located based on accessibility and proximity to the Umgeni, Karkloof, and Lions Rivers.

Various sources were targeted for sample collection to capture all water bodies of the Umgeni Catchment's hydrological system. Rainwater, wetlands, rivers, lakes, springs, and boreholes were sampling points. This diverse selection aimed to account for different sources of meteoric waters and their potential differences in evaporated signals influencing the depletion and enrichment of isotope signals.

The sampling strategy accounted for significant impoundments that could influence the isotope signals. Key impoundments included tributaries, the Midmar Dam, Albert Falls Dam, Nagle Dam, and Inanda Dam. Factors such as sharp turns, changing geology, structures, land uses, and stream geometry were considered when determining sampling sites. The selection

process aimed to cover a range of environmental conditions and influences within the Umgeni Catchment. Field sampling was conducted in the wet (1st February to 30th March) and dry seasons (1st August to 30th September) of 2023. The seasonal approach allowed for assessing variations in water quality and isotopic composition under different hydrological regimes.

Sampling followed a highland-lowland transect along the course of the Umgeni, Karkloof, and Lions Rivers. This transects approach enabled the examination of changes in isotopic composition and environmental characteristics across different elevations and landscapes within the catchment. The locations where samples were taken are represented on the map below (**Figure 3.11**). This map is a visual reference for the spatial distribution of sampling sites across the Umgeni Catchment. The collected samples will undergo thorough analysis to characterise rainfall, surface water, and groundwater isotope signals.

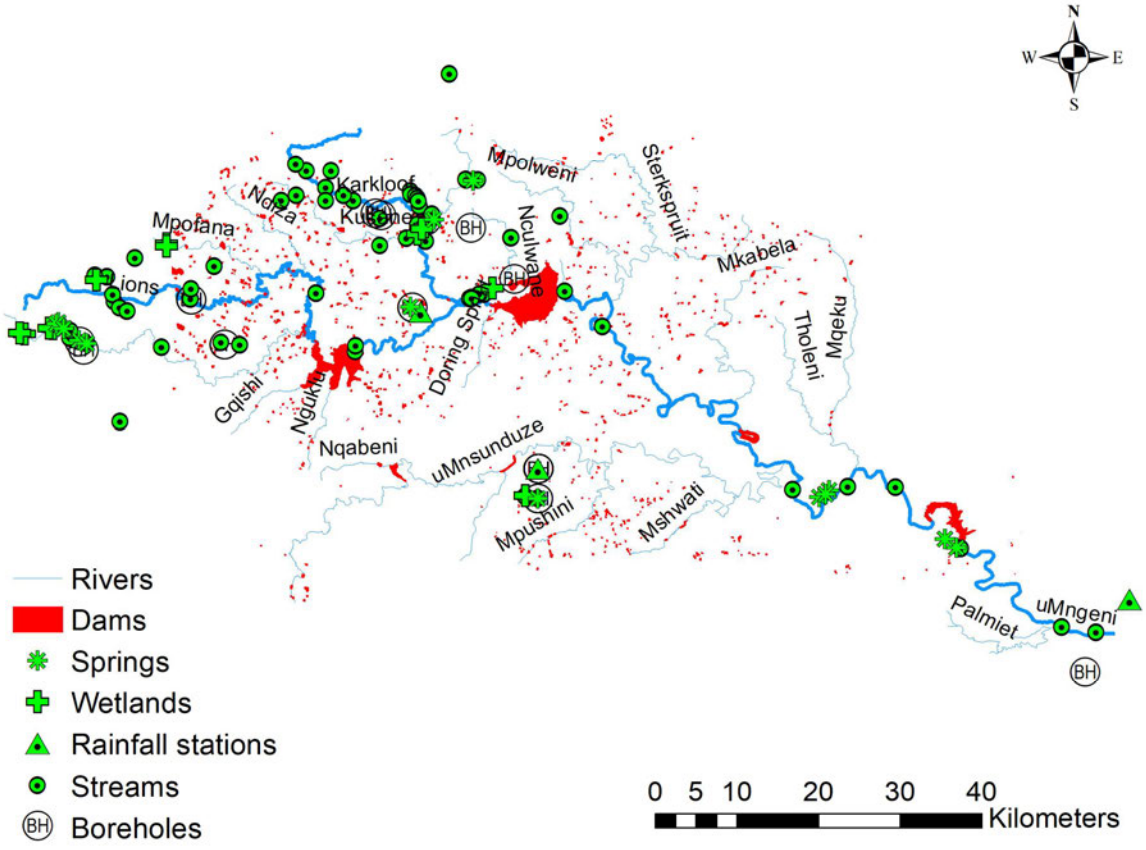

Figure 3.11 Sampled sites in the Umgeni Catchment (rainwater, groundwater, rivers and wetlands).

3.4 Methods

3.4.1 Hydrochemistry

The *in-situ* temperature, pH and EC measurements were conducted in rainfalls, surface waters and groundwater. Temperature measurements were essential for radon conversions, providing insights into groundwater discharge. The pH measurements, initially collected to assess the acidity or alkalinity of the water and complement the hydrochemical analysis, were no longer used in the analysis. EC measurements, on the other hand, were utilized to classify the salinity levels of the streams and groundwater, helping to assess the overall water quality and identify any potential influences from saltwater intrusion or contamination.

The measurements were performed using a Waterproof Conductivity Meter (HI-98129 and HI-98130 models) manufactured by Hanna Instruments based in the United States. The conductivity meter was calibrated using solutions with known conductivity values before starting the measurements. Conductivity meters were checked to be clean and free from debris or residues in preparation for testing. The boreholes were allowed to flow for at least five minutes before collecting the sample to ensure that the sample reflected the deeper groundwater. The measurements were conducted by directly immersing the conductivity meter in the water (river, spring or borehole), or where not possible, the measurements were conducted through a beaker, as shown in the figure below (**Figure 3.12**). A few seconds to a minute would be taken to allow the reading to stabilise, and records were made from the meter display, taking caution of the units to be in micro siemens per centimetre (µS/cm).

Figure 3.12 Measurements of the hydrochemistry parameters (EC, temperature and pH) using the Waterproof Portable Meter. (a) immersed directly into a stream, (b) immersed in a beaker.

3.4.2 Stable isotopes

A survey of the two principal isotopes of water molecules (Oxygen-18 (^{18}O) and deuterium (^{2}H)) was conducted for all samples collected (rainfall, groundwater and surface waters). The water samples were collected directly from the source using 15 ml conical centrifuge plastic test tubes equipped with screw caps manufactured by Ackers, Inc. The bailer was used when the stream was observed unsafe for collecting by hand. The vials were kept clean and dry before sample collection to avoid contamination. The bailer would be rinsed three times before collecting to avoid alterations from previous samples. Following the successful collection of the sample, the vials were labelled with different codes (location and date) to facilitate proper documentation and tracking.

To ensure the reliability of the isotope samples, special care was taken to avoid head space in the bottles during collection. Therefore, bottles were completely filled to eliminate any air gaps. All collected samples were stored at cool temperatures in the laboratory (Hydrology Isotope Lab at the University of KwaZulu-Natal, Pietermaritzburg). The samples were stored at a cool temperature to minimise isotopic fractionation for approximately 4-10 weeks before the ^{2}H and ^{18}O isotope ratios were analysed.

In preparation for the analysis, the samples were filtered using different laboratory equipment such as syringes (5 ml), vials (12x32 mm) with sample vial septa and filter units (0.45 µm),

all shown in the figure below (**Figure 3.13**). The filtering process was conducted to prevent damage to sensitive instrument components such as the (Lot Gatos Syringe) and ensure no decline in the instrument performance (precision and accuracy). The samples were transferred from the vials to the syringe, ensuring that air bubbles were minimised. The syringe was connected to the filter unit and inserted into the new vial, slowly pushing the syringe's plunger to pass water through the filter. Once filtered, the samples were loaded into the sample tray according to the Laboratory Information Management System (LIMS) layout sequence and analysed within 24 hours.

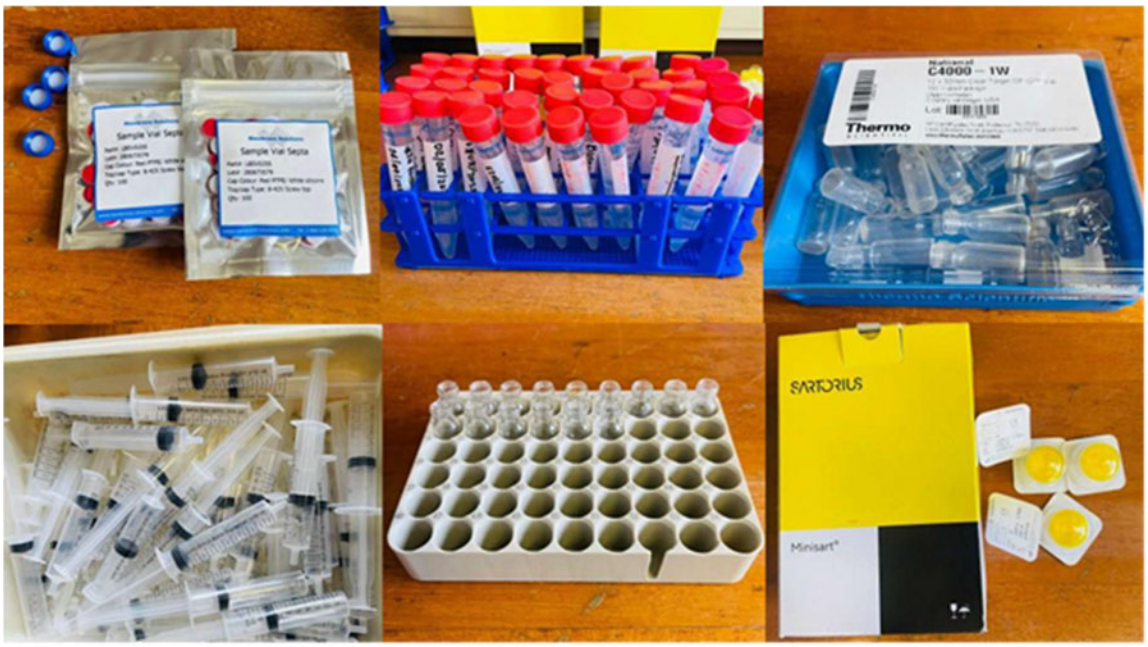

Figure 3.13 Apparatuses used to collect and filter samples in preparation for ^{2}H and ^{18}O analysis.

3.4.3 Radon

The Big Bottle System, fitted with a RAD7 detector meter, was used for radon measurements. The measurements followed the sampling protocol detailed in the Durrige manual (Durrige Company Inc., 2020). The Big Bottle system employs a closed-loop aeration scheme, as shown in the figure below (**Figure 3.14**). The system allows air to flow and recirculate through the water, extracting more radon until equilibrium. The air and water volumes are constant and independent of the flow rate for the Big Bottle system. However, the extraction efficiency of radon from the water sample is temperature-dependent. The RAD7 detector meter must be free of radon and dry before making a new measurement. The RAD7

instrument is dried by purging it with dry air for approximately 15 minutes. During this process, the relative humidity inside the RAD7 must be reduced to less than 10%. If the relative humidity does not reach this threshold after 15 minutes of purging, the process is continued until the desired humidity level is achieved. The Big Bottle System has lower detection limit of 1 picocuries per litre (pCi/L) or 40 becquerel per cubic metres (Bq/m^3) and the upper limit is 10 000 pCi/L (400 000 Bq/m^3) for radon in water.

Radon measurements were undertaken across various surface water bodies, springs, and boreholes in the Umgeni Catchment. The choice of sampling sites was based on accessibility. Sites where water can be directly collected from the source were preferred. All the samples collected were ensured to be not from water tanks or collected before reaching treatment processes. In the case of boreholes, the water was run for 5-10 minutes before being collected to ensure the sample came from the deep part of the source. The samples were collected by lowering the empty 2.5 ℓ glass bottle to a depth that allows water to flow, displacing air. The cap was placed while relocating, and a few mL of water was discarded to create space for air circulation. In this study, each aeration cycle was set to 15 minutes and conducted over one hour in four cycles since the system needs aeration for more than 10 minutes to reach equilibrium. On-site, the water temperature was measured to convert radon in the air to radon in water.

Figure 3.14 The Big Bottle System connected to the RAD7 detector meter.

3.5 Data Processing and Analysis

The maps showing the composition and structure of the soils of the surface water and the groundwaters were created using ArcMap (GIS) version 10.6. The maps present the geology, topography, fractures, LULC, stream nature, and geomorphology across the Umgeni Catchment. Following the survey and sampling program of the Umgeni catchment, the *in-situ* measurements of temperature and EC were recorded and analysed using Microsoft Excel.

3.5.1 Stable isotopes (^{2}H and ^{18}O)

Stable isotope ratios of H ($^{2}H/^{1}H$) and O ($^{18}O/^{16}O$) were analysed at the University of KwaZulu-Natal (Pietermaritzburg campus) using the liquid water series analyser (LGR-ICOS GLA431) coupled with the autoinjector (ABB-PAL3 LSI) shown in **Figure 3.15**. The GLA431 isotope analyser utilises a cavity ring-down spectroscopy technique to measure isotopic compositions with high sensitivity and precision. The analyser has an internal computer controlling the number of injection cycles and stores the results for post-analysis.

A total of 400 samples were analysed (220 rainwater samples, 18 springs, 105 streams and 15 wetlands and 43 boreholes). Each sample underwent nine analytical sessions or injections to represent the sample better. The machine produces results within the accuracy of approximately 0.2‰ ($\delta^{18}O$) and 2‰ ($\delta^{2}H$) in samples. Where fluxes were observed, reruns were conducted. The $\delta^{18}O$ to $\delta^{2}H$ results were calculated using the delta (δ) notation and reported in per mill (‰). The δ is calculated as the relative deviation of a given sample with respect to a standard value. The first standard was the Vienna-Standard Mean Ocean Water (Vsmow). The second standard was tap water (Midmar water) enclosed in a sealed tank to preserve its composition. The third standard was the mixture of the two.

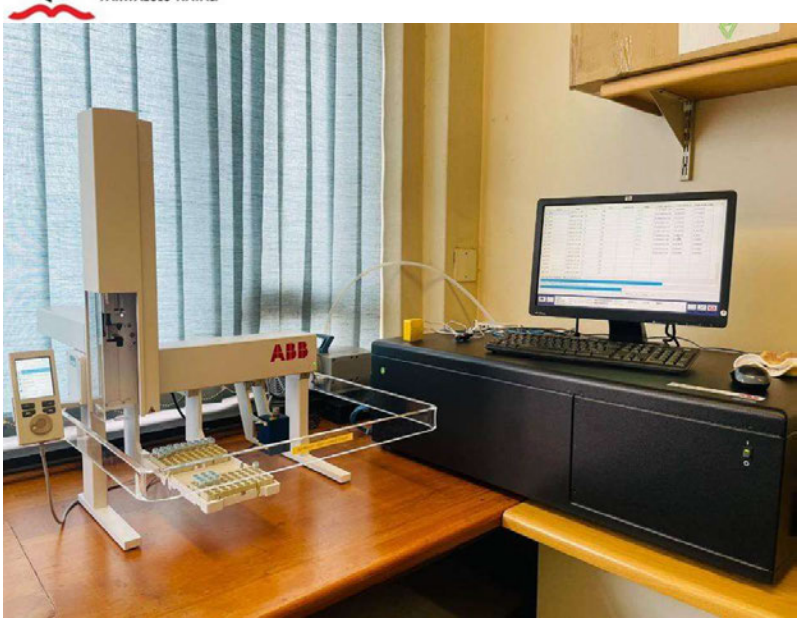

Figure 3.15 Liquid water isotope analyser GLA431.

3.5.2 Radioactive isotope (^{222}Rn)

DURRIDGE provides a freely accessible software utility for Windows called CAPTURE, which can be used to download RAD7 data, graph and analyse, perform real-time RAD7 monitoring, and store data on a cloud-based internet server. The RAD7 was connected to a computer through a StarTech USB to serial adaptor cable to download the device's data. Once data has been downloaded and saved, the CAPTURE software displays all the data. Graphs can be displayed, allowing the selection of the data points within a specific range. Out of the four radon cycles, the first one was discarded and the average of the remaining readings was taken as the mean radon concentration of that specific site. The temperature recorded on site was used to convert air radon to water.

3.5.3 Baseflow separation

The BFI was calculated using river discharge data downloaded from the Department of Water and Sanitation (DWS) page: https://www.dws.gov.za/. The twelve drainage regions (U20A, U20B, U20C, U20D, U20E, U20F, U20G, U20H, U20J, U20K, U20L and U20M) of the Umgeni catchment had 23 river stations identified. The locations of the river stations in the Umgeni catchment are shown in the map below (**Figure 3.16**). The additional data is in the appendices (**Appendix C: Baseflow Separation**)

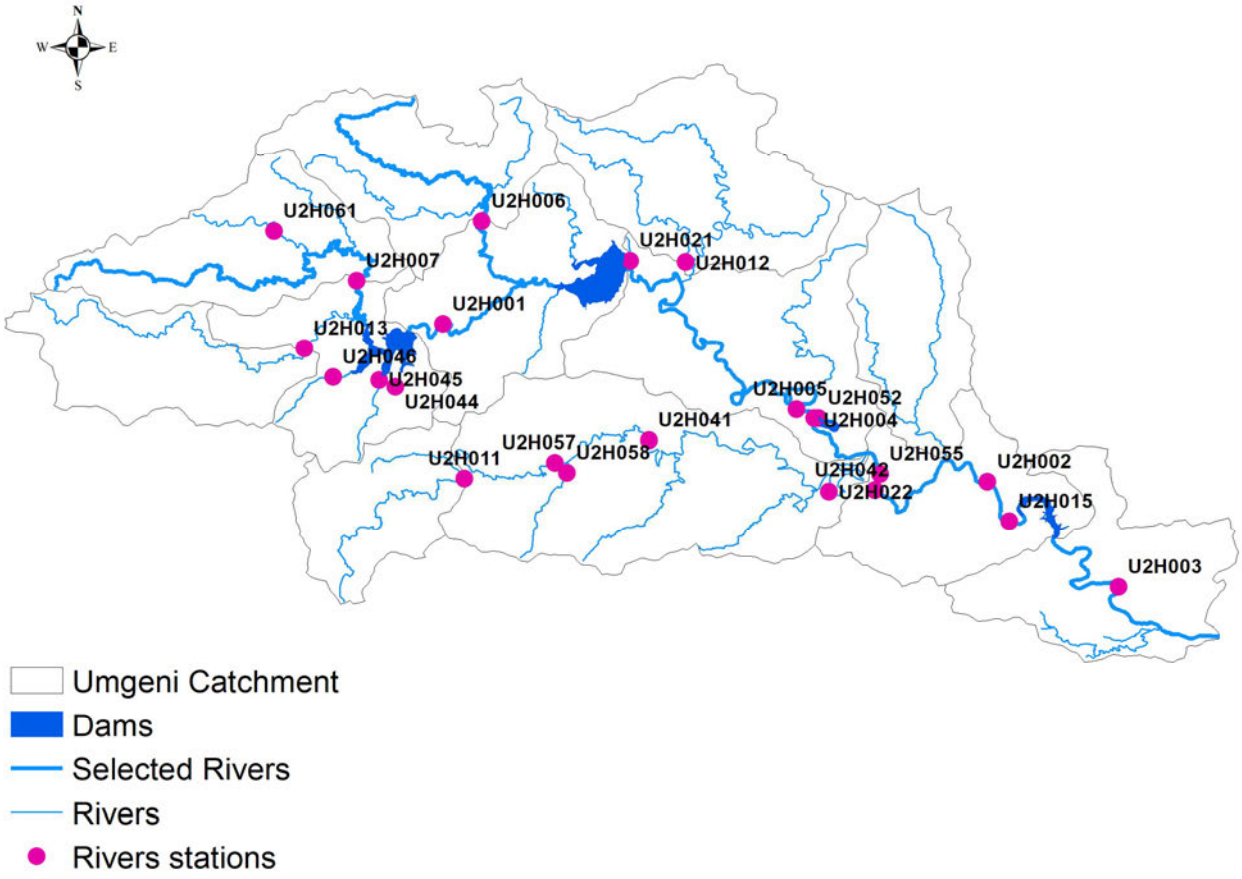

Figure 3.16 Location of river stations in the Umgeni Catchment.

The BFI+ 3.0 of HydroOffice 2010 software (developed by Milos Gregor) was used to analyse and separate baseflow for the total river discharge of Umgeni Catchment. The BFI+ generated the baseflow indexes using the local minimum method. The local minimum approach examines each day to determine discharge within a specified range; the lowest discharge is one-half the interval minus one day [0.5(2N*-1) days] before and after the day is being considered. The local minimum method requires two parameters N and F. The parameter N is calculated using the formula ($N = A^{0.2}$), where A represents the area of the region being considered and F is a constant factor, typically set to 0.9.

3.5.4 Piezometry

The piezometer approach provides point measurements of the hydraulic heads (Kalbus *et al.*, 2006). Piezometers are quick and easy to install, however, this study used pre-existing data on groundwater level changes over the years (2015 to 2023). The groundwater levels were represented using freely available hydraulic head measurements on nine boreholes that were

downloaded from the National Groundwater Archive (NGA) of South Africa page. The figure (**Figure 3.17**) presents the borehole sites located in the Umgeni Catchment.

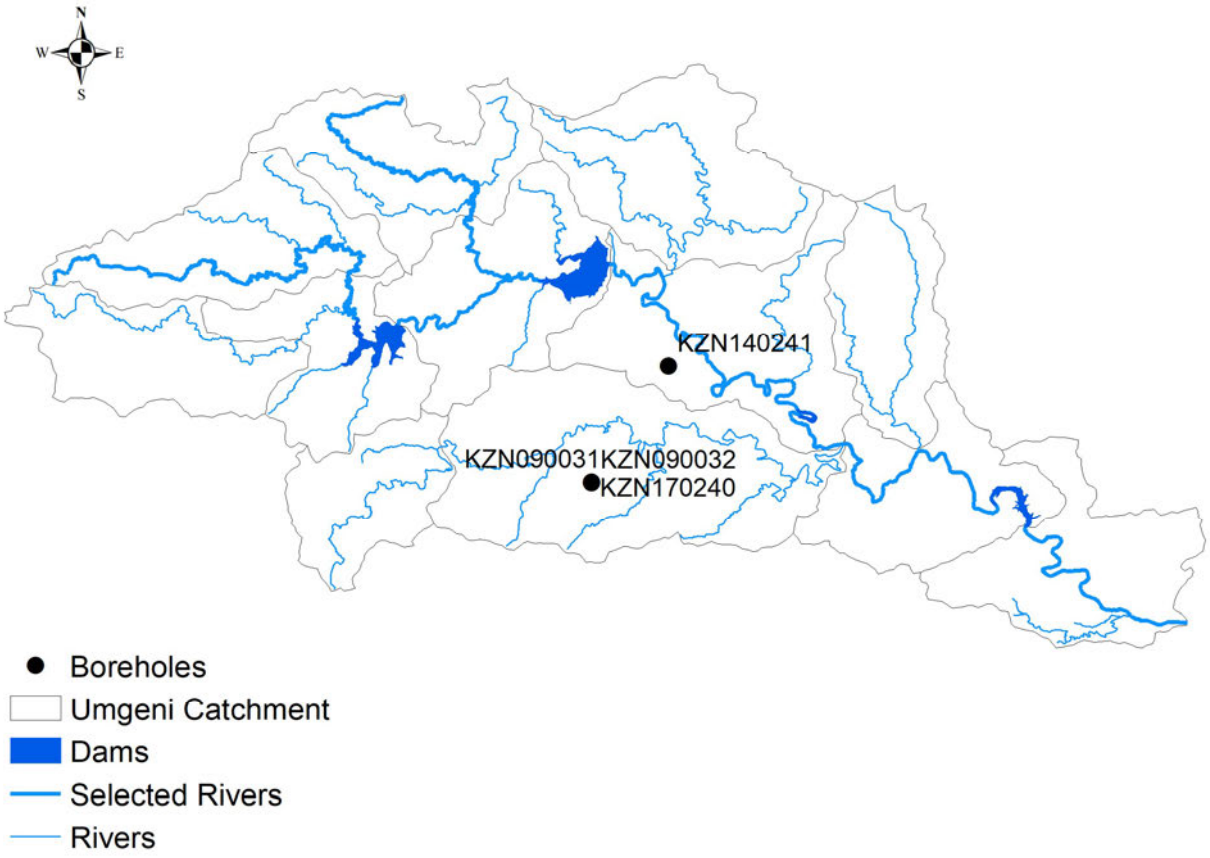

Figure 3.17 Borehole locations in the Umgeni Catchment.

4. RESULTS

4.1 Introduction

This chapter reports the study's findings, starting by characterising the composition of rainfall isotopes. The rainfall signals are presented on three bases: the d-excess, Pietermaritzburg Local Meteoric Water Line (PtLMWL), and the isotope effects. The following component is characterising the isotope signals of groundwater and surface waters. The ^{222}Rn concentrations in the different parts of the catchment are explained with a major focus on detecting sites of groundwater connection to surface waters and geologic control on ^{222}Rn in groundwaters. The last component presents the results of EC, water levels and baseflow separation assessment.

4.2 Rainfall Isotope Signals

A comprehensive analysis of the two-year records of rainfall isotope across Umgeni Catchment was conducted to aid in understanding groundwater recharge mechanisms and determine sources of moisture responsible for rainfall events. In addition, we examined the effects of precipitation amounts and altitude on the rainfall isotopes compositions in the catchment.

The table (**Table 8.1**) presents the daily rainfall collected in Pietermaritzburg between March 2022 and January 2024. The daily rainfall ranged from 0.3 to 107 mm. The δ^2H and $\delta^{18}O$ ranged from −90.9‰ to +36.7‰ and −13.11‰ to +4.36‰, respectively in Pietermaritzburg. The rainfall amount weighted mean was calculated to be -3.21‰ for $\delta^{18}O$ and -9.12‰ for δ^2H.

In Howick, the monthly rainfall ranged from 12 to 237 mm. The **Table *8.2*** shows the isotopic composition of precipitation collected from Howick (February 2023 to January 2024) ranging from −7.34‰ to +7.75‰ ($\delta^{18}O$) and −47.3‰ to +43.3‰ (δ^2H). The amount weighted mean was calculated to be -3.31‰ ($\delta^{18}O$) and -11.80‰ (δ^2H).

In Durban, the monthly rainfall ranges from 20 to 288 mm. The **Table *8.3*** shows the isotopic composition of precipitation collected from Durban (March 2023 to January 2024). The isotope signatures ranged from −5.7‰ to +0.76‰ ($\delta^{18}O$) and −35.5‰ to +14.1‰ (δ^2H). The weighted mean average was calculated to be -3.01‰ ($\delta^{18}O$) and - 53 9.33‰ (δ^2H).

4.2.1 D-excess

The d-excess values provide insight into the humidity and evaporation process of the source of moisture. Previous studies have linked high d-excess with low humidity and high evaporation conditions (Diamond, 2022). The d-excess values were calculated as follows:

$D = \delta^2H - 8* \delta^{18}O$

The d-excess was calculated for all collected rainfall samples (n = 217). At Pietermaritzburg, the d-excess values ranged between −5.38‰ and 27.7‰. For Howick, d-excess values ranged from −18.7‰ to 27.5‰, while values between 8.02‰ to 20.8‰ were found in Durban. The results indicate variations in humidity conditions and evaporation processes at different locations. Despite these variations, there was no significant difference in the d-excess values among the stations, suggesting that other factors could overshadow the isotopic fractionation along the trajectory (West *et al.*, 2014).

4.2.2 Pietermaritzburg local meteoric water line (PtLMWL)

The LMWL is a linear relationship derived from the correlation of δ^2H-$\delta^{18}O$ over a period of time. The daily stable water isotopes (δ^2H-$\delta^{18}O$) compositions rainfall from Pietermaritzburg (PMB) was used to construct the LMWL and is compared against the GMWL: $\delta^2H = 8*\delta^{18}O + 10$. Unlike the GMWL, the LMWL reflects the local weather conditions, including the sources of atmospheric moisture. The least square regression line representing the PtLMWL was $\delta^2H = 7.37 * \delta^{18}O + 14.3$ (**Error! Reference source not found.**). The PtLMWL lies above the GMWL with a slope (7.37), slightly close to the GMWL (8) (Craig, 1961). The d-intercept (14.3) was higher for the PtLMWL than the GMWL (10.8). This indicates the contribution of land surface re-evaporated moisture to rainfall.

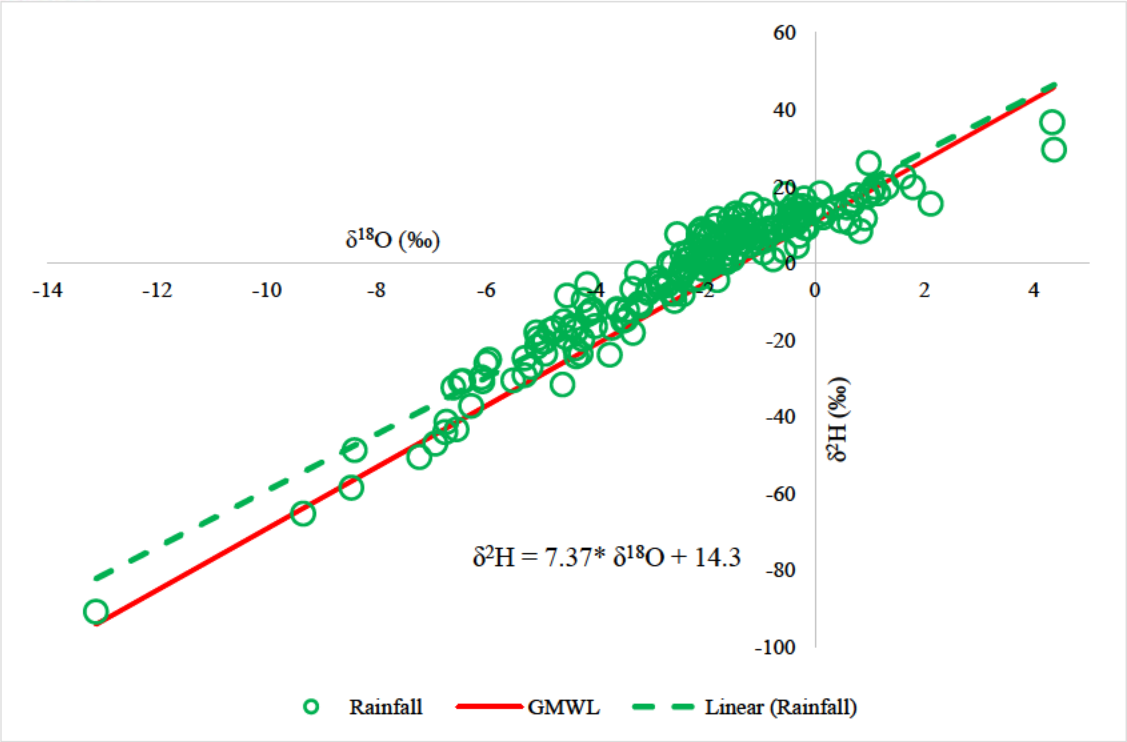

Figure 4.1 Distribution of daily rainfall isotope composition (δ^2H-$\delta^{18}O$) in Pietermaritzburg, the established Umgeni Local Meteoric Water Line (ULMWL) plotted and the Global Meteoric Water Line (GMWL).

4.2.3 Wet and dry season LMWL's

There is expected seasonal variation in isotope signatures of precipitation of the catchment as the winter months (April to September) are colder and dominated by drizzles compared to the wet season (October to March) (Miller *et al.*, 2017). In this study, rainfall data was divided into the summer/wet season and the winter/dry season to examine the seasonal effect (**Error! Reference source not found.**). The established LMWLs for winter and summer were $\delta^2H = 7.46\ \delta^{18}O + 15.9$ and $\delta^2H = 7.48\ \delta^{18}O + 13.7$, respectively. Previous studies have highlighted that there can be differences between the diffusion fractionation factors for ^2H-^1H and ^{18}O - ^{16}O. This was shown by the slopes having a negligible difference of 0.02, whereas the d-excess of the winter LMWL (15.9) was higher than that of the summer (13.7). Basically, the slope is the ratio between the equilibrium isotope fractionations of hydrogen and oxygen for the rain condensation process (Diamond, 2022). Notably, the slope comes closer to equilibrium in the summer due to slightly increasing humidity and less fractionation (8).

The intercept on the δ^2H axis of the LMWL/GMWL is known as the d-excess. The d-excess is an indicator of the source, with highly humid sources generating low d-excess. This is evident by the winter's higher d-excess, indicating that the moisture source has lower humidity. Generally, Pietermaritzburg shows a good correlation between d-excess and rainfall season compared to other regions in South Africa, such as Pretoria (Abiye, 2011) and Cape Town (Harris *et al.*, 2010).

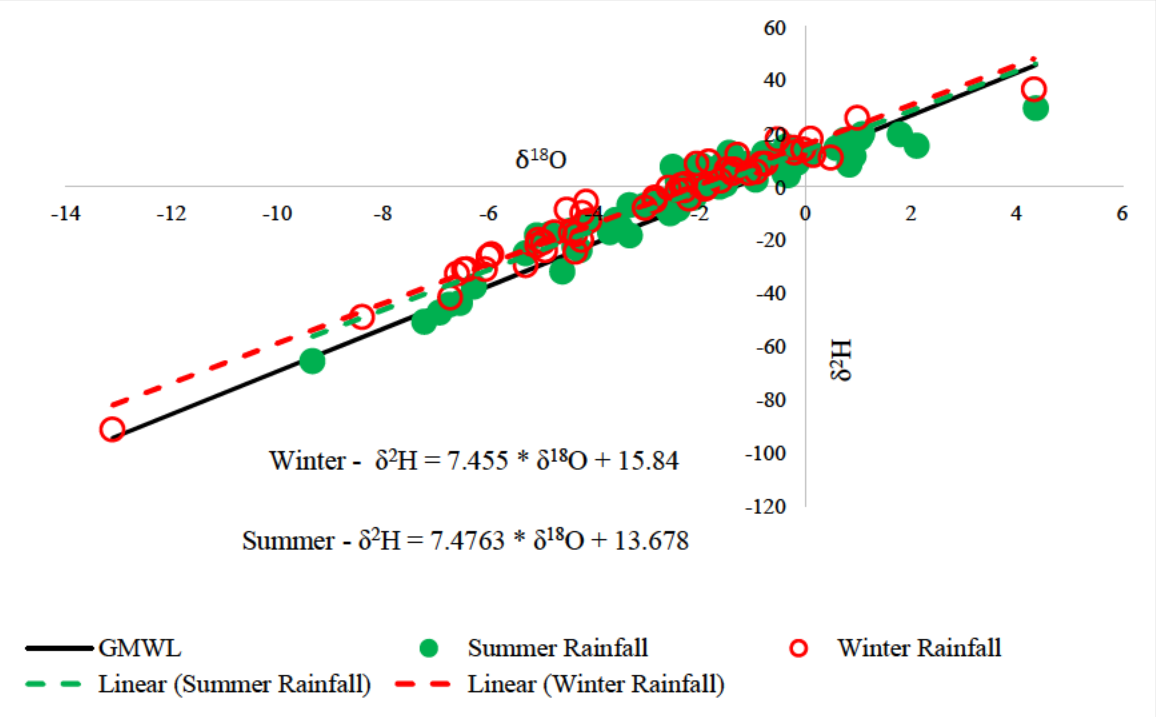

Figure 4.2 Pietermaritzburg dry and wet season LWMLs.

4.2.4 Comparison with other South African LMWLs

The PtLMWL ($\delta^2H = 7.37 * \delta^{18}O + 14.3$) was compared to the GMWL ($\delta^2H = 8*\delta^{18}O + 10$; Craig., 1961) and Africa Local Meteoric Water Line (ALMWL: $\delta^2H = 7.4 * \delta^{18}O + 10.1$; Cohen et al., 1997) shown in **Error! Reference source not found.**. The PtLMWL shows a slope similar to the ALMWL (7.4) and close to the GMWL (8). The slope suggests that the raindrops occur in equilibrium conditions. The slope of the LMWL is a function of the relative humidity of the source, with regions under low relative humidity plotting further left of the GMWL (Diamond, 2022). In comparison of the PtLMWL with other studies in South Africa, such as the Cape Town Local Meteoric Water Line (CLMWL: $\delta^2H = 6.8 * \delta^{18}O +$ 10.5; Harris et al., 1999), Pretoria Local Meteoric Water Line (PLMWL: $\delta^2H = 6.55 * \delta^{18}O +$

7.9; Abiye et al., 2011) and Thohoyandou Local Meteoric Water Line (TLMWL: $\delta^2H = 7.56 * \delta^{18}O + 10.64$; Durowoju et al., 2019), the local slopes were found to be slightly different.

The d-excess was found to be significantly high in the PtLMWL. The different d-excess values result from varying humidity levels in moisture sources during evaporation, which creates moisture masses. Notably, the higher d-excess in PtLMWL than the rest of the LMWLs suggests high local moisture recycling.

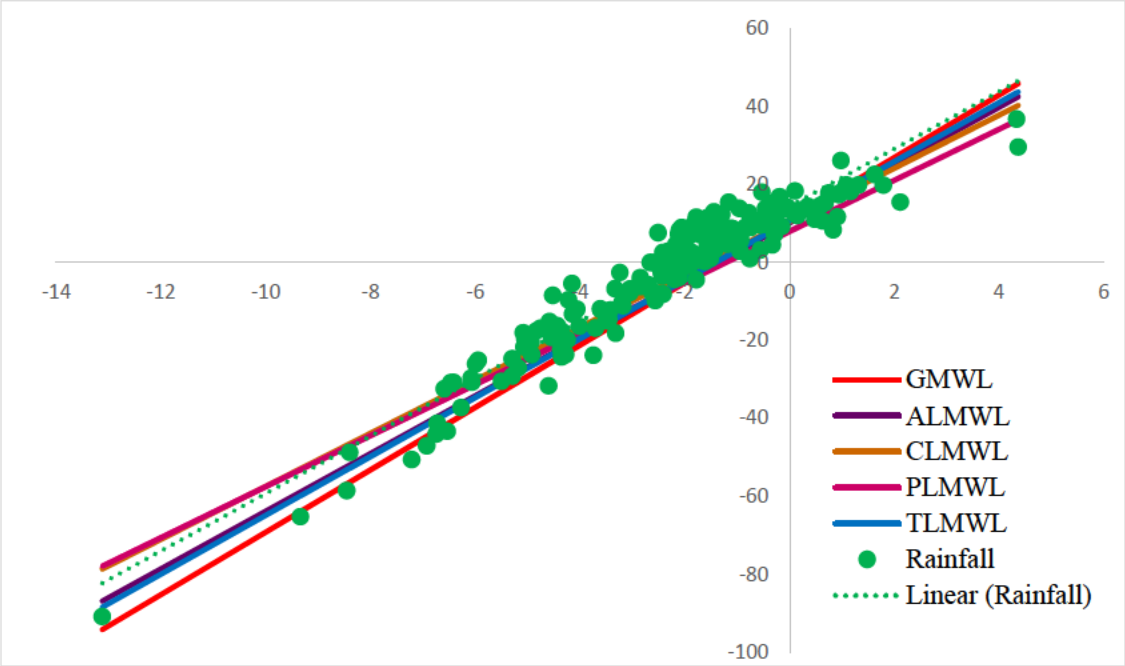

Figure 4.3 Different LMWLs including PtLMWL, GMWL, ALMWL, CLMWL, PLMWL and TLMWL.

4.3 Isotope Effects

4.3.1 Amount effect

Several processes that occur during transportation and precipitation influence the isotopic composition of rainfall, such as moisture source conditions, the distance between sources and sinks, the seasonality and the amount of rainfall. Heavy rainfalls tend to remove more vapor and cloud droplets in the air, resulting in increased rainfall amounts that are more isotopically depleted. The effect of rainfall amount was assessed by plotting rainfall (mm) against δ^2H-$\delta^{18}O$ for the Pietermaritzburg station. The δ^2H-$\delta^{18}O$ of rainfall was plotted with the size of each data point corresponding to the rainfall amount (**Error! Reference source not found.**).

The rainfall amount effect was observed in Pietermaritzburg, shown by the shift to a more depleted end associated with larger total precipitation amounts, as shown in Error! Reference source not found. and Error! Reference source not found.. The highest rainfall amounts were received on the 5th (point 1) and the 17th (point) of April 2022. The variations in the isotope composition of each rainfall event can be related to the type of event and its duration. The total amount of rainfall events is high, but the intensity and duration of points 1 and 3 may differ. The findings are in line with the global findings where the tropical atmospheric circulation systems have been found to have a good correlation between decreasing isotope composition and increasing rainfall amount (Yang *et al.*, 2011). High rainfall amount effect has also been observed in other summer rainfall regions in South Africa, such as Pretoria and Northen KZN. However, in the winter rainfall regions, the rainfall amount effect was found to be weak due to the low temperatures and high rainfall amount that alter the isotope compositions during winter (Abiye *et al.*, 2013; Braun *et al.*, 2017).

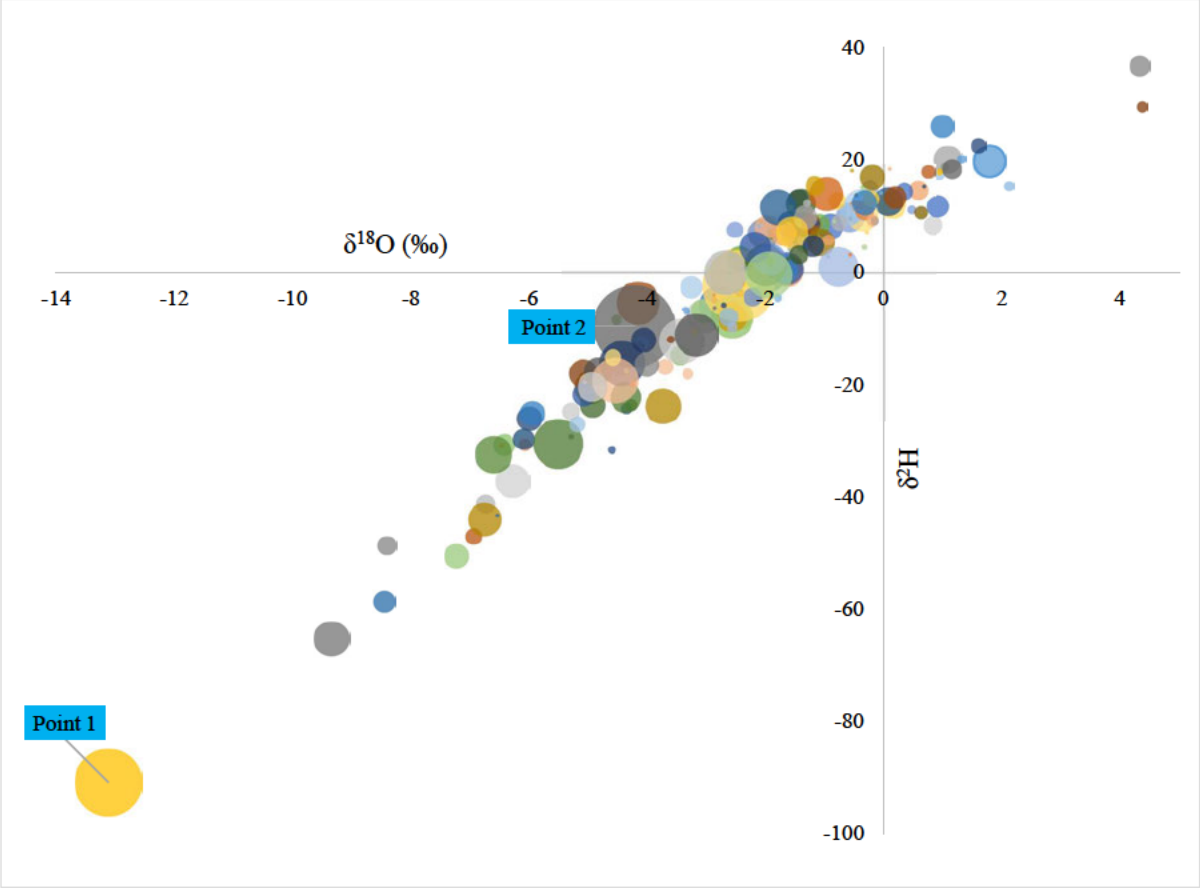

Figure 4.4 δ^2H-$\delta^{18}O$ of rainfall in Pietermaritzburg is plotted with the size of each data point corresponding to the rainfall amount (mm).

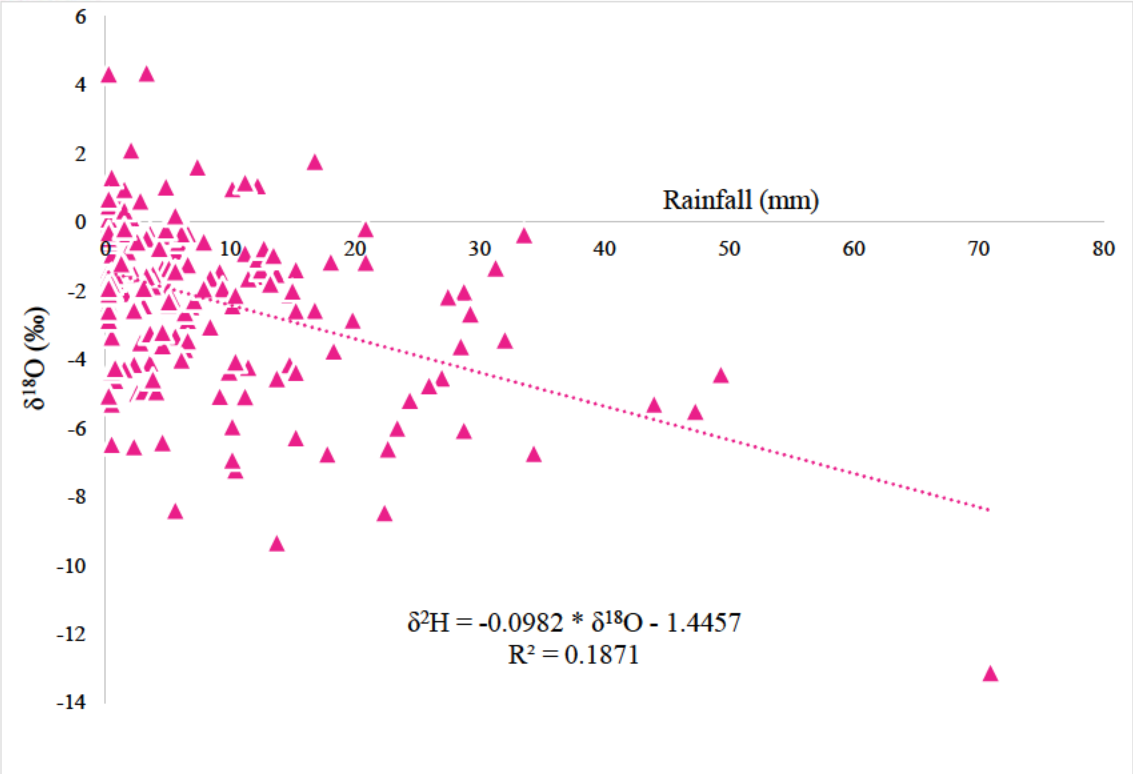

Figure 4.5 Variation of $\delta^{18}O$ with rainfall amount.

4.3.2 Seasonal effect

Rainwater isotope signatures represent the specific local environmental conditions and the processes that influence rain formation, meaning the amount effect is relatively close to rainout. In **Error! Reference source not found.**, the three-year data showed a predominant seasonal effect. Notably, the three most depleted signals were recorded in the wet season months: the 5th of April 2022 (-13.11‰), the 15th of February 2023 (-9.33‰) and the 17th of October 2023 (-8.45‰). The findings from the Pietermaritzburg rainfall indicate a strong seasonal and rainfall amount effect which has been globally observed and well-documented for low-latitude regions (Yang *et al.*, 2011; Diamond, 2022). In South Africa, the arid regions, including Northen KZN have been found to have a good seasonal effect (Abiye *et al.*, 2013)

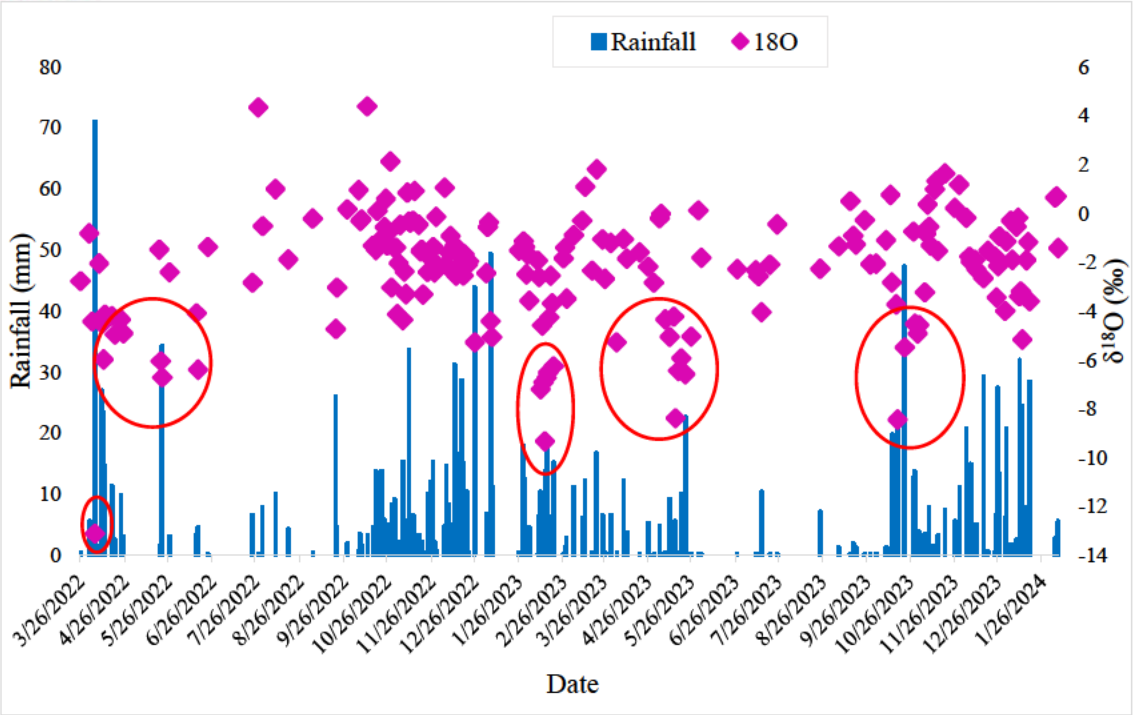

Figure 4.6 Monthly variations (2022 – 2024) in precipitation and of $\delta^{18}O$ with the red circles showing the highly depleted values.

4.3.3 Altitude effect

The altitude effect, driven by orographic lifting and decreasing temperatures at high altitudes, can be examined as the decrease in $\delta^{18}O$ values per 100m of elevation. The altitude effect was examined for the Umgeni Catchment. The weighted mean isotope compositions are presented in **Figure 4.7** moving from Durban (-3.01‰) to Pietermaritzburg (-3.21‰) and Howick (-3.31‰). However, in **Error! Reference source not found.** the gradient change is generally weak (-.0.03‰/100m) compared to the global average reported to be -0.28 by 100m (Poage, 2001; Liu *et al.*, 2024). Globally, the weak altitude effect has been reported to be due to the mixing of multiple moisture sources (Jing *et al.*, 2022).

The stations in the upper catchment fall under different moisture sources moving in different directions that can lead to mixing and high turbulence moving towards the Drakensberg. Therefore, the weak altitude effect can be attributed to the different moisture sources reported in the different parts of the catchment (Ndlovu *et al.*, 2021). Again, a lack of strong temperature lapse rate has been reported in the Northeastern Drakensburg due to the prominent thermal inversions (Grab, 2013). Thus, the complex behavior in the Drakensberg

could be a driving factor behind the weak altitude lapse rate observed in the Umgeni Catchment. In South Africa, Cape Town, Pretoria and Northern KZN were found to have weak altitude effects. However, the case was found to be different for Oxbow and Lesotho (Abiye *et al.*, 2013).

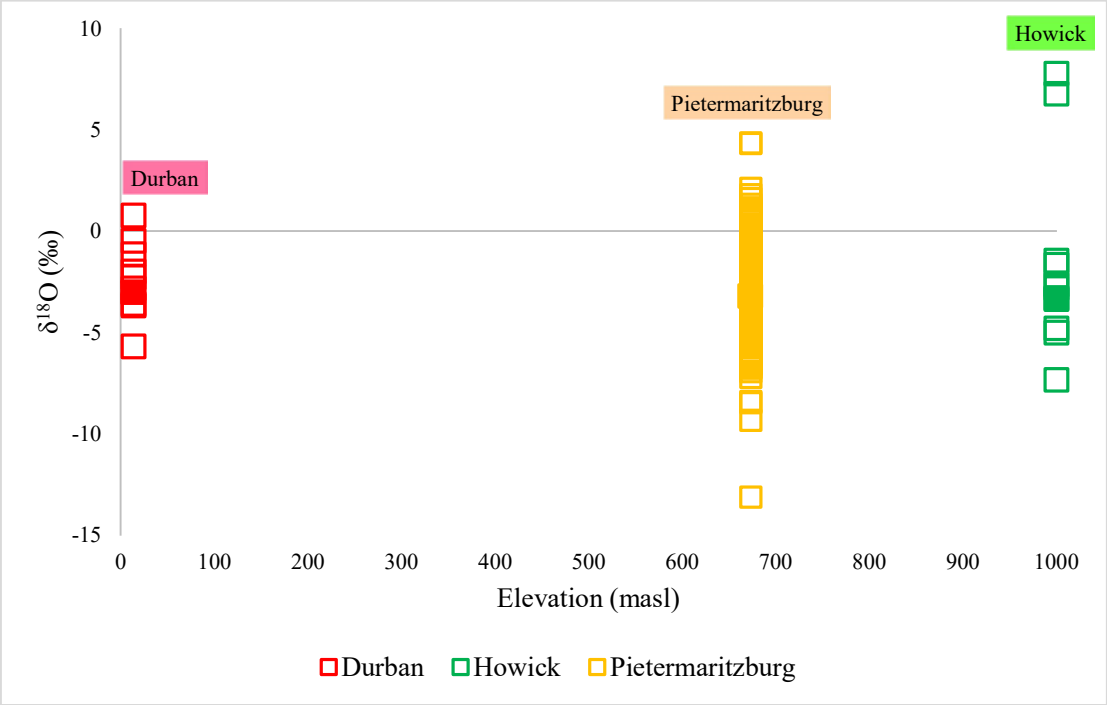

Figure 4.7 Change in $\delta^{18}O$ with increasing elevation (Durban to Howick).

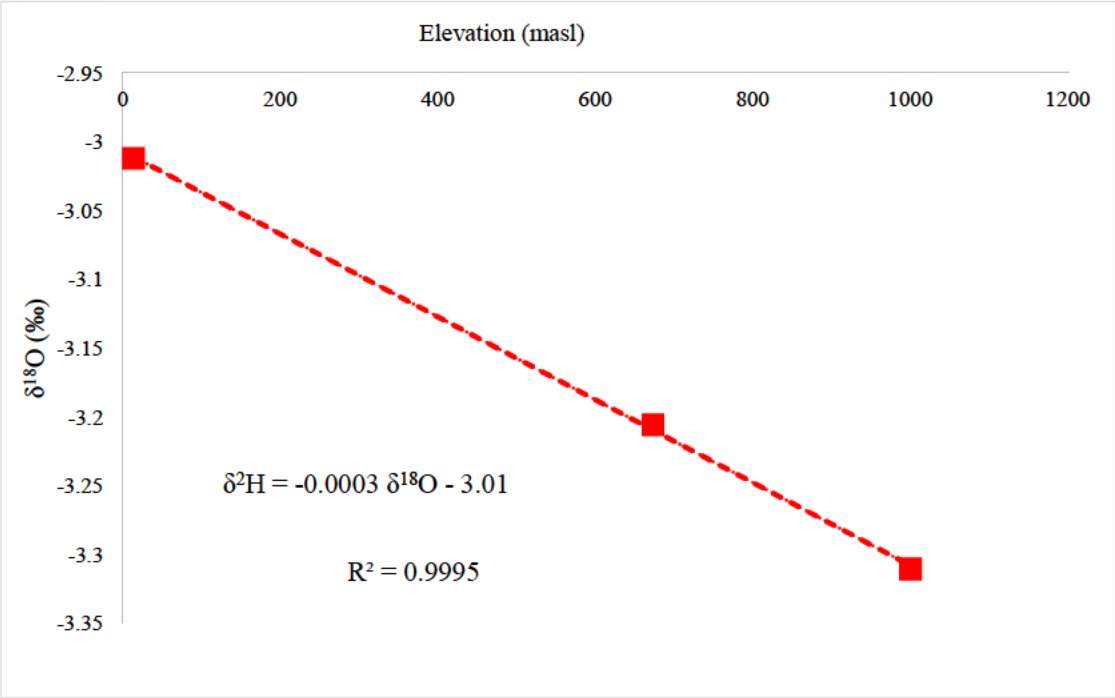

Figure 4.8 The weighted mean composition of $\delta^{18}O$ with changing elevation (masl).

4.4 The $\delta^{18}O$-$\delta^{2}H$ Composition of Groundwater and Surface Water

The isotopic compositions of GW and SWs are examined to understand recharge, flow and discharge processes. The groundwater $\delta^{18}O$ ranged from -3.77‰ to -1.42‰ (wet season) and -3.63‰ to -0.35‰ (dry season). The ranges are within the groundwater isotope ranges derived for South Africa -6.8 ‰ to 1.1‰ for $\delta^{18}O$ (West *et al.*, 2014). The $\delta^{2}H$-$\delta^{18}O$ were plotted against the PtLMWL to understand the effect of secondary processes such as evaporation, on rainfall before it reaches aquifers. (**Error! Reference source not found.** and **Error! Reference source not found.**).

The streams in the lower part of the catchment clustered above the groundwaters and to the right of the PtLMWL. The ranges in $\delta^{18}O$ and $\delta^{2}H$ of groundwater downstream are -2.91‰ to -1.42‰ and -9.6‰ to -4.1‰, respectively. In comparison, the ranges in surface waters were -2.34‰ to -2.15‰ in $\delta^{18}O$ and -8.2‰ to -6.0‰ in $\delta^{2}H$. During the dry season, groundwater and surface waters in the lower catchment plotted along and below the evaporation line, indicating significant evaporation prior to recharge. The ranges in $\delta^{18}O$ and $\delta^{2}H$ of groundwater are -2.06‰ to -0.35‰ and -5.1‰ to -1.6‰ respectively. On the other hand, surface waters ranged from -2.06‰ to -0.97‰ in $\delta^{18}O$ and -6.2‰ to -2.6‰ in $\delta^{2}H$. The groundwaters showed more enrichment than surface water during the dry season, indicating

recharge from recent precipitation. The findings are similar to those of a study conducted in this region but extend to nearby areas outside the Umgeni catchment. The study focused on the eThekwini Metropolitan District (Mtshali, 2021). The isotope compositions of all waters ranged from -4.18‰ to 2.22‰ in $\delta^{18}O$ and $\delta^{2}H$ averaged to -8.78‰.

The surface waters in the headwaters, including Lions River (-3.56‰ to -2.94‰), Karkloof River (-3.86 to -2.58) and Umgeni Vlei wetland (-3.36‰), exhibit the most depleted $\delta^{18}O$ signatures. In the wet season, the groundwaters (-3.55‰ in $\delta^{18}O$; -13.6‰ in $\delta^{2}H$) are clustered with the surface waters (ranging from -3.86% to -1.72‰ in $\delta^{18}O$; -13.9‰ to -5.7‰ in $\delta^{2}H$). Suggesting a strong connection between groundwater and surface water in the catchment.

During the dry season, the groundwaters (ranging from -3.58 to -1.95 in $\delta^{18}O$; -17.8 to -7.8 in $\delta^{2}H$) are slightly depleted than the surface waters (ranging from -3.51 to 0.78 in $\delta^{18}O$; -13.2 to 1.8 in $\delta^{2}H$). The clustering of isotope signatures of surface waters along the LMWL indicates that the main source of recharge is rainfall during the wet season. Rapid runoff generations resulted in surface waters plotting above the PtLMWL. The presence of dams influences the isotope compositions of the river waters by enriching them as we move downstream. Nevertheless, the GW and SW compositions continue to cluster in both seasons, suggesting a contribution of groundwater discharge in streams.

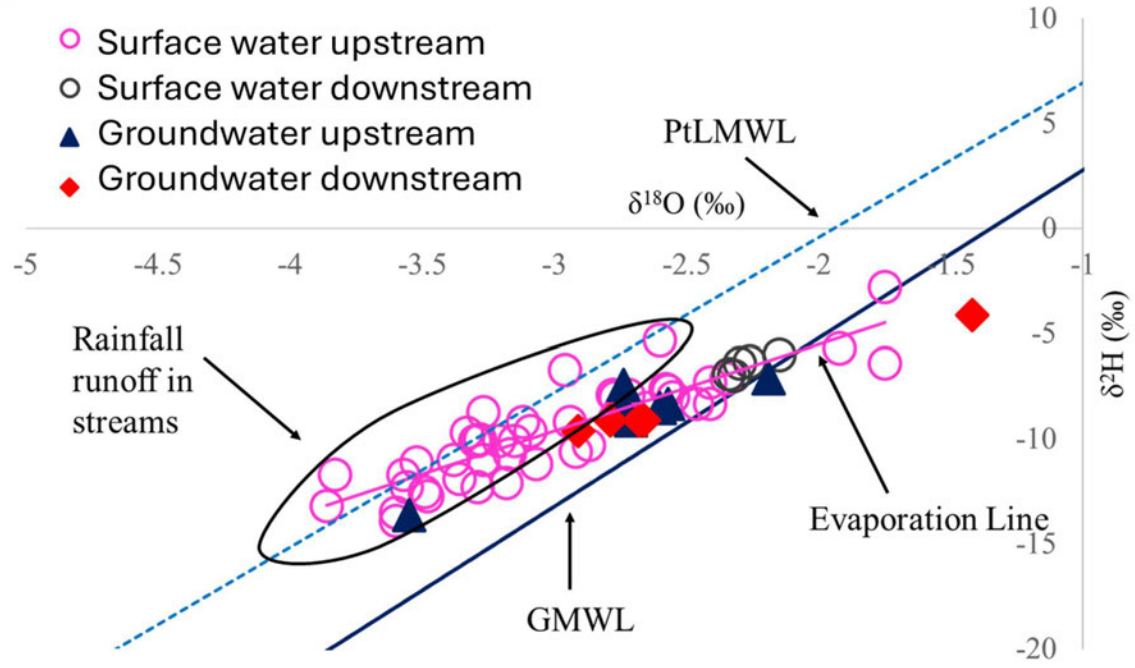

Figure 4.9 $\delta^{18}O$-$\delta^{2}H$ values (groundwater and surface waters) collected in the downstream and upstream areas of the Umgeni Catchment during the wet season 2023 (February to March).

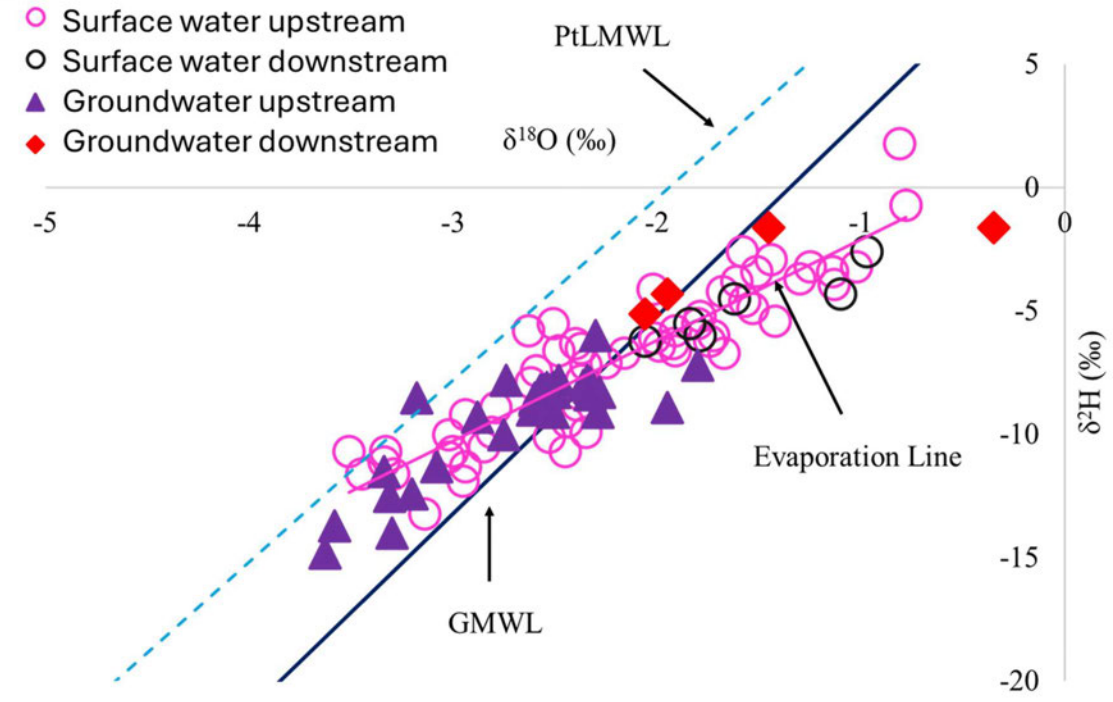

Figure 4.10 $\delta^{18}O$-$\delta^{2}H$ values for data (groundwater and surface waters) collected in downstream and upstream areas of the Umgeni Catchment during the dry season 2023 (August to September).

Pietermaritzburg's two-year data (March 2022 to January 2024) was used to distinguish the isotopic compositions of the summer and winter seasons. The high rainfall amounts during the wet season had a clear depletion trend. The low rainfall amounts from light showers and drizzles showed signs of re-evaporation. The findings suggest high secondary evaporation in light rainfalls of both seasons. Previous studies (Kruger and Nxumalo, 2017; Ndlovu *et al.*, 2021) anticipated a change in the seasonal distribution of rainfall in South Africa, which can potentially influence a decrease in the rainout effect and an increase in rainfall secondary evaporation (Ramudzuli, 2021).

The re-evaporation of light rainfalls can influence groundwater recharge. Unfortunately, the study only looked at the offset of the wet season in terms of specific groundwater recharge (**Error! Reference source not found.**). Nevertheless, the weighted mean precipitation (-3.2059‰ for $\delta^{18}O$ and -9.1227‰ for $\delta^{2}H$) plot below the Pietermaritzburg borehole's isotopic signatures ranging from (-2.75 ‰ to -2.26 ‰ in $\delta^{18}O$) and (-10.0 ‰ to -6 ‰ in $\delta^{2}H$), indicating that the borehole water is isotopically enriched in $\delta^{18}O$ compared to the weighted mean precipitation. Probably, the light rainfall recharges the borehole predominantly.

Similarly, a study recently conducted in the Upper Vall River Catchment found the winter rainfalls occurring between May and October to be the main source of recharge (Banda *et al.*, 2023).

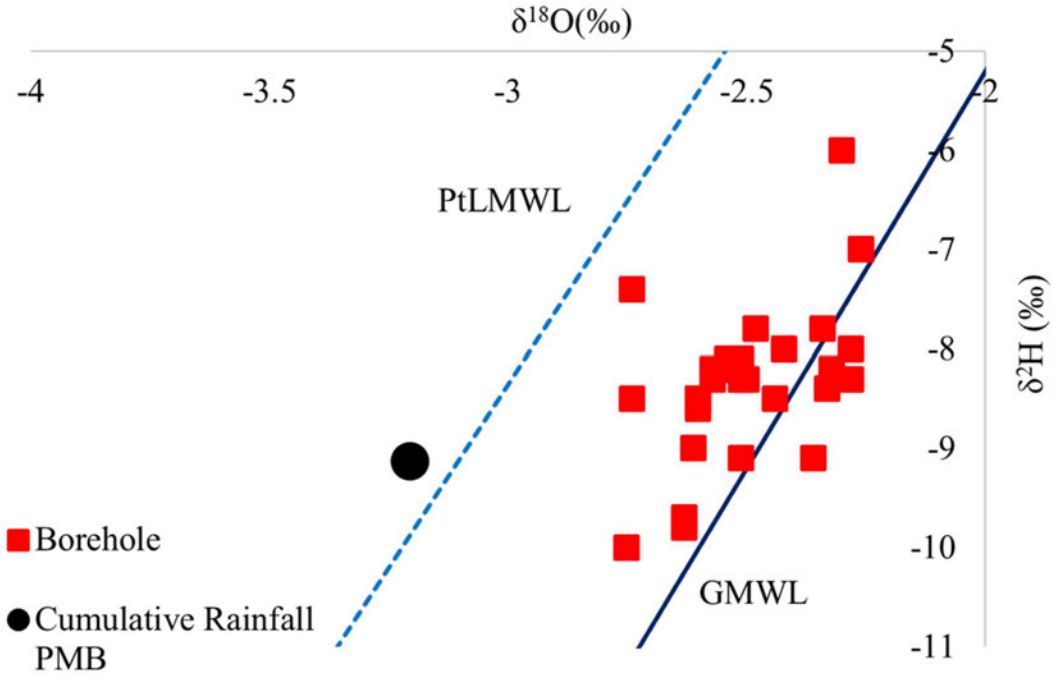

Figure 4.11 Weighted mean rainfall of Pietermaritzburg rainfall vs nearby borehole in UKZN Campus.

4.5 Environmental Radioactive Isotope (^{222}Rn)

Sixty measurements of ^{222}Rn were conducted across the catchment during the wet and dry seasons and the corresponding data is presented in the appendices (**Appendix B: Radon**). The **Error! Reference source not found.** shows the radon concentrations (Bq/m^3) measured during the wet season. Most measurements were conducted on the surface waters (streams and wetlands) and few were conducted on boreholes. In the dry season, the surface waters were repeated with an addition of seven water samples from boreholes (**Error! Reference source not found.**). The concentrations of ^{222}Rn showed significant variation among the stream networks upstream and downstream. Low values below 40 Bq/m^3 in wet and dry seasons were measured in the Umgeni River downstream. The river downstream flows on basement rocks (Dwyka, Mapumulo Group, and the Oribi George Suite), contributing to poor groundwater and surface water interactions.

High concentrations of ^{222}Rn in the 140 to 18000 Bq/m^3 range were measured in the stream networks upstream of the catchment. The streams flow over the Ecca Group, comprising shale, sandstone, siltstone, mudstones and diamictites with dolerite intrusions at different angles forming a network. The area has permeable rocks with fracture networks that favour groundwater discharge. ^{222}Rn has a short half-life (~4 days) and the consistent increase along the rivers moving downstream proves multiple discharge points. Therefore, these areas are identified as the local groundwater discharge zones due to the consistently high ^{222}Rn concentrations.

In addition, the Karkloof River mainly flows over the Volksrust Formation and comprises siltstone, shale, and minor sandstone. It was observed during fieldwork that shale and siltstone contribute to the formation of waterlogged areas, resulting in permanent and seasonal wetlands. The minor sandstone may also influence localised groundwater flow. For instance, the ^{222}Rn upstream of the wetland (200 Bq/m^3) was lower than downstream of the wetland (395 Bq/m^3) during the wet season. Again, in the dry season, the ^{222}Rn upstream of the wetland (1280 Bq/m^3) was significantly lower than downstream (7800 Bq/m^3). The high concentrations of ^{222}Rn downstream of the wetland during the dry season shows that the wetland stores groundwater during the wet months and slowly releases the water during the dry months. This can also be supported by the increase in ^{222}Rn concentration of the Umgeni Vlei wetland, from 1930 Bq/m^3 in the wet season to 17180 Bq/m^3 in the dry season.

The ranges of ^{222}Rn concentration in surface waters of the Umgeni Catchment are significantly high (0-17180 Bq/m^3) compared to other global studies. For instance, a similar study has been recently conducted in Ethiopia and the ^{222}Rn values in surface waters were found to be 2.9-1467 Bq/m^3 (Tadesse *et al.*, 2023). Other studies globally recorded 122-2085 Bq/m^3 in Southern Australia (Cartwright *et al.*, 2014) and 10-8940 Bq/m^3 in China (Wang, 2002). However, a recent study in South Africa in the Western Cape province reported higher ranges of 905–64 550 Bq/m^3 (Mazvimavi *et al.*, 2022).

The high ^{222}Rn in the streams suggests that significantly high uranium-bearing groundwater discharges into the streams. The rocks over which groundwater and surface water flow in the study area are rich in Uranium as shown in **Table 2.2**. The groundwaters were found to have abundant concentrations compared to surface waters in both seasons. During the wet season, the measured ^{222}Rn in groundwater ranged from 1350 to 27 570 Bq/m^3 and surface waters

ranged from 0 to 2210 Bq/m^3. During the dry season, the measured ^{222}Rn values were elevated in groundwaters (148 to 289 500 Bq/m^3) and surface waters (0 to 18260 Bq/m^3).

All the sampled boreholes are found in the intergranular and fractured (0.5 – 2.0 l/s) zones (**Error! Reference source not found.**). However, the alignment of geological units and the distribution of the dykes vary within the catchment. The highest ^{222}Rn concentrations were detected in the Volksrust Formation (289 500, 103 500 and 14980 Bq/m^3). The Volkrust comprises high uranium rocks, which include (shale, siltstone, mudstone and sandstone) (Bezuidenhout, 2021). The ^{222}Rn concentration of 289 500 Bq/m^3 was measured in a borehole in a farm located in the Dargle Valley (30.05748; -29.4919). The concentrations are above the WHO limit (0.5 Bq/L for gross and 1 Bq/L for gross beta activities) and may pose health risks as households in the Sinkle farm area use the borehole. In South Africa, similar results have been recently reported in the Nuwejaars Catchment of Western Cape. The high ^{222}Rn values ranging from 1081 – 332 250 Bq/m^3 were found in the Table Mountain Group and shales.

The Balfour Formation made up of mudstone, siltstone and subordinate sandstone, follows with the second highest ^{222}Rn concentrations (19420 Bq/m^3). The concentrations of ^{222}Rn varied among the Pietermaritzburg Formation (14700, 6040 and 148 Bq/m^3), predominantly shale with thin siltstone and sandstone. Moderate values were measured in the Maputaland Formation (13920 Bq/m^3), comprising sandy or clayey colluvial and alluvial sediments with conglomerate and redistributed sand. They were followed by the Karoo Dolerite Suite (12 440 Bq/m^3), which is dolerite and ultrabasic rocks. The lowest was measured in the Vryheid Formation (227 Bq/m^3), which comprises fine to coarse-grained sandstone, shale and coal seams.

The results also show that the siltstones, mudstones, and shale have a high ^{222}Rn concentration. The dykes were found to be the significant control of high ^{222}Rn in groundwaters. In addition, the findings complement a similar study that was conducted in the Table Mountain aquifers in the Western Cape province, South Africa (Strydom *et al.*, 2021), where the granitic geology and the proximity of fractures was found to be the major control of high ^{222}Rn concentration in groundwater.

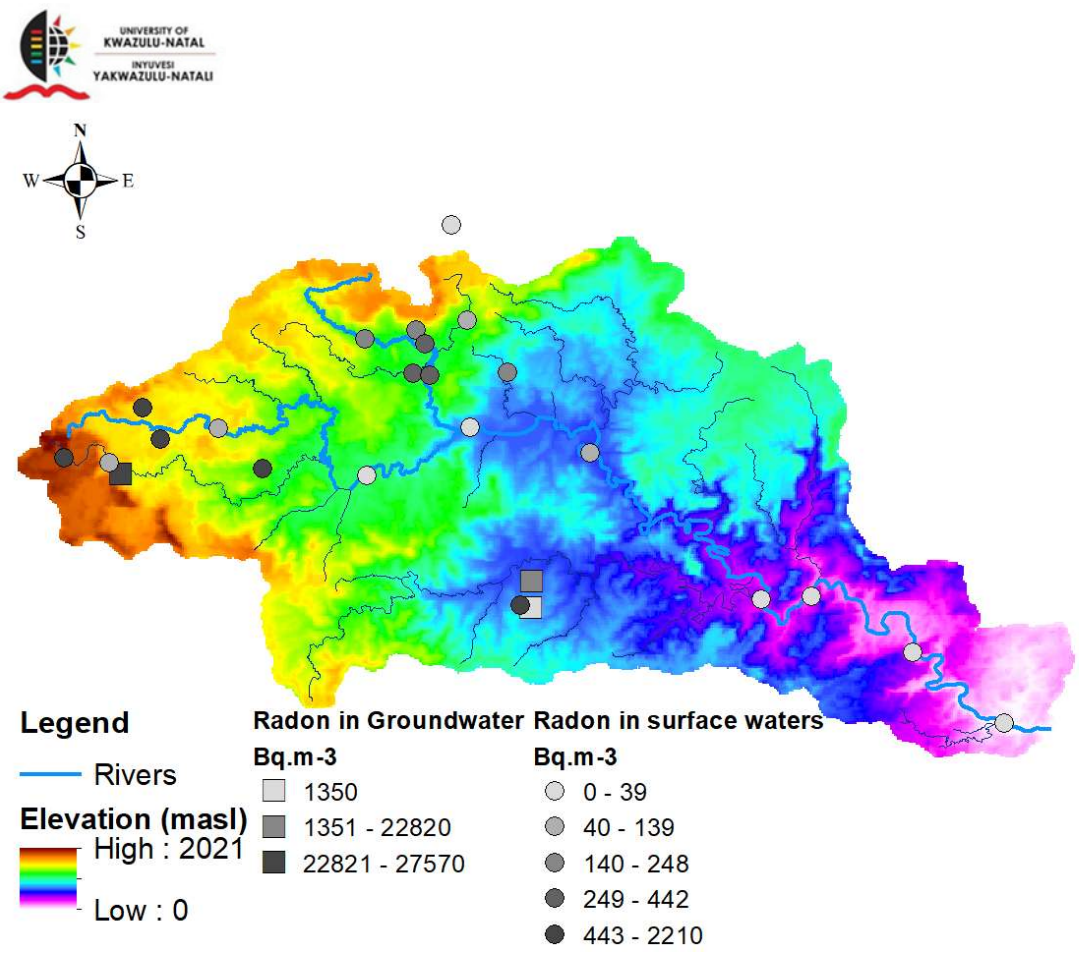

Figure 4.12 Concentration of ^{222}Rn (Bq/m^3) in groundwaters and surface waters of the Umgeni Catchment in the wet season 2023.

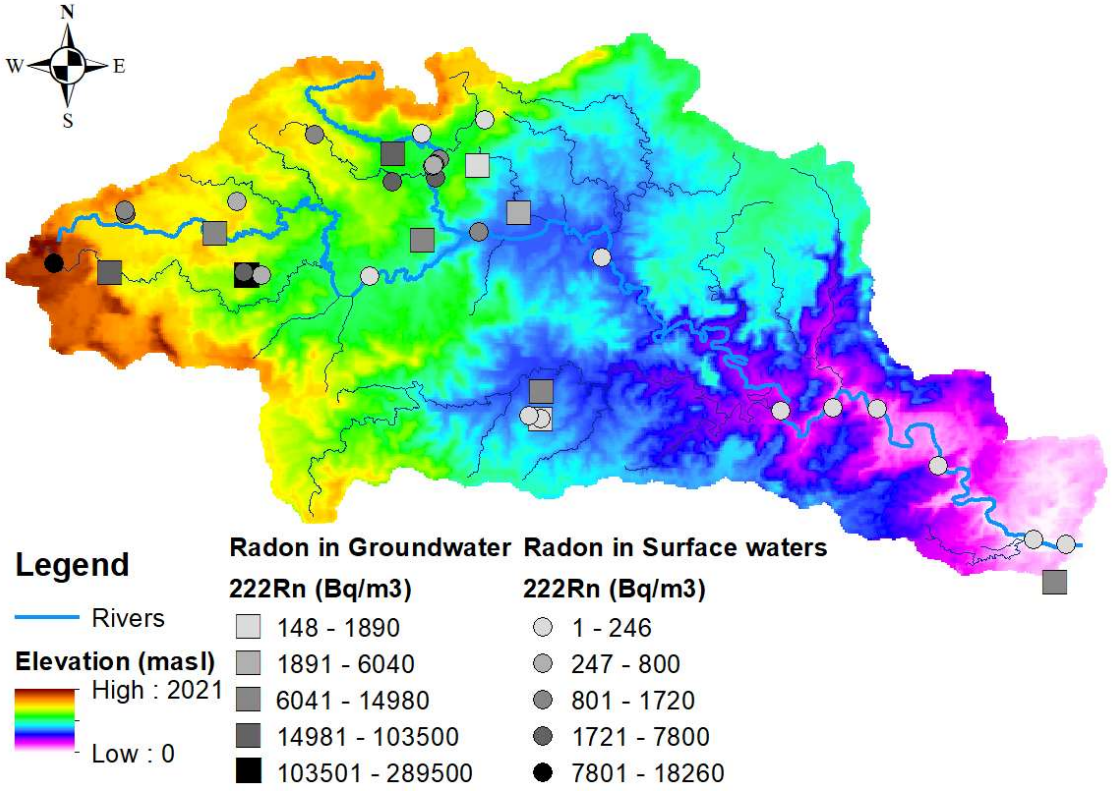

Figure 4.13 Concentration of ^{222}Rn (Bq/m^3) in groundwaters and surface waters of the Umgeni Catchment in the dry season 2023.

4.6 Electrical Conductivity

During the sampling season, the EC was measured on-site while collecting isotope samples. The EC in rainwaters varied from 5 µS/cm to 1650 µS/cm for all seasons and locations (**Figure 4.14**). The rainfall station in Durban consistently had the highest EC levels each month compared to the stations in Howick and Pietermaritzburg. The highest rainfall EC was recorded in October (1650 µS/cm) in Durban. The high EC levels found in Durban are due to the proximity of the Durban rainfall station to the sea, and the rainfall gets most of the sea dust.

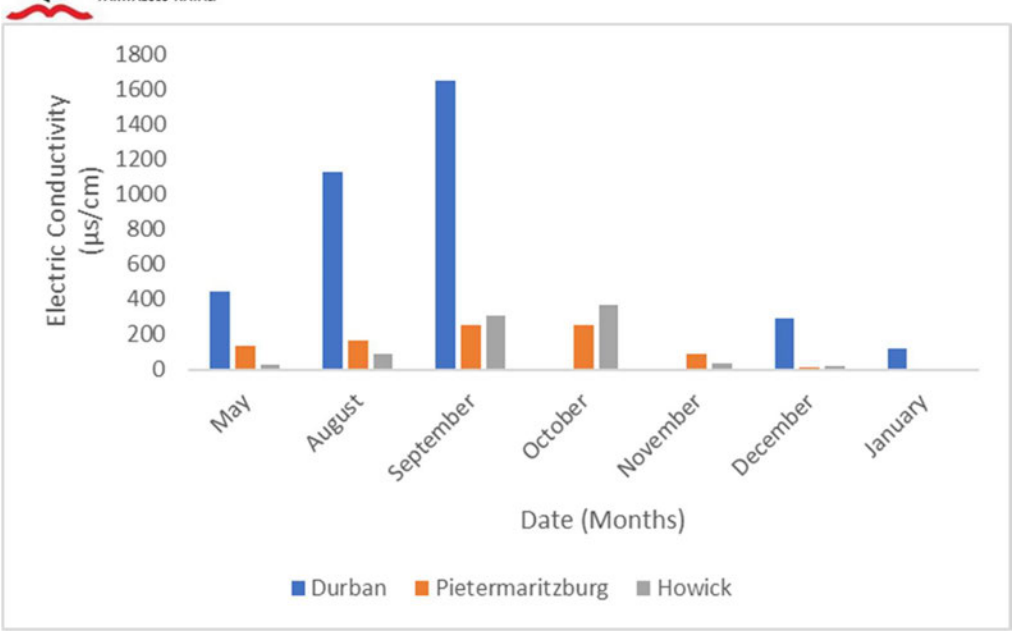

Figure 4.14 EC variations in three rainfall stations in Durban, Pietermaritzburg and Howick.

EC indicates how long water resides in a catchment area. Water that stays in contact with rocks for extended periods tends to have higher EC concentrations (Kebede *et al.*, 2005; Liu and Yamanaka, 2012). The results (**Figure 4.15** and **Figure 4.16**) show progressive EC increase in stream water moving from the highlands to lowlands. Groundwater EC ranged from 29-928 µS/cm during wet and 38-813 µS/cm during dry seasons. The results show that the groundwater of the catchment falls into the freshwaters (<1500 µS/cm) category (Mondal *et al.*, 2008).

Stream water EC ranged from 18—617 µS/cm during the wet season and 30—4000 µS/cm during the dry season. The high EC (4000 µS/cm) measured in Durban was subject to pollution, not necessarily groundwater inflow, and the site measured is a sewage area. The results indicate that groundwater and surface water are characterised by low EC values, respectively, indicating low salinity. The low EC values can be attributed to rapid aquifer discharge and minimum resident time in saturated and unsaturated zones. The EC values indicate local groundwater circulation rather than regional groundwater contribution to discharge. The low EC values were also observed in granitic /crystalline basement formations. Furthermore, the low EC values can demonstrate a significant recharge contribution from preferential flow paths (Ngubo *et al.*, 2022).

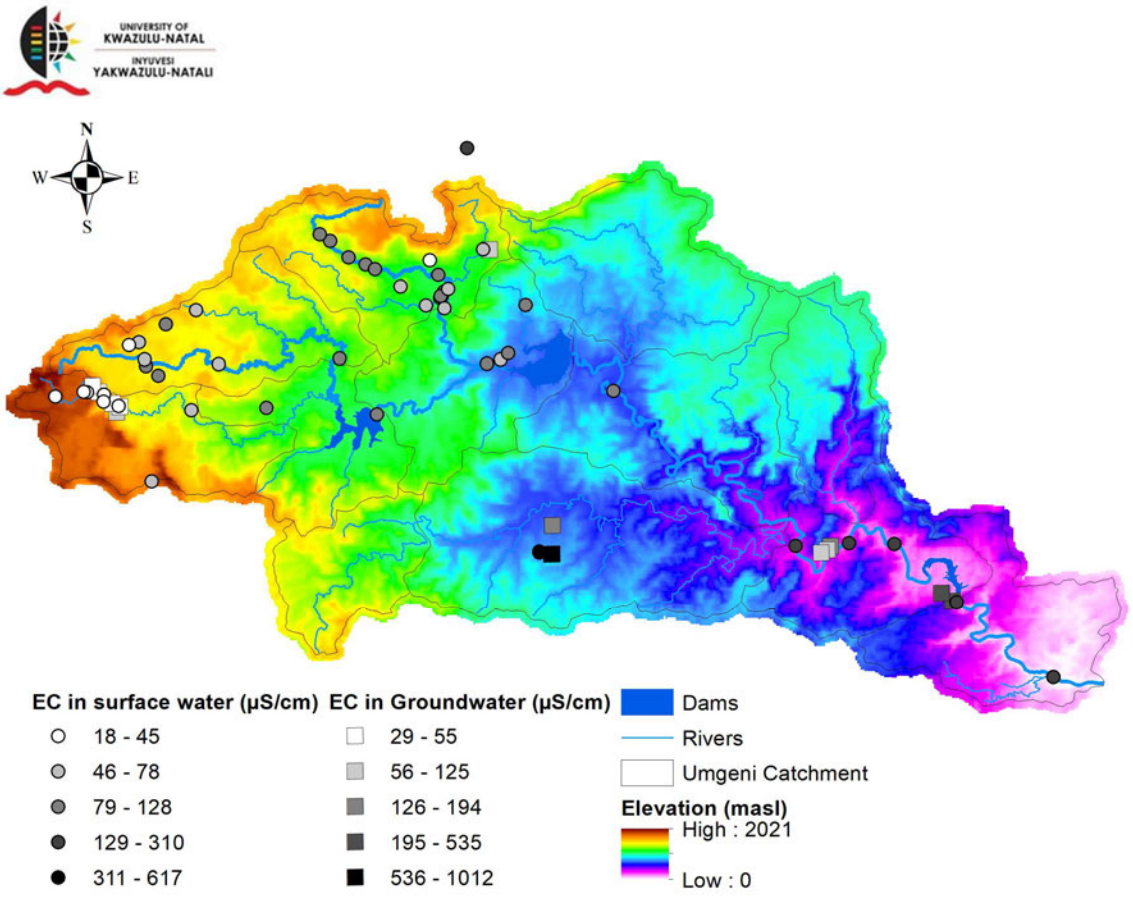

Figure 4.15 EC variations in groundwater and surface waters along the Umgeni Catchment in the wet season.

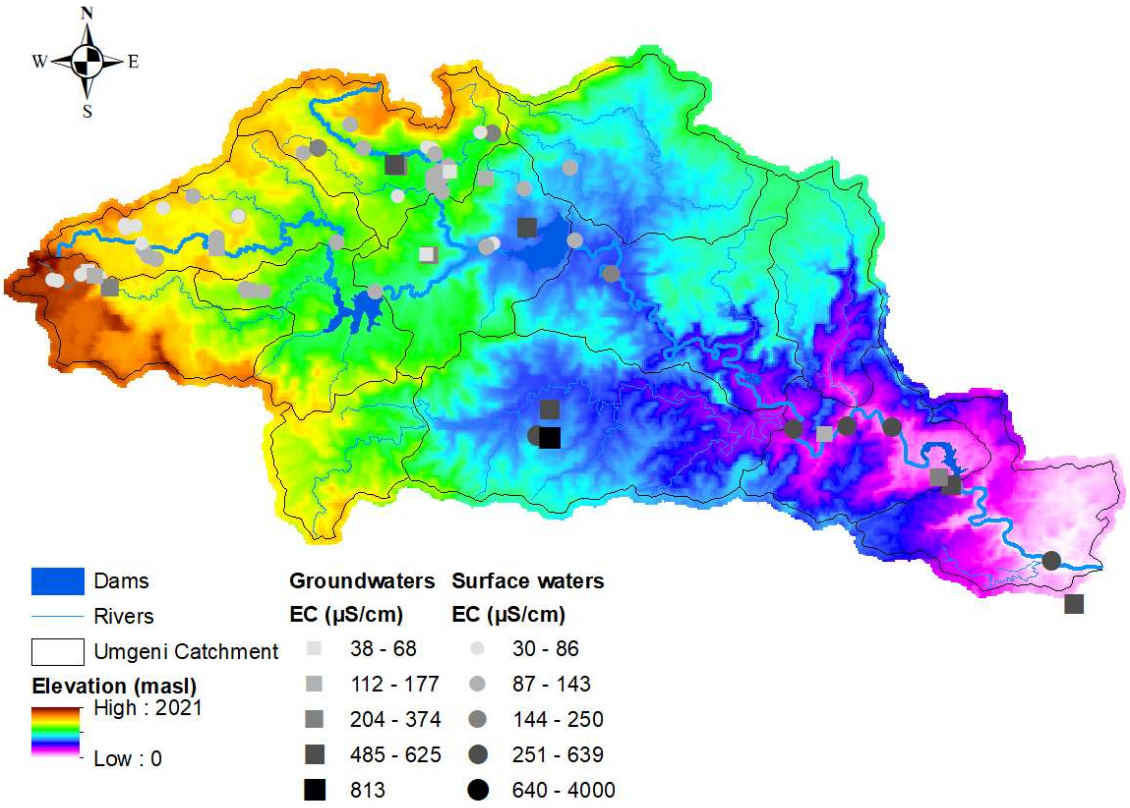

Figure 4.16 EC variations in groundwater and surface water along the Umgeni Catchment in the dry season.

4.7 The Relation Between Rainfalls and Groundwater Levels

Over eight years, groundwater level changes (2015 – 2023) were assessed to understand how aquifers respond to rainfall seasons. During 2015-2016, South Africa experienced the worst El Nino related drought on record in 23 years (Strydom *et al.*, 2020). This period shows a general decrease in the groundwater levels in all boreholes. However, the overall observation from the boreholes indicates that there was no major decrease in the groundwater levels over the years. It can be noted that some wells may be subject to local pumping, such activities could affect the groundwater levels, potentially making them less reflective of natural water level fluctuations.

The borehole (KZN140241) is found in the Dwyka Group. The rock is categorised as a low permeability aquifer with a low storage capacity (Woodford and Chevallier, 2002). The other three boreholes are found in the Pietermaritzburg Formation. The Pietermaritzburg Formation also has decreasing hydraulic conductivity with increasing depth (Woodford and Chevallier,

2002; Bordy *et al.*, 2017). The KZN140241 showed fluctuations compared to other boreholes, with a slight decrease at the dry season's end. Nevertheless, there was a less observed response to the exceptional heavy rainfalls of 2016, 2022 and 2023 in all boreholes.

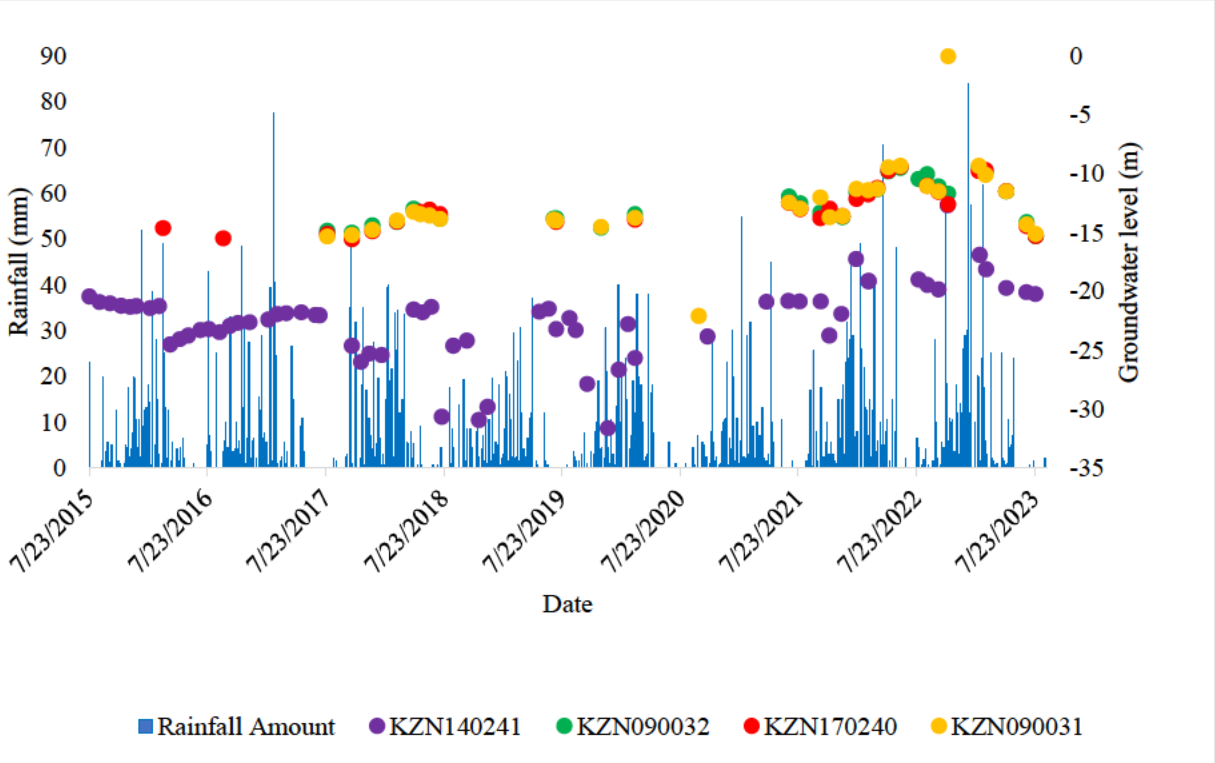

Figure 4.17 Groundwater levels response to changing rainfall from 2015 to 2023.

4.8 Baseflow Separation

The mean annual baseflow index was analysed to supplement the ^{222}Rn findings. The ^{222}Rn was used to indicate groundwater inflow sites, and BFI gives insight into groundwater's overall contribution to streamflow over a year. Nevertheless, the high ^{222}Rn should correlate with high BFI. Notably, the stations in the outlet of the dams showed relatively high BFI (0.69 – 0.81) in **Error! Reference source not found.**. The high values may not indicate groundwater inflow. Instead, they can be linked to the contribution of artificial releases from dams.

The upstream stations showed a high mean annual baseflow index (BFI ranges from 0.36 to 0.88). One of the stations in the upstream part of the catchment, including the Karkloof River, shows a higher BFI of 0.88. The results are similar to a recent study conducted in the headwater streams in the Jonkershoek Valley in the Western Cape (Mokua *et al.*, 2024). The

baseflow was estimated to contribute about 36% to 86% across the Table Mountain Group geology region.

The findings in the headwaters are consistent with the ^{222}Rn findings. The combination of the results indicates that the region is dominated by groundwater inflow compared to surface runoff due to the permeable formations. The areas have permeable geological units, which include the Karoo Dolerite Suite, Balfour, Vryheid and Pietermaritzburg Formation. A similar study was conducted in the Buffalo River Catchment in the Eastern Cape to investigate the influence of geological formations on stream flow dynamics (Owolabi *et al.*, 2020). The results revealed that the porosity network of the fracture system in dolerite influences high baseflow discharge.

On the other hand, the downstream parts of the basin showed a lower baseflow index (BFI 0.36 – 0.68). As observed with the ^{222}Rn results, there is no significant groundwater contribution due to the impermeable geological units in the downstream parts of the catchment. Notably, the outlet of the catchment has high baseflow index (BFI 0.82 — 0.88).

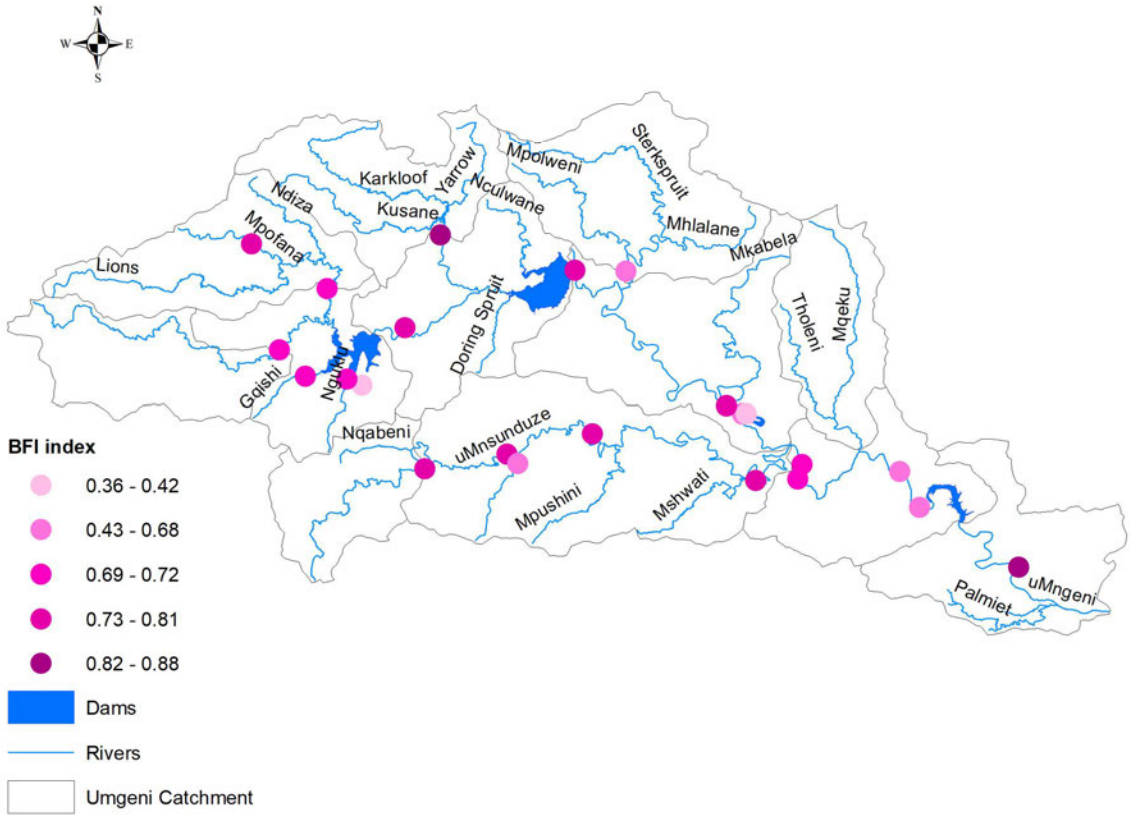

Figure 4.18 Baseflow contribution across the Umgeni catchment derived from the calculated baseflow indexes.

5. DISCUSSION

5.1 Introduction

The interactions between GW and SW at the catchment scale are poorly understood yet significantly affect water resource management. The study aimed to shed light on the groundwater flow processes and its connection with the surface waters of the Umgeni Catchment of KwaZulu-Natal province in South Africa and develop a conceptual GW and SW interactions model. The findings are significant in understanding groundwater recharge mechanisms, flows, and interactions with surface waters in the Umgeni Catchment. The study integrated multiple methodologies, including stable water isotope (δ^2H and $\delta^{18}O$), ^{222}Rn measurements, hydrochemistry (EC), piezometric analysis and baseflow separation. All methods have been previously applied in South Africa to assess different hydrological and hydrogeological aspects. However, this is the first documented study to characterise GW and SW interactions in the Umgeni Catchment. This section discusses the implications of the various results with respect to the objectives of the study.

5.2 Characterising Isotope Signals of Rainfall

The hydrological cycle includes various processes that involve evaporation, vapour transport, condensation and near-surface flows. The water vapour that evaporates from the seas and land surfaces is transported across the earth by atmospheric circulation. This vapour condenses and precipitates over both land and ocean surfaces. Overland, a portion of this precipitation is intercepted by vegetation. The remaining water can follow several paths: it can generate runoff over the land surface, infiltrate the ground, flow through the soil as subsurface flow, or reach aquifers, contributing to groundwater recharge. Groundwater is then discharged into surface waters as baseflow, completing the system. The environmental isotopes have been successfully applied to understand these hydrological processes.

The isotope composition of precipitations provides valuable input for understanding and characterising catchment hydrological systems. Globally, the isotopes of precipitation have been applied to determine the origins and ages of different water bodies (Araguas *et al.*, 1998; Abiye, 2011; Chen *et al.*, 2024), to understand the mixing time and scale (Cartwright *et al.*, 2014; Cai *et al.*, 2020), to quantify the velocity of groundwater flow (Fleckenstein *et al.*, 2010; Gibrilla *et al.*, 2022) and to determine the location of groundwater recharge and discharge (Bourke *et al.*, 2014; Mabokela, 2021; Adyasari *et al.*, 2023; Banda *et al.*, 2023).

Previous studies used LMWLs as fundamental initial tools to represent the relationship between $\delta^{18}O$ and $\delta^{2}H$ in rainfall. The LMWLs derived from local rainfall data was used to understand the local recharge processes, origin, and interactions between groundwater and surface waters. The GMWL, defined by Craig (1961) with the equation $\delta^{2}H = 8*\delta^{18}O + 10$, serve as a global reference.

The PtLMWL equation ($\delta^{2}H= 7.36\delta^{18}O + 14.3$) has a slope close to the GMWL, suggesting conditions that are close to equilibrium. Again, the African Local Meteoric Water Line (LMWL) exhibits a similar slope of 7.4, reinforcing the notion of equilibrium conditions across a regional scale. This implies that the process of precipitation formation in Pietermaritzburg within the Umgeni Catchment occurs in equilibrium conditions with a minor evaporation effect when raining. However, it's worth noting that some regions in South Africa, such as Cape Town, exhibit lower slopes on their LMWLs (6.8) (Harris *et al.*, 2010). This discrepancy can be attributed to different local climatic conditions such as moisture sources, proximity to the sea and evaporation influences in different regions. For instance, compared to Pietermaritzburg, which receives mostly summer rainfall, Cape Town receives most of its rainfall during the winter (Harris *et al.*, 2010). In addition, the PtLMWL was found to have the highest d-excess compared to all the LMWLs; this suggests high local moisture recycling in the Umgeni Catchment.

Precipitation shows isotopic variation across locations and times that are consistent with earlier findings in the catchment (Diamond, 2022). Spatial differences in isotopic composition become more pronounced over larger areas, reflecting climatic complexities, such as the presence of multiple weather systems and variations in terrain, particularly changes in altitude. Temporal variations can occur in a minute within individual rain events and over extended periods of years.

The dense data collection across the Umgeni Catchment allowed us to assess the spatial variations in rainfall isotopic compositions and the potential of using isotopes in hydrological studies. The spatial and temporal variation in isotopes will serve as the basis for tracing the origin of water and its movement through catchments. The three rainfall stations are located at 0 to 1000 masl, giving an altitude difference of ~500 masl. The weighted mean isotope values for each station worked out to an altitude gradient of -0.03‰ $\delta^{18}O$ per 100m. This altitude effect is at the far end of the spectrum, compared to the effect reported by other

studies close to the global average of -0.28‰/100m reported by Poage, 2001. A possible explanation for this low altitude effect is the considerable influence of escarpments, which alter moisture sources and transport pathways (Grab, 2013; Jing *et al.*, 2022).

Globally, a weak altitude effect has been observed in various studies (Harris and Diamond, 2013; Jing *et al.*, 2022), mainly in the lower and mid-latitudes, such as Asia, North Africa and North America. A recent study by Jing et al. (2022) highlighted this phenomenon, indicating an inverse altitude effect on a global scale. The major drivers were found to be the supply of moisture from distant moisture sources and the intense mixing along the transport pathways. Similar findings have been observed in South Africa, including a study conducted by Harris and Diamond (2013), which also identified a weak altitude effect (0.085‰/100m). The weak altitude was explained to be possibly due to the turbulent effect the Table Mountain has on the winter frontal systems. The study emphasised that Table Mountain has higher rainfall on the lee side compared to the windward side and concluded that the isotopic behavior is affected by the turbulence, causing a local depression in temperature and bringing conditions that are higher up in the cloud to mid and lower elevations, further suppressing the altitude effect.

Similarly, the Umgeni catchment highlands stretching to the Drakensberg Mountains have a more complex climate (Ndlovu *et al.*, 2021). The variation in the temperature in the Drakensberg Escarpment has been assessed (Grab, 2013), and the near-surface temperature lapse rates were found to be weak. The escarpment wall separates the maritime moist air to the east (Indian Ocean) from dry air to the west, likely influencing the temperature lapse rates. Again, the Northeastern slopes of the Drakensberg were found to have lower temperatures with frequent thermal inversions that can cause complex variations in temperature with elevation. Therefore, the Drakensberg escarpment along the eastern side contributes to orographic uplifting, blocking the circulation and advection of coastal airflow towards the central interior, bringing high elevation conditions back to the lower elevations as illustrated in **Error! Reference source not found.**. Thus, the different moisture sources were found to be the possible major influence on the weak altitude lapse rate in the Umgeni Catchment.

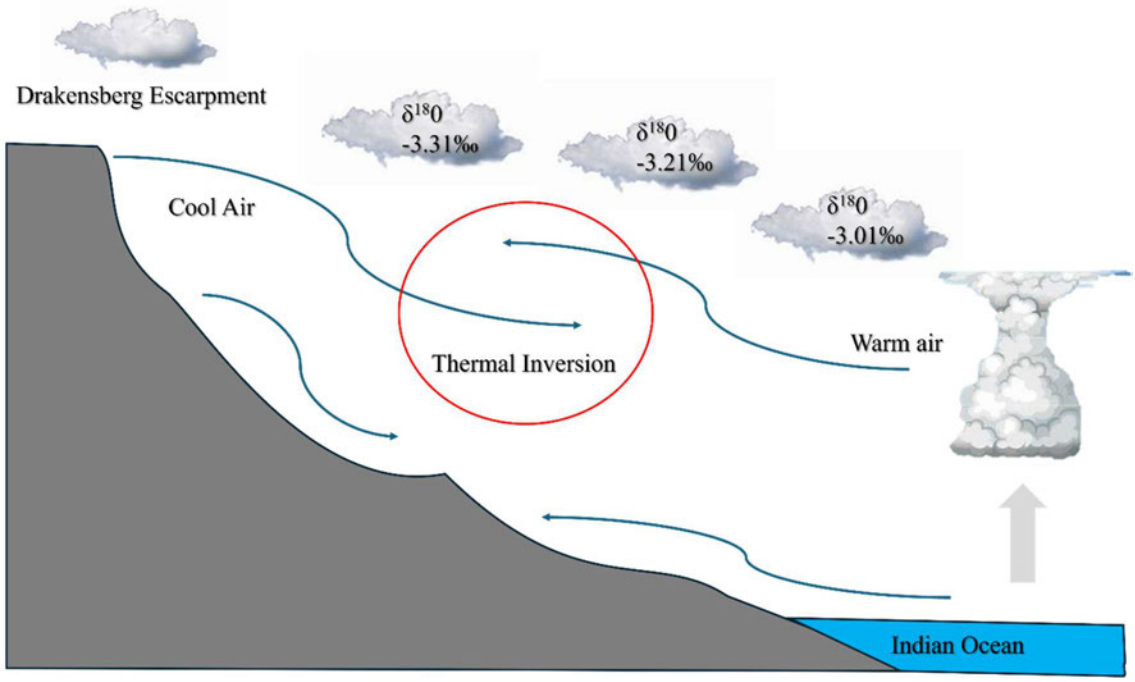

Figure 5.1 Air circulation across the Umgeni Catchment

Despite the weak altitude effect observed on the eastern side of the Drakensberg Escarpment, a high-altitude effect has been reported between KZN (Estcourt) and Lesotho (Oxbow), which is -0.13‰/100m. The high altitude effect moving to the western direction indicates that the warm moisture in the Escourt gives enriched rainfall, but the Oxbow, which faces the western side, has more depleted rainfall. Nevertheless, the weak altitude effect observed in the Umgeni Catchment challenges the application of stable isotopes in tracing regional groundwater flows. Therefore, the limited understanding on the influence of the escarpments on the mixing and pathways of moisture sources in South Africa necessitates further investigation.

The rainfall collected during the intense storm (April 2022) exhibits the most depleted δ^2H and $\delta^{18}O$. Proving a significant impact of tropical cyclones on isotopic composition during extreme precipitation events. The findings are consistent with existing literature on isotope fractionation during intense precipitation events (Diamond, 2014). The isotope compositions varied seasonally, with the dry season having more enriched signals indicating the effect of evaporation. The high rainfall amount effect in the Umgeni Catchment provided valuable insights into recharge mechanisms. The results revealed that recharge occurs through both direct and indirect mechanisms, with upstream areas experiencing significant groundwater

contribution and downstream regions rely mainly on direct recharge, highlighting the role of geological formations in controlling groundwater flow.

Pietermaritzburg's weighted average isotope composition was plotted against its nearby borehole to assess the contribution of different rainfall events on groundwater recharge and the seasonal variability, aiming to provide recharge patterns. The light rainfalls showed to predominantly recharge the groundwater (**Figure 4.11**). This observation contradicts other studies that found exceptional rainfall events as significant contributors to groundwater recharge (Cheng *et al.*, 2021). The prevalence of light rainfall recharge in Pietermaritzburg can be attributed to the underlying shale of the Pietermaritzburg Formation having shallower groundwater systems (Bordy *et al.*, 2017). Such phenomena have been reported in other regions of South Africa, where light rainfall effectively recharges shallow aquifers (Banda *et al.*, 2023).

5.3 Groundwater Recharge, Discharge and Controls that Govern the Connections.

Groundwaters and stream networks fed by groundwaters have proven resilient against global climate change. Thus, the study compared the isotope compositions of rainfall, surface waters and groundwater to assess the interactions of these components in the Umgeni Catchment. The aim was to identify the sites of GW and SW interactions and evaluate groundwater's contribution to the stream networks. The results were integrated with ^{222}Rn, EC, BFI and groundwater water levels, giving insight into the catchment's GW and SW interactions. The upper section of the catchment showed high ^{222}Rn, BFI and depleted $\delta^{18}O$ signals. Based on the observations, the headwater streams of the catchment have the potential of indirectly recharging the groundwaters through preferential pathways. The indirect recharge has been reported in Eastern Cape and it was found to be due to the permeability of dykes, which act as conduits for groundwater flow, facilitating recharge (Sami, 1992).

Groundwater was found to locally discharge as springs and seepages to streams. Local springs in the catchment can be linked to the shallow depths of the underlying sedimentary rock, with many springs remerging upstream of the dykes (Woodford and Chevallier, 2002). The dykes have also been found to restrict groundwater flow (Woodford and Chevallier, 2002). The Natal Sandstone Group outcropping around the Valley of a Thousand Hills acts as a barrier to the groundwater movement. The catchment is restricted to deep regional groundwater flow and lacks evidence of intermediate flows.

The low concentrations of ^{222}Rn detected in the streams in the lower parts of the catchment indicate no groundwater inflow to surface waters. The $\delta^{18}O$ of rainfall resembles the springs, suggesting that local groundwaters are fed by rainfall. The stream beds of the rivers in the lower part of the catchment are impervious due to the underlying basement rocks restricting groundwater inflow. Therefore, the findings suggest that rainfall significantly contributes to groundwater recharge and streamflow generation in lowland areas. Similar findings have been reported on the Natal Group Sandstone (Demlie and Titus, 2015).

5.4 Delineating Groundwater Recharge and Discharge Protection Zones

The integrated analysis of the methods (EC,^{222}Rn, stable isotopes, water levels and baseflow separation) assisted in defining the high recharge and discharge potential areas. The areas that require protection due to strategic importance will be detailed in this section. The overall aim of delineating groundwater recharge and discharge zones is to protect the various sources of water that contribute to the catchment water availability. The findings are significant in enhancing sustainable water supply, monitoring and management, minimising the impact of land use, and assisting in developing proper catchment management plans.

The combination of the findings suggests that dominant recharge occurs upstream of the catchment. The recharge processes include a combination of direct recharge from rainfall and indirect recharge through preferred pathways in the streams influenced by the proximity of dykes. The applied methods (^{222}Rn and BFI) showed that the rivers are consistently fed by groundwater in the highlands. Therefore, protecting headwaters can ensure that the recharge zones remain active and groundwater continues to discharge to streams. Additionally, properly managing the streams in the upper regions can sustain water availability in the catchment, especially during the dry seasons, supporting ecological systems and water supply needs.

Along the eastern region of the catchment, direct recharge from rainfall is dominant. Based on the observed stable isotope compositions, the lowland streams and groundwater were found to rely on rainfall. In the past years, the region has been reported to face significant water quality degradation. The reliance on rainfall can make the stream vulnerable to prolonged drought seasons. Groundwater discharge was evident in springs, wetlands, and freely flowing boreholes, as shown in **Error! Reference source not found.** and **Error! Reference source not found.**. For instance, the findings suggested that the springs are locally

recharged from the observed low EC values.

Figure 5.2 Springs located in different locations, such as Umgeni Vlei, Howick, and Durban

Figure 5.3 Freely flowing boreholes in Pietermaritzburg and Durban

The wetlands were found to store groundwater during the high rainfall season and release it to streams during the dry season. The ^{222}Rn results indicated that these wetlands are mainly fed by groundwater. The wetlands have been found to contribute to water purification from polluted streams, and they vitally maintain the health of ecosystems and water supply

downstream. Unfortunately, wetland loss in the Umgeni has been reported (WRC, 2002) due to unauthorised mining, dumping and land degradation activities.

The study provided no evidence of regional groundwater flows, which could be restricted by the decreased hydraulic conductivity with depth in the underlying rocks (Bordy *et al.*, 2017). Previous studies (Ngubo *et al.*, 2022; Glanville *et al.*, 2023) have found that vegetation such as woody plantations develop root systems that can extract large volumes of groundwater, leading to groundwater and vegetation interactions. This has been investigated by looking at the distribution, diversity, structure, and function of groundwater-dependent vegetation worldwide (Glanville *et al.*, 2023). Nevertheless, the dependence of vegetation on groundwater plays a role in the GW and SW interactions by influencing the direct and indirect recharge (Le Maitre *et al.*, 1999). In South Africa, the woody plants have been documented to have deep roots that can extract large volumes of groundwater from depths 10m and above.

The changes from grassland to tall vegetation significantly impact groundwater recharge, baseflow and groundwater levels (Ngubo *et al.*, 2022). This can be linked with the reported replacement of grassland by indigenous trees and shrub thornveld dominated by *Acacias* in the Umgeni Catchment (WRC, 2002). Similarly, *Acacia* species encroached grasslands in the Northern KwaZulu-Natal along the Drakensberg foothills (Grellier *et al.*, 2011). In these regions, the geology consists of fine-grained sandstone, shale, mudstone, and siltstone from the Ecca and Beaufort Groups of the Karoo Supergroup. *Acacia* crops in these areas were found to extract groundwater directly from shallow (40 cm) and deeper layers (80 cm).

Ngubo et al. (2022) conducted a study on *Acacia* plantations within the Natal Metamorphic Province, also found in the Umgeni Catchment. *Acacia* was found to extract water in the unsaturated zone, affecting the recharge amount for groundwater root uptake and contributing to reduced baseflow rates. Given that similar thornveld vegetation (**Error! Reference source not found.**) and geological conditions are found in the Umgeni Catchment, the same processes are probably occurring in this region. Therefore, the vegetation in the Umgeni Catchment, particularly the *Acacia* species, can potentially be taking up groundwater at both shallow and deep levels. Further investigation is needed to quantify the contribution of groundwater discharge to natural vegetation and better understand the effects of deep-rooted plants on groundwater discharge in the Umgeni Catchment.

Figure 5.4 Natural Vegetation in the Umgeni Catchment (Source: Google Earth; Author, 2024).

5.5 Conceptual Model

The global increase in groundwater demand, pollution threats and changing climate patterns have generated great interest in understanding groundwater recharge, flows and discharge processes. The environmental isotopes have been previously applied to understand the hydrological processes, including identifying sites/sources of groundwater recharge, groundwater origin, potential influence of climate change in groundwaters and sources of contamination. Previous studies have substantiated the environmental data with hydrochemistry, groundwater level analysis, baseflow separation and geological surveys to characterise groundwater movement and develop conceptual models. Similarly, the findings from the hydrological and geological methods that include $\delta^{18}O$-$\delta^{2}H$, ^{222}Rn, EC, BFI and groundwater levels were integrated to develop a conceptual model.

The model illustrates the groundwater recharge mechanisms, flow processes and connection with the surface waters of the Umgeni Catchment (**Error! Reference source not found.**). In the north-western section of the Umgeni Catchment, the findings from $\delta^{18}O$-$\delta^{2}H$ revealed that direct groundwater recharge from rainfall and indirect recharge from preferential pathways occur. The area was proven to have consistent groundwater inflow, as indicated by the increasing ^{222}Rn values moving down the river. The high ^{222}Rn and BFI index values suggest significant GW and SW interactions that contribute to the perennial nature of the headwaters.

Additionally, the EC concentrations were used to classify the groundwater as freshwater. Thus, the headwaters of the catchment were found to have shallow groundwater inputs.

Geologically, the upstream section of the catchment is underlined by permeable geological units, predominantly shale and sandstone, with dense networks of dykes. The sandstones in the Karoo Basin are reported to experience a decrease in hydraulic conductivity, resulting in low porosity and permeability with increasing depth. Similarly, the porosity of shale and other Karoo sediments may appear to be high in the upper layers but decrease with depth due to lithostatic pressures and varying temperatures. The shales and sandstone influence the observed shallow groundwater system in the Umgeni Catchment. A low permeability zone is reached as the water percolates downward, restricting further downward percolation. Groundwater was found to reemerge as diffuse springs upstream of the dykes. The additional downward circulation and deep regional groundwater flow could also be restricted by the prevalence of the dense crisscrossing dykes network. As it has been previously observed that the dykes serve as pathways to the reemergence of springs. In Northern KwaZulu-Natal, previous findings show that more than 80% of high-yielding boreholes, with yields exceeding 0.13 l/s, are directly associated with dolerite intrusions (Woodford and Chevallier, 2002).

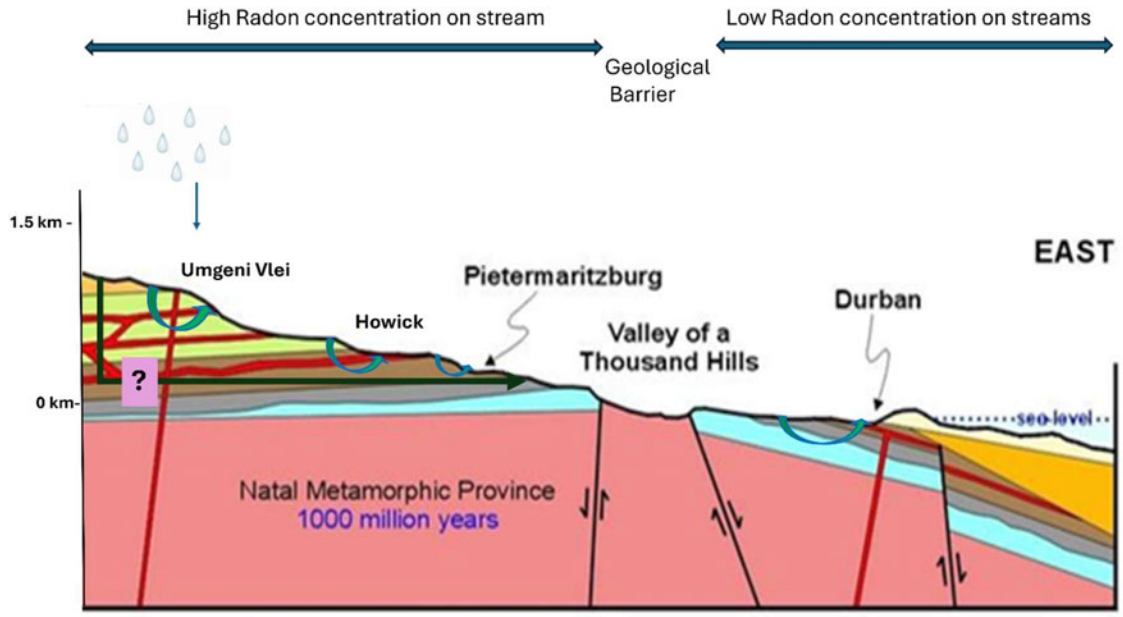

Figure 5.5 Hydrogeological Conceptual Model of the Umgeni Catchment (Modified from STEC@UKZN).

6 CONCLUSIONS AND RECOMMENDATIONS

6.1 Conclusions

Environmental, hydrochemical, baseflow separation, groundwater levels and hydrogeological findings were integrated to conceptualise the groundwater flow processes and its connection with the surface waters of the Umgeni Catchment. The model attempted to conceptualise how groundwater is being recharged, how it joins the surface waters, where it joins and what controls its connection to the surface waters of the catchment. All the inferences on GW and SW interactions in the Umgeni Catchment were made with confidence as the applied methods complemented each other.

Diffuse recharge was found to initially occur in the catchment's highlands, which produce freshwater aquifers. Therefore, highlands were identified as the primary recharge areas that must be protected to sustain groundwater recharge and water quality. The recharged aquifers locally emerge as springs and seepages that connect with the surface waters. The analysis revealed significant groundwater contributions to streamflow in the upstream regions. Direct seepage of groundwater onto stream networks and wetlands was evident. The high ^{222}Rn levels and mean annual baseflow index (BFI) values (above 0.5, reaching up to 0.88 at certain stations) indicated a dominant groundwater inflow, largely attributed to the permeable geological formations such as the Volksrust formation and proximity to dykes.

The geology was found to be the major control of groundwater movement in the catchment. The deep-regional groundwater flows were found to be restricted by the outcrop of the Natal Group sandstone in the Valley of a Thousand Hills, separating the catchment into two segments. The study proved that local groundwater flows play a significant role in maintaining the Umgeni Catchment's surface waters. However, there is no evidence of intermediate groundwater flows.

The catchment was found to have high Uranium barring rocks that influenced high concentrations of ^{222}Rn. The rocks comprising shale, siltstone and mudstone produced the highest ^{222}Rn concentrations. The influence of the prevalence of dykes was significant. The findings suggest a need to assess ^{222}Rn levels in terms of geology and identify any health risks associated with the high concentrations in the Umgeni Catchment.

The ^{222}Rn results showed little groundwater contribution in the downstream section of the catchment due to basement rocks. The nonexistence of GW and SW interactions in the river

downstream suggests a high dependence on rainfall. The downstream area relied on rainfall for groundwater recharge, springs, and streamflow maintenance. This catchment section may be highly susceptible to the global anticipated changes in the rainfall patterns. In addition, the lowlands have been reported to face challenges such as water quality degradation, unauthorised mining, rapid population growth and the invasion of alien species. Implementing a robust water resource management plan is crucial for the Umgeni Catchment, especially the lowlands. To ensure the protection of natural vegetation, minimise pollutants from land uses, monitor water quality, reduce biodiversity losses, secure water supply and promote resilience of the stream networks.

6.2 Recommendations

- The stable isotope analysis indicates a lack of a clear altitude effect, highlighting the need for a dense rainfall sampling network to understand the meteorological processes in rainwater better.
- The highlands were identified as the primary regions for groundwater recharge, discharging into springs, wetlands, and streams. The local groundwater systems present a better opportunity to protect and manage groundwaters within the catchment.
- Light rainfall predominantly recharges the groundwater, warranting further investigation through long-term piezometric observations.
- Groundwater extraction by deep-rooted plantations such as the indigenous and thornveld also present in the Umgeni Catchment influences the GW AND SW interactions. An improved understanding of the beneficial and adverse effects of groundwater extractions by vegetation can be employed in ongoing and future related studies.

7 REFERENCES

Abiye, T. 2011. Provenance of groundwater in the crystalline aquifer of Johannesburg area, South Africa. *International Journal of Physical Sciences* 6.

Abiye, T, Mengistu, H, Masindi, K and Demlie, M. 2015. Surface water and groundwater interaction in the upper crocodile river basin johannesburg, South Africa: Environmental isotope approach. *South African Journal Of Geology* 118 1-10.

Abiye, T, Verhagen, B, Freese, C, Harris, C, Orchard, C, Van Wyk, E, Tredoux, G, Pickles, J, Kollongei, J and Xiao, L. 2013. The use of isotope hydrology to characterize and assess water resources in South (ern) Africa. *WRS Report No TT* 570 13.

Abumurad, KM and Tamimi, M. 2001. Emanation power of radon and its concentration in soil and rocks. *Radiation Measurements* 34 (1): 423-426.

Adyasari, D, Dimova, NT, Dulai, H, Gilfedder, BS, Cartwright, I, McKenzie, T and Fuleky, P. 2023. Radon-222 as a groundwater discharge tracer to surface waters. *Earth-Science Reviews* 238 104321.

Allen, S, Sprenger, M, Bowen, G and Brooks, J. 2022. Spatial and temporal variations in plant source water: O and H isotope ratios from precipitation to xylem water. In.

Anderson, MP. 2005. Heat as a ground atwer tracer. *Groundwater* 43 (6): 951-968.

Araguas, L, Froehlich, K and Rozanski, K. 1998. Stable isotope composition of precipitation over southeast Asia. *Journal of Geophysical Research: Atmospheres* 103 (D22): 28721-28742.

Banda, VD, Mengistu, H and Kanyerere, T. 2023. Assessment of catchment scale groundwater-surface water interaction in a non-perennial river system, Heuningnes catchment, South Africa. *Scientific African* 20 19.

Banks, EW, Simmons, CT, Love, AJ, Cranswick, R, Werner, AD, Bestland, EA, Wood, M and Wilson, T. 2009. Fractured bedrock and saprolite hydrogeologic controls on groundwater/surface-water interaction: a conceptual model (Australia). *Hydrogeology Journal* 17 (8): 1969-1989.

Barrie, CJ, Rasmussen, TC, Tollner, EW, Golladay, SW and Brantley, ST. 2022. Steady vs dynamic stream-aquifer interactions: Lower Flint River Basin, Southwest Georgia, USA. *Journal of Hydrology: Regional Studies* 40 101046.

Barthel, R and Banzhaf, S. 2016. Groundwater and surface water interaction at the regional-scale – a review with focus on regional integrated models. *Water Resources Management* 30 (1): 1-32.

Bezuidenhout, J. 2021. Estimating indoor radon concentrations based on the uranium content of geological units in South Africa. *Journal of Environmental Radioactivity* 234 106647.

Bordy, E, Spclman, S, Cole, DI and Mthembi, P. 2017. Lithostratigraphy of the Pietermaritzburg Formation (Ecca Group, Karoo Supergroup), South Africa. *South African Journal of Geology* 120 293-302.

Botha, G and Botha, RCN. 2002. Geological description of sheet 2930CB Pietermaritzburg, Explanation: 1:50 000 Geological Series.

Bourke, SA, Cook, PG, Shanafield, M, Dogramaci, S and Clark, JF. 2014. Characterisation of hyporheic exchange in a losing stream using radon-222. *Journal of Hydrology* 519 94-105.

Brannen, R, Spence, C and Ireson, A. 2015. Influence of shallow groundwater–surface water interactions on the hydrological connectivity and water budget of a wetland complex. *Hydrological Processes* 29 (18): 3862-3877.

Braun, K, Bar-Matthews, M, Ayalon, A, Zilberman, T and Matthews, A. 2017. Rainfall isotopic variability at the intersection between winter and summer rainfall regimes in coastal South Africa (Mossel Bay, Western Cape Province). *South African Journal of Geology* 120 (3): 323-340.

Brodie, HD.2005. A review of techniques for analysing baseflow from stream.

Cai, Z, Wang, W, Zhao, M, Ma, Z, Lu, C and Li, Y. 2020. Interaction between surface water and groundwater in Yinchuan Plain. *Water* 12 (9): 2635.

Cantor, A, Owen, D, Harter, T, Green Nylen, N and Kiparsky, M. 2018. Navigating groundwater-surface water interactions under the Sustainable Groundwater Management Act.

Cartwright, I, Hofmann, H, Gilfedder, B and Smyth, B. 2014. Understanding parafluvial exchange and degassing to better quantify groundwater inflows using 222Rn: The King River, southeast Australia. *Chemical Geology* 380 48-60.

Cavazza, S and Pagliara, S. 2009. Groundwater and surface water interactions. *Groundwater-Volume I* 96.

Chamine, HI, Carvalho, JM, Teixeira, J and Freitas, L. 2015. Role of hydrogeological mapping in groundwater practice: back to basics. *European Geologist Journal* 40 34-42.

Chen, L, Zhu, G, Lin, X, Li, R, Lu, S, Jiao, Y, Qiu, D, Meng, G and Wang, Q. 2024. The complexity of moisture sources affects the altitude effect of stable isotopes of precipitation in inland mountainous regions. *Water Resources Research* 60 (6): e2023WR036084.

Cheng, L, Si, B, Wang, Y and Liu, W. 2021. Groundwater recharge mechanisms on the Loess Plateau of China: New evidence for the significance of village ponds. *Agricultural Water Management* 257 107148.

Chiluwe, QW. 2014. Assessing the role of property rights in managing water demand: the case of Umgeni River catchment. *Monash South Africa: Johannesburg, South Africa*.

Condon, LE, Markovich, KH, Kelleher, CA, McDonnell, JJ, Ferguson, G and McIntosh, JC. 2020. Where Is the Bottom of a Watershed? *Water Resources Research* 56 (3): e2019WR026010.

Cook, PG. 2020. Introduction to isotopes and environmental tracers as indicators of groundwater flow. Guelph, ontario, canada.

Craig, H. 1961. Isotopic variations in meteoric waters. *Science* 133 (3465): 1702-1703.

Demlie, M and Titus, R. 2015. Hydrogeological and hydrogeochemical characteristics of the Natal Group sandstone, South Africa. *South African Journal of Geology* 118 (1): 33-44.

Diamond, R. 2022. Stable isotope hydrology. Guelph, Ontario, Canada.

Diamond, RE. 2014. Stable isotope hydrology of the Table Mountain group. Unpublished thesis, University of Cape Town.

Dlamini, AE and Demlie, M. 2020. Integrated hydrogeological, hydrochemical and environmental isotope investigation of the area around the Kusile Power Station, Mpumalanga, South Africa. *Journal of African Earth Sciences* 172 103958.

Duncan, HP. 2019. Baseflow separation – A practical approach. *Journal of Hydrology* 575 308-313.

Durowoju, OS, Ekosse, G-IE and Odiyo, JO. 2019. Determination of isotopic composition of rainwater to generate local meteoric water line in Thohoyandou, Limpopo Province, South Africa. *Water SA* 45 (2): 183-189.

Durrige Company Inc. 2020. https://durrige.com/products/big-bottle-system.

Eilers, A, Miller, J, Swana, K, Botha, R, Talma, S, Newman, R, Murray, R and Vengosh, A. 2015. Characterisation of radon concentrations in karoo groundwater, south africa, as a prelude to potential shale-gas development. *Procedia Earth and Planetary Science* 13 269-272.

Fleckenstein, JH, Krause, S, Hannah, DM and Boano, F. 2010. Groundwater-surface water interactions: New methods and models to improve understanding of processes and dynamics. *Advances in Water Resources* 33 (11): 1291-1295.

Geppert, M, Hartmann, K, Kirchner, I, Pfahl, S, Struck, U and Riedel, F. 2022. Precipitation over southern africa: Moisture sources and isotopic composition. *Journal of Geophysical Research: Atmospheres* 127 (21): e2022JD037005.

Gibrilla, A, Fianko, JR, Ganyaglo, S, Adomako, D, Stigter, TY, Salifu, M, Anornu, G, Zango, MS and Zakaria, N. 2022. Understanding recharge mechanisms and surface water contribution to groundwater in granitic aquifers, Ghana: Insights from stable isotopes of δ2H and δ18O. *Journal of African Earth Sciences* 192 104567.

Glanville, K, Sheldon, F, Butler, D and Capon, S. 2023. Effects and significance of groundwater for vegetation: A systematic review. *Science of the Total Environment* 875 162577.

Gleeson, T and Manning, AH. 2008. Regional groundwater flow in mountainous terrain: Three-dimensional simulations of topographic and hydrogeologic controls. *Water Resources Research* 44 (10).

Gonfiantini, R, Roche, M-A, Olivry, J-C, Fontes, J-C and Zuppi, GM. 2001. The altitude effect on the isotopic composition of tropical rains. *Chemical Geology* 181 (1): 147-167.

Grab, SW. 2013. Fine-scale variations of near-surface-temperature lapse rates in the high Drakensberg Escarpment, South Africa: environmental implications. *Arctic, antarctic, and alpine research* 45 (4): 500-514.

Grellier, S, Janeau, J-L, Richard, P, Ward, D, Bariac, T and Lorentz, S. 2011. Water uptake adaptations of Acacia sieberiana in a woody plant encroached grassland of South Africa. *Invasion ligneuse par l'Acacia sieberiana dans un pâturage raviné du KwaZulu-Natal (Afrique du Sud)* 127.

Harris, C, BURGERS, C, MILLER, J and RAWOOT, F. 2010. O and H isotope record of cape town rainfall from 1996 to 2008, and its application to recharge studies of table mountain groundwater, south africa. *South African Journal of Geology* 113 (1): 33-56.

Harris, C and Diamond, R. 2013. Oxygen and hydrogen isotopes record of cape town rainfall and its application to recharge studies of Table Mountain groundwater. *The Use of Isotope Hydrology to Characterize and Assess Water Resources in South (ern) Africa* 38-52.

Herbert, C and Compton, J. 2007. Depositional environments of the lower Permian Dwyka diamictite and Prince Albert shale inferred from the geochemistry of early diagenetic concretions, southwest Karoo Basin, South Africa. *Sedimentary Geology* 194 (3-4): 263-277.

Hicks, N. 2010. Extended distribution of Natal Group within southern KwaZulu-Natal, South Africa: implications for sediment sources and basin structure. *South African Journal of Geology* 113 287-306.

Hughes, C, de Winnaar, G, Schulze, R, Mander, M and Jewitt, G. 2018. Mapping of water-related ecosystem services in the uMngeni catchment using a daily time-step hydrological model for prioritisation of ecological infrastructure investment - Part 1: Context and modelling approach. *Water SA* 44 577-589.

Indarto, Novita, E and Wahyuningsih, S. 2016. Preliminary Study on Baseflow Separation at Watersheds in East Java Regions. *Agriculture and Agricultural Science Procedia* 9 538-550.

Jing, Z, Yu, W, Lewis, S, Thompson, LG, Xu, J, Zhang, J, Xu, B, Wu, G, Ma, Y, Wang, Y and Guo, R. 2022. Inverse altitude effect disputes the theoretical foundation of stable isotope paleoaltimetry. *Nature Communications* 13 (1): 4371.

Kalbus, E, Reinstorf, F and Schirmer, M. 2006. Measuring methods for groundwater–surface water interactions: a review. *Hydrology and Earth System Sciences* 10 (6): 873-887.

Karar, E, Pillay, M and Howard, J. 1999. Evaluation of water resource management practices.

Kebede, S, Charles, K, Godfrey, S, MacDonald, A and Taylor, RG. 2021. Regional-scale interactions between groundwater and surface water under changing aridity: evidence from the River Awash Basin, Ethiopia. *Hydrological Sciences Journal* 66 (3): 450-463.

Kebede, S, Travi, Y, Alemayehu, T and Ayenew, T. 2005. Groundwater recharge, circulation and geochemical evolution in the source region of the Blue Nile River, Ethiopia. *Applied Geochemistry* 20 (9): 1658-1676.

Kebede, S and Zewdu, S. 2019. Use of 222Rn and δ18O-δ2H isotopes in detecting the origin of water and in quantifying groundwater inflow rates in an alarmingly growing lake, Ethiopia. *Water* 11 (12): 2591.

Khan, S and Davidson, I. 2016. Aquifer underground pumped hydroelectric energy storage in south africa.

King, G. 1997. The development potential of KwaZulu-Natal aquifers for rural water supply. Unpublished thesis, Rhodes University.

Kruger, AC and Nxumalo, M. 2017. Historical rainfall trends in South Africa: 1921–2015. *Water Sa* 43 (2): 285-297.

Kusangaya, S, Toucher, MLW, van Garderen, EA and Jewitt, GPW. 2016. An evaluation of how downscaled climate data represents historical precipitation characteristics beyond the means and variances. *Global and Planetary Change* 144 129-141.

Kusangaya, S, Warburton Toucher, ML and van Garderen, EA. 2018. Evaluation of uncertainty in capturing the spatial variability and magnitudes of extreme hydrological events for the uMngeni catchment, South Africa. *Journal of Hydrology* 557 931-946.

Le Maitre, DC, Scott, DF and Colvin, C. 1999. A review of information on interactions between vegetation and groundwater. *Water SA* 25 (2): 137-152.

Leaney, FW and Herczeg, AL. 1995. Regional recharge to a karst aquifer estimated from chemical and isotopic composition of diffuse and localised recharge, South Australia. *Journal of Hydrology* 164 (1): 363-387.

Leketa, K and Abiye, T. 2020. Investigating stable isotope effects and moisture trajectories for rainfall events in Johannesburg, South Africa. *Water Sa* 46 (3): 429-437.

Leketa, K, Abiye, T and Butler, M. 2018. Characterisation of groundwater recharge conditions and flow mechanisms in bedrock aquifers of the Johannesburg area, South Africa. *Environmental Earth Sciences* 77 (21): 727.

Levy, J and Xu, Y. 2012. Groundwater management and groundwater/surface-water interaction in the context of South African water policy. *Hydrogeology journal* 20 (2): 205-226.

Liao, F, Wang, G, Shi, Z, Cheng, G, Kong, Q, Mu, W and Guo, L. 2018. Estimation of groundwater discharge and associated chemical fluxes into Poyang Lake, China: approaches using stable isotopes (δD and δ18O) and radon. *Hydrogeology Journal* 26 (5): 1625-1638.

Liu, F, Conklin, MH and Shaw, GD. 2024. Elevational control of isotopic composition and application in understanding hydrologic processes in the mid Merced River catchment, Sierra Nevada, California, USA. *Hydrol. Earth Syst. Sci.* 28 (10): 2239-2258.

Liu, J, Fu, G, Song, X, Charles, SP, Zhang, Y, Han, D and Wang, S. 2010. Stable isotopic compositions in Australian precipitation. *Journal of Geophysical Research: Atmospheres* 115 (D23).

Liu, Y and Yamanaka, T. 2012. Tracing groundwater recharge sources in a mountain–plain transitional area using stable isotopes and hydrochemistry. *Journal of Hydrology* 464-465 116-126.

London, L, Dalvie, MA, Nowicki, A and Cairncross, E. 2005. Approaches for regulating water in South Africa for the presence of pesticides. *Water SA* 31 (1): 53-59.

Lorentz, S, Riddell, ES, Nel, J, Van Tol, J, Fundisi, D, Jumbi, F and van Niekerk, A. 2020. Groundwater-surface water interactions in an ephemeral savanna catchment, Kruger National Park. *Koedoe: African Protected Area Conservation and Science* 62 (2): 1-14.

Lorimer, B. 2012. Some, for all, forever: a case study of participation in water management in south africa's umgeni river catchment.

Mabokela, SP. 2021. Hydrogeological investigations of groundwater and surface water interactions in the Berg River catchment, Western Cape, South Africa. Unpublished thesis, Cape Peninsula University of Technology.

Madlala, T, Kanyerere, T, Oberholster, P and Butler, M. 2021. Assessing the groundwater dependence of valley bottom wetlands in coal-mining environment using multiple environmental tracers, Mpumalanga, South Africa. *Sustainable Water Resources Management* 7 (4): 23.

Madlala, TE. 2015. Determination of groundwater-surface water interaction, upper Berg River catchment, South Africa.

Madzunya, D, Dudu, V, Mathuthu, M and Manjoro, M. 2020. Radiological health risk assessment of drinking water and soil dust from Gauteng and North West Provinces, in South Africa. *Heliyon* 6 (2).

Makaya, N, Dube, T, Seutloali, K, Shoko, C, Mutanga, O and Masocha, M. 2019. Geospatial assessment of soil erosion vulnerability in the upper uMgeni catchment in KwaZulu Natal, South Africa. *Physics and Chemistry of the Earth, Parts A/B/C* 112 50-57.

Manickum, T, John, W, Terry, S and Hodgson, K. 2014. Preliminary study on the radiological and physicochemical quality of the Umgeni Water catchments and drinking water sources in KwaZulu-Natal, South Africa. *Journal of Environmental Radioactivity* 137 227-240.

Markovich, KH, Manning, AH, Condon, LE and Jennifer. 2019. Mountain-block recharge: A review of current understanding. *Water Resources Research* 55 (11): 8278-8304.

Mazvimavi, D, Clarke, S, Day, J, Dube, T, Kanyerere, T, Machingura, J, Malijani, E, Mkunyana, Y and Swartbooi, E. 2022. Understanding of surface water-groundwater interactions from headwaters to lowlands or catchment scale sustainable water resources management.

McDonald, AK, Sheng, Z, Hart, CR and Wilcox, BP. 2013. Studies of a regulated dryland river: surface–groundwater interactions. *Hydrological Processes* 27 (12): 1819-1828.

Miller, JA, Dunford, AJ, Swana, KA, Palcsu, L, Butler, M and Clarke, CE. 2017. Stable isotope and noble gas constraints on the source and residence time of spring water from the Table Mountain Group Aquifer, Paarl, South Africa and implications for large scale abstraction. *Journal of Hydrology* 551 100-115.

Modie, LT, Kenabatho, PK, Stephens, M and Mosekiemang, T. 2022. Investigating groundwater and surface water interactions using stable isotopes and hydrochemistry in the Notwane River Catchment, South East Botswana. *Journal of Hydrology: Regional Studies* 40 101014.

Mokua, RA, Glenday, J and Mazvimavi, D. 2024. Evaluating the spatial and temporal variation in baseflow across headwater streams in the Jonkershoek valley, South Africa. *Proc. IAHS* 385 239-246.

Mondal, N, Singh, V, Saxena, V and Prasad, R. 2008. Improvement of groundwater quality due to fresh water ingress in Potharlanka Island, Krishna delta, India. *Environmental Geology* 55 595-603.

Mook, W and Rozanski, K. 2000. Environmental isotopes in the hydrological cycle. *IAEA Publish* 39.

Mothusi, D. 2014. Seasonal analysis of water and sediment along the umgeni river, south africa. Unpublished thesis, School of Chemistry and Physics, University of KwaZulu-Natal, South Africa.

Mtshali, S. 2021. Characterisation of groundwater and surface water interaction in the eThekwini Metropolitan District, KwaZulu-Natal, South Africa. Unpublished thesis.

Namugize, JN, Jewitt, G and Graham, M. 2018. Effects of land use and land cover changes on water quality in the uMngeni river catchment, South Africa. *Physics and Chemistry of the Earth, Parts a/b/c* 105 247-264.

Ndlovu, M, Clulow, AD, Savage, MJ, Nhamo, L, Magidi, J and Mabhaudhi, T. 2021. An Assessment of the Impacts of Climate Variability and Change in KwaZulu-Natal Province, South Africa. *Atmosphere* 12 (4): 427.

Ndlovu, MS. 2018. Hydrogeological and hydrochemical investigation of the Durban Metropolitan District, Eastern South Africa. Unpublished thesis.

Ndlovu, MS and Demlie, M. 2018. Statistical analysis of groundwater level variability across KwaZulu-Natal Province, South Africa. *Environmental Earth Sciences* 77 (21): 739.

Ngcobo, S and Jewitt, G. 2017. Multiscale drivers of sugarcane expansion and impacts on water resources in Southern Africa. *Environmental Development* 24 63-76.

Ngubo, CZ, Demlie, M and Lorentz, S. 2022. Investigation of hydrological processes and the impacts of Acacia mearnsii plantations on groundwater in secondary aquifers: Case study at the two-stream research catchment, South Africa. *Journal of Hydrology: Regional Studies* 40 101018.

Owolabi, ST, Madi, K, Kalumba, AM and Alemaw, BF. 2020. Assessment of recession flow variability and the surficial lithology impact: A case study of Buffalo River catchment, Eastern Cape, South Africa. *Environmental Earth Sciences* 79 (8): 187.

Petersen, RM, Nel, JM, Strydom, T, Riddell, E, Coetsee, C and February, E. 2023. The use of stable isotopes to identify surface water-groundwater interaction in the Kruger National Park, South Africa. *Water Sa* 49 (2): 96-102.

Poage, MA. 2001. Empirical relationships between elevation and the stable isotope composition of precipitation and surface waters: Considerations for studies of paleoelevation change. *American Journal of Science* 301 1-15.

Poage, MA and Chamberlain, CP. 2001. Empirical relationships between elevation and the stable isotope composition of precipitation and surface waters: Considerations for studies of paleoelevation change. *American Journal of Science* 301 (1): 1-15.

Ramudzuli, KE. 2021. Potential impacts of climate change on groundwater recharge in South Africa using stable isotopes of water. Unpublished thesis, Stellenbosch: Stellenbosch University.

Rangeti, I and Dzwairo, BR. 2021. Umngeni basin water quality trend analysis for river health and treatability fitness. In: river basin management-sustainability issues and planning strategies. *Intechopen*.

Rorabaugh, MI, Geological, S and United States Department of the, I. 1956. Ground water in northeastern Louisville, Kentucky : With reference to induced infiltration. U.S. G.P.O., Washington, D.C.

Sami, K. 1992. Recharge mechanisms and geochemical processes in a semi-arid sedimentary basin, Eastern Cape, South Africa. *Journal of Hydrology* 139 (1): 27-48.

Scanlon, B, Tachovsky, J, Reedy, R, Nicot, J, Keese, K, Slade, R, Merwad, V, Howard, M, Wells, G and Mullins, G. 2005. Groundwater–surface water interactions in Texas. *Implications for Water Resources and Contaminant Transport (TCEQ), Bureau of Economic Geology, the University of Texas at Austin* 129-131.

Scanlon, BR, Jolly, I, Sophocleous, M and Zhang, L. 2007. Global impacts of conversions from natural to agricultural ecosystems on water resources: Quantity versus quality. *Water Resources Research* 43 (3).

Schaller, MF and Fan, Y. 2009. River basins as groundwater exporters and importers: Implications for water cycle and climate modeling. *Journal of Geophysical Research: Atmospheres* 114 (D4).

Sechu, GL, Nilsson, B, Iversen, BV, Møller, AB, Greve, MB, Troldborg, L and Greve, MH. 2022. Mapping groundwater-surface water interactions on a national scale for the stream network in Denmark. *Journal of Hydrology: Regional Studies* 40 101015.

Sloto, RA and Crouse, MY. 1996. *HYSEP:* A Computer Program for Streamflow Hydrograph Separation and Analysis. 96-4040. Reston, VA.

Sophocleous, M. 2002a. Interactions between groundwater and surface water: The state of the science. *Hydrogeology Journal* 10 52-67.

Sophocleous, M. 2002b. Interactions between groundwater and surface water: the state of the science. *Hydrogeology Journal* 10 (1): 52-67.

Stellato, L, Petrella, E, Terrasi, F, Belloni, P, Belli, M, Sansone, U and Celico, F. 2008. Some limitations in using 222Rn to assess river–groundwater interactions: the case of Castel di Sangro alluvial plain (central Italy). *Hydrogeology Journal* 16 (4): 701-712.

Strydom, S, Jewitt, GPW, Savage, MJ and Clulow, AD. 2020. Long-term trends and variability in the microclimates of the uMngeni Catchment, KwaZulu-Natal, South

Africa and potential impacts on water resources. *Theoretical and Applied Climatology* 140 (3): 1171-1184.

Strydom, T, Nel, J, Nel, M, Petersen, R and Ramjukadh, C. 2021. The use of Radon (Rn222) isotopes to detect groundwater discharge in streams draining Table Mountain Group (TMG) aquifers. *Water SA* 47 (2): 194-199.

Tadesse, E, Azagegn, T and Alemayehu, T. 2023. Characterizing groundwater and surface water interaction using geological, environmental tracers (222Rn, EC, δ18O, and δ2H) and baseflow index methods for part of the Upper Awash and the adjacent Blue Nile Basin, Ethiopia. *Journal of African Earth Sciences* 205 104992.

Thomas, R, von Brunn, V. and Marshall, C. 1990. A tectono-sedimentary model for the Dwyka Group in southern Natal, South Africa. *South African Journal of Geology* 93 (4): 809-817.

Tian, Y, Zheng, Y, Wu, B, Wu, X, Liu, J and Zheng, C. 2015. Modeling surface water-groundwater interaction in arid and semi-arid regions with intensive agriculture. *Environmental Modelling & Software* 63 170-184.

Toran, L. Groundwater–surface water interaction. In: *Encyclopedia of Water*.

Tredoux, G and Talma, A. 2006. Nitrate pollution of groundwater in southern Africa. In: *Groundwater pollution in Africa*. CRC Press.

Uhl, A, Hahn, HJ, Jäger, A, Luftensteiner, T, Siemensmeyer, T, Döll, P, Noack, M, Schwenk, K, Berkhoff, S, Weiler, M, Karwautz, C and Griebler, C. 2022. Making waves: pulling the plug - climate change effects will turn gaining into losing streams with detrimental effects on groundwater quality. *Water Research* 220 118649.

Uhlenbrook, S, Frey, M, Leibundgut, C and Maloszewski, P. 2002. Hydrograph separations in a mesoscale mountainous basin at event and seasonal timescales. *Water Resources Research* 38 (6): 31-1-31-14.

Valett, HM and Reinhold, AM. 2022. Groundwater and surface water interaction. In: eds. Mehner, T and Tockner, K, *Encyclopedia of Inland Waters (Second Edition)*. Elsevier, Oxford.

Van Tonder, G, Bardenhagen, I, Riemann, K, Van Bosch, J, Dzanga, P and Xu, Y. 2002. Manual on pumping test analysis in fractured-rock aquifers. *Water Research Commission (WRC) of South Africa, Report* 1116 (1).

Vandas, S, Winter, TC and Battaglin, WA. 2002. Water and the Environment. American Geological Institute.

Viviroli, D and Weingartner, R. 2004. The hydrological significance of mountains: from regional to global scale. *Hydrology and Earth System Sciences* 8 (6): 1017-1030.

Wang, W, Zhang, Z, Duan, L, Wang, Z, Zhao, Y, Zhang, Q, Dai, M, Liu, H, Zheng, X and Sun, Y. 2018. Response of the groundwater system in the Guanzhong Basin (central China) to climate change and human activities. *Hydrogeology journal* 26 (5): 1429-1441.

Wang, Z. 2002. Natural radiation environment in China. *International Congress Series* 1225 39-46.

Welgus, MN and Abiye, TA. 2022. Surface water and groundwater interaction in the Vredefort Dome, South Africa: a stable isotope and multivariate statistical approach. Unpublished thesis, Environmental Monitoring and Assessment.

West, AG, February, EC and Bowen, GJ. 2014. Spatial analysis of hydrogen and oxygen stable isotopes ("isoscapes") in ground water and tap water across South Africa. *Journal of Geochemical Exploration* 145 213-222.

West, C, Rosolem, R, MacDonald, AM, Cuthbert, MO and Wagener, T. 2022. Understanding process controls on groundwater recharge variability across Africa through recharge landscapes. *Journal of Hydrology* 612 127967.

Wilson, JL and Guan, H. 2004. Groundwater Recharge in a Desert Environment: The Southwestern United States. *Water Science and Application*.

Wilson, JW, Erhardt, AM and Tobin, BW. 2022. Isotopic and geochemical tracers of groundwater flow in the Shivwits Plateau, Grand Canyon National Park, USA. *Hydrogeology Journal* 30 (2): 495-510.

Winter, TC. 1999. Relation of streams, lakes, and wetlands to groundwater flow systems. *Hydrogeology Journal* 7 (1): 28-45.

Woodford, A and Chevallier, L. 2002. Hydrogeology of the Main Karoo Basin: Current knowledge and future research needs. *Water Research Commission Report No. TT* 179 (02): 482.

Xu, W, Su, X, Dai, Z, Yang, F, Zhu, P and Huang, Y. 2017. Multi-tracer investigation of river and groundwater interactions: a case study in Nalenggele River basin, northwest China. *Hydrogeology Journal* 25 (7): 2015-2029.

Yang, X, Yao, T, Yang, W, Yu, W and Qu, D. 2011. Co-existence of temperature and amount effects on precipitation δ18O in the Asian monsoon region. *Geophysical Research Letters* 38 (21).

Zega, BN, He, S and Lubis, AM. 2020. Characteristics of Stable Isotope Compositions (δ18O and δ2H) of Surface Water in Bengkulu City. *Atom Indonesia* 46 85.

8 APPENDICES

8.1 Appendix A: Stable Isotope Signals and Hydrochemistry

This appendix presents the data from stable isotopes of rainfall, groundwater, and surface water, along with the measured EC and temperature. Additionally, the calculated deuterium excess (D-excess) values are included.

Table 8.1 Stable isotope composition of rainfall from Pietermaritzburg station.

Sample code	δ^2H (‰)	$\delta^{18}O$ (‰)	Date of collection (m/d/y)	Season	Rainfall Amount (mm)	D-excess (‰)	EC	Temperature
UKZN Rainfall 1	-5.8	-2.79	3/26/2022	Summer	23.364	16.52		
UKZN Rainfall 2	8.8	-0.83	4/1/2022	Summer	0.508	15.44		
UKZN Rainfall 3	-17	-4.44	4/3/2022	Summer	5.588	18.52		
UKZN Rainfall 4	-90.9	-13.11	4/5/2022	Summer	71.12	13.98		
UKZN Rainfall 5	8.8	-2.06	4/8/2022	Summer	0.254	25.28		
UKZN Rainfall 6	-8.5	-4.52	4/10/2022	Summer	2.032	27.66		
UKZN Rainfall 7	-26.1	-5.99	4/11/2022	Summer	9.91	21.82		
UKZN Rainfall 8	-5.5	-4.15	4/12/2022	Summer	30.23	27.7		
UKZN Rainfall 9	-9.7	-4.22	4/17/2022	Summer	107.4	24.06		
UKZN Rainfall 10	-20.6	-4.96	4/19/2022	Summer	17.53	19.08		
UKZN Rainfall 11	-24.3	-4.35	4/23/2022	Summer	2.032	10.5		
UKZN Rainfall 12	-23.7	-4.92	4/25/2022	Summer	9.91	15.66		
UKZN Rainfall 13	6.6	-1.49	5/20/2022	Winter	11.682	18.52		
UKZN Rainfall 14	-30.8	-6.06	5/21/2022	Winter	2.794	17.68		

UKZN Rainfall 15	-41.4	-6.72	5/22/2022	Winter	5.588	12.36		
UKZN Rainfall 16	-1.1	-2.42	5/27/2022	Winter	59.18	18.26		
UKZN Rainfall 17	-12.6	-4.09	6/15/2022	Winter	3.048	20.12		
UKZN Rainfall 18	-30.8	-6.41	6/16/2022	Winter	8.13	20.48		
UKZN Rainfall 19	5.2	-1.38	6/23/2022	Winter	2.286	16.24		
UKZN Rainfall 20	-5.1	-2.85	7/24/2022	Winter	1.016	17.7		
UKZN Rainfall 21	36.7	4.33	7/28/2022	Winter	6.604	2.06		
UKZN Rainfall 22	17.9	-0.53	7/31/2022	Winter	0.254	22.14		
UKZN Rainfall 23	26	0.98	8/9/2022	Winter	8.128	18.16		
UKZN Rainfall 24	-0.7	-1.9	8/18/2022	Winter	14.478	14.5		
UKZN Rainfall 25	14.8	-0.23	9/4/2022	Winter	4.826	16.64		
UKZN Rainfall 26	-17	-4.75	9/20/2022	Winter	1.016	21		
UKZN Rainfall 27	-7.8	-3.04	9/21/2022	Winter	18.29	16.52		
UKZN Rainfall 28	11.9	0.15	9/28/2022	Winter	12.442	10.7		
UKZN Rainfall 29	17.3	0.94	10/6/2022	Summer	2.54	9.78		
UKZN Rainfall 30	4.4	-0.33	10/7/2022	Summer	0.508	7.04		
UKZN Rainfall 31	11.8	-0.26	10/8/2022	Summer	3.556	13.88		
UKZN Rainfall 32	29.5	4.36	10/12/2022	Summer	1.778	-5.38		
UKZN Rainfall 33	7	-1.33	10/16/2022	Summer	3.302	17.64		
UKZN Rainfall 34	1	-1.51	10/18/2022	Summer	4.064	13.08		
UKZN Rainfall 35	12.5	0.08	10/19/2022	Summer	13.46	11.86		
UKZN Rainfall 36	6.9	-1.04	10/22/2022	Summer	0.508	15.22		
UKZN Rainfall 37	9.7	-0.57	10/24/2022	Summer	13.72	14.26		
UKZN Rainfall 38	14.5	0.59	10/25/2022	Summer	5.842	9.78		
UKZN Rainfall 39	5.1	-1.34	10/26/2022	Summer	5.588	15.82		

UKZN Rainfall 40	12.6	-0.78	10/27/2022	Summer	5.588	18.84		
UKZN Rainfall 41	15.4	2.11	10/28/2022	Summer	1.524	-1.48		
UKZN Rainfall 42	-6.9	-3.04	10/29/2022	Summer	9.91	17.42		
UKZN Rainfall 43	12.9	-1.44	10/31/2022	Summer	6.858	24.42		
UKZN Rainfall 44	7.8	-1.41	11/1/2022	Summer	1.27	19.08		
UKZN Rainfall 45	-13.3	-4.14	11/2/2022	Summer	2	19.82		
UKZN Rainfall 46	-1.6	-2.05	11/3/2022	Summer	1.302	14.8		
UKZN Rainfall 47	9.7	-0.49	11/4/2022	Summer	2.286	13.62		
UKZN Rainfall 48	-22.3	-4.37	11/6/2022	Summer	15.24	12.66		
UKZN Rainfall 49	-1.1	-2.39	11/7/2022	Summer	0.254	18.02		
UKZN Rainfall 50	-18.2	-3.32	11/8/2022	Summer	2.032	8.36		
UKZN Rainfall 51	8.3	0.83	11/9/2022	Summer	5.842	1.66		
UKZN Rainfall 52	10.1	-0.35	11/10/2022	Summer	16.385	12.9		
UKZN Rainfall 53	11.9	-0.39	11/11/2022	Summer	16.385	15.02		
UKZN Rainfall 54	14.2	-0.32	11/13/2022	Summer	1.524	16.76		
UKZN Rainfall 55	11.6	0.91	11/14/2022	Summer	8.13	4.32		
UKZN Rainfall 56	11.7	-0.47	11/17/2022	Summer	2.286	15.46		
UKZN Rainfall 57	4	-1.57	11/18/2022	Summer	0.508	16.56		
UKZN Rainfall 58	8.4	-1.49	11/19/2022	Summer	1.778	20.32		
UKZN Rainfall 59	-6.8	-3.33	11/20/2022	Summer	1.016	19.84		
UKZN Rainfall 60	2.4	-2.42	11/23/2022	Summer	10.16	21.76		
UKZN Rainfall 61	8.5	-1.57	11/25/2022	Summer	10.92	21.06		
UKZN Rainfall 62	2.8	-1.91	11/26/2022	Summer	2.794	18.08		
UKZN Rainfall 63	7.6	-1.38	11/27/2022	Summer	18.54	18.64		
UKZN Rainfall 64	-3.7	-2.43	11/28/2022	Summer	1.524	15.74		

UKZN Rainfall 65	9.1	-0.15	11/29/2022	Summer	1.27	10.3		
UKZN Rainfall 66	18.5	1.04	12/5/2022	Summer	1.016	10.18		
UKZN Rainfall 67	-4	-2.11	12/6/2022	Summer	4.064	12.88		
UKZN Rainfall 68	0.1	-1.62	12/8/2022	Summer	15.49	13.06		
UKZN Rainfall 69	2.7	-0.94	12/9/2022	Summer	0.254	10.22		
UKZN Rainfall 70	-8.2	-2.41	12/11/2022	Summer	8.638	11.08		
UKZN Rainfall 71	5.4	-1.32	12/12/2022	Summer	4.318	15.96		
UKZN Rainfall 72	-8	-2.56	12/13/2022	Summer	30.48	12.48		
UKZN Rainfall 73	0.6	-1.63	12/14/2022	Summer	17.27	13.64		
UKZN Rainfall 74	6.8	-1.51	12/15/2022	Summer	1.016	18.88		
UKZN Rainfall 75	6.8	-2.02	12/17/2022	Summer	15.244	22.96		
UKZN Rainfall 76	-8	-2.57	12/18/2022	Summer	14.99	12.56		
UKZN Rainfall 77	0.6	-1.69	12/19/2022	Summer	13.97	14.12		
UKZN Rainfall 78	6.7	-1.92	12/20/2022	Summer	2.032	22.06		
UKZN Rainfall 79	7.1	-2.12	12/21/2022	Summer	6.35	24.06		
UKZN Rainfall 80	8	-1.97	12/22/2022	Summer	8.89	23.76		
UKZN Rainfall 81	-24.8	-5.29	12/26/2022	Summer	5.08	17.52		
UKZN Rainfall 82	-2.5	-2.45	1/3/2023	Summer	83.556	17.1		
UKZN Rainfall 83	10.1	-0.57	1/4/2023	Summer	6.858	14.66		
UKZN Rainfall 84	15.1	-0.37	1/5/2023	Summer	0.254	18.06		
UKZN Rainfall 85	-16.3	-4.43	1/6/2023	Summer	33.53	19.14		
UKZN Rainfall 86	-18.1	-5.08	1/7/2023	Summer	13.715	22.54		
UKZN Rainfall 87	-17.6	-4.83	1/8/2023	Summer	12	21.04		
UKZN Rainfall 88	9.2	-1.53	1/26/2023	Summer	1.715	21.44		
UKZN Rainfall 89	6.6	-1.15	1/29/2023	Summer	0.508	15.8		

UKZN Rainfall 90	12.1	-1.39	1/30/2023	Summer	14.73	23.22		
UKZN Rainfall 91	7.5	-2.51	1/31/2023	Summer	4.318	27.58		
UKZN Rainfall 92	6.9	-1.69	2/1/2023	Summer	10.67	20.42		
UKZN Rainfall 93	-12.3	-3.59	2/2/2023	Summer	1.27	16.42		
UKZN Rainfall 94	0.3	-1.95	2/8/2023	Summer	9.144	15.9		
UKZN Rainfall 95	-8	-2.62	2/9/2023	Summer	6.096	12.96		
UKZN Rainfall 96	-50.6	-7.21	2/10/2023	Summer	9.65	7.08		
UKZN Rainfall 97	-31.7	-4.6	2/11/2023	Summer	1.27	5.1		
UKZN Rainfall 98	-47.1	-6.92	2/12/2023	Summer	4.826	8.26		
UKZN Rainfall 99	-65.3	-9.33	2/13/2023	Summer	19.56	9.34		
UKZN Rainfall 100	-44.1	-6.74	2/14/2023	Summer	17.78	9.82		
UKZN Rainfall 101	-43.4	-6.53	2/15/2023	Summer	0.254	8.84		
UKZN Rainfall 102	-23.7	-4.27	2/16/2023	Summer	2.286	10.46		
UKZN Rainfall 103	-9.9	-2.56	2/17/2023	Summer	1.778	10.58		
UKZN Rainfall 104	-16.9	-3.7	2/18/2023	Summer	4.318	12.7		
UKZN Rainfall 105	-37.3	-6.27	2/19/2023	Summer	19.3	12.86		
UKZN Rainfall 106	2.3	-1.85	2/26/2023	Summer	0.254	17.1		
UKZN Rainfall 107	8.8	-1.41	2/27/2023	Summer	1.27	20.08		
UKZN Rainfall 108	-15.1	-3.5	2/28/2023	Summer	2.794	12.9		
UKZN Rainfall 109	8	-0.9	3/5/2023	Summer	11.18	15.2		
UKZN Rainfall 110	10.9	-0.32	3/11/2023	Summer	6.096	13.46		
UKZN Rainfall 111	19.8	1.08	3/13/2023	Summer	12.196	11.16		
UKZN Rainfall 112	-2.1	-2.36	3/18/2023	Summer	0.508	16.78		
UKZN Rainfall 113	19.7	1.79	3/21/2023	Summer	16.76	5.38		
UKZN Rainfall 114	8.5	-1.08	3/25/2023	Summer	6.604	17.14		

UKZN Rainfall 115	-5.8	-2.69	3/27/2023	Summer	0.508	15.72		
UKZN Rainfall 116	8.6	-1.23	3/31/2023	Summer	6.604	18.44		
UKZN Rainfall 117	-29.3	-5.29	4/4/2023	Summer	0.508	13.02		
UKZN Rainfall 118	5.3	-1.06	4/9/2023	Summer	12.19	13.78		
UKZN Rainfall 119	0.1	-1.86	4/11/2023	Summer	3.81	14.98		
UKZN Rainfall 120	2.4	-1.61	4/20/2023	Summer	0.254	15.28		
UKZN Rainfall 121	-4.4	-2.2	4/26/2023	Summer	5.334	13.2		
UKZN Rainfall 122	-4	-2.85	4/30/2023	Summer	0.254	18.8		
UKZN Rainfall 123	8.8	-0.75	5/3/2005	Winter	4.318	14.8		
UKZN Rainfall 124	13	-0.21	5/4/2023	Winter	4.826	14.68		
UKZN Rainfall 125	14.1	-0.04	5/5/2023	Winter	0.254	14.42		
UKZN Rainfall 126	-17.7	-4.35	5/8/2023	Winter	0.508	17.1		
UKZN Rainfall 127	-21.8	-5.07	5/11/2023	Winter	9.148	18.76		
UKZN Rainfall 128	-19.9	-4.24	5/14/2023	Winter	0.762	14.02		
UKZN Rainfall 129	-48.8	-8.39	5/15/2023	Winter	5.588	18.32		
UKZN Rainfall 130	-30.9	-6.46	5/17/2023	Winter	0.508	20.78		
UKZN Rainfall 131	-25.2	-5.94	5/19/2023	Winter	10.16	22.32	10	
UKZN Rainfall 132	-32.5	-6.59	5/22/2023	Winter	22.61	20.22		
UKZN Rainfall 133	-19.7	-5.05	5/26/2023	Winter	0.254	20.7		
UKZN Rainfall 134	18.2	0.1	5/31/2023	Winter	0.254	17.4		
UKZN Rainfall 135	9.6	-1.83	6/2/2023	Winter	0.254	24.24		
UKZN Rainfall 136	-1.2	-2.29	6/27/2023	Winter	0.254	17.12		
UKZN Rainfall 137	0.8	-2.35	7/10/2023	Winter	0.254	19.6		
UKZN Rainfall 138	-0.2	-2.59	7/12/2023	Winter	0.254	20.52		
UKZN Rainfall 139	-12.1	-4.06	7/14/2023	Winter	10.41	20.38		

UKZN Rainfall 140	1.3	-2.11	7/20/2023	Winter	0.254	18.18		
UKZN Rainfall 141	13.7	-0.46	7/25/2023	Winter	0.254	17.38		
UKZN Rainfall 142	1.1	-2.28	8/24/2023	Winter	1.016	19.34		
UKZN Rainfall 143	-29.8	-6.08	9/1/2023	Winter	7.366	18.84		
UKZN Rainfall 144	6.6	-1.36	9/6/2023	Winter	0.508	17.48		
UKZN Rainfall 145	11	0.48	9/14/2023	Winter	1.27	7.16		
UKZN Rainfall 146	5.7	-0.93	9/16/2023	Winter	2.032	13.14		
UKZN Rainfall 147	12.2	-1.29	9/18/2023	Winter	1.27	22.52		
UKZN Rainfall 148	7.1	-0.29	9/24/2023	Winter	0.254	9.42	163	19.4
UKZN Rainfall 149	8.2	-2.1	9/28/2023	Winter	0.254	25	70	18.5
UKZN Rainfall 150	4.3	-2.08	10/2/2023	Summer	0.254	20.94	156	29.3
UKZN Rainfall 151	8.7	-1.12	10/9/2023	Summer	0.508	17.66	251	19.3
UKZN Rainfall 152	17.7	0.75	10/12/2023	Summer	3.048	11.7		
UKZN Rainfall 153	-6.3	-2.84	10/13/2023	Summer	0.254	16.42	18	19.7
UKZN Rainfall 154	-23.9	-3.74	10/16/2023	Summer	20.574	6.02	26	16
UKZN Rainfall 155	-58.6	-8.45	10/17/2023	Summer	7.366	9	16	18.9
UKZN Rainfall 156	-30.6	-5.5	10/22/2023	Summer	40.898	13.4	51	15.8
UKZN Rainfall 157	0.9	-0.76	10/28/2023	Summer	25.65	6.98	67	15.4
UKZN Rainfall 158	-19.3	-4.54	10/29/2023	Summer	33.78	17.02	39	12.1
UKZN Rainfall 159	-20.5	-4.93	10/31/2023	Summer	13.972	18.94		
UKZN Rainfall 160	-15.2	-4.58	11/1/2023	Summer	4.572	21.44	90	16.1
UKZN Rainfall 161	-2.7	-3.24	11/5/2023	Summer	7.874	23.22		
UKZN Rainfall 162	9	-0.84	11/6/2023	Summer	0.254	15.72	92	32.9
UKZN Rainfall 163	14.3	0.35	11/7/2023	Summer	5.08	11.5	8	21.6
UKZN Rainfall 164	3.1	-0.56	11/8/2023	Summer	0.254	7.58	36	18.0

UKZN Rainfall 165	9.7	-1.32	11/9/2023	Summer	9.4	20.26		
UKZN Rainfall 166	17.7	0.96	11/12/2023	Summer	0.762	10.02		
UKZN Rainfall 167	19.8	1.31	11/13/2023	Summer	1.27	9.32		
UKZN Rainfall 168	11.4	-1.56	11/14/2023	Summer	0.508	23.88		
UKZN Rainfall 169	22.5	1.62	11/19/2023	Summer	3.556	9.54	38	30.0
UKZN Rainfall 170	13.2	0.2	11/26/2023	Summer	8.636	11.6		
UKZN Rainfall 171	18.1	1.16	11/29/2023	Summer	5.588	8.82		
UKZN Rainfall 172	16.8	-0.19	12/4/2023	Summer	10.418	18.32		
UKZN Rainfall 173	11.5	-1.78	12/6/2023	Summer	20.83	25.74		
UKZN Rainfall 174	1.2	-1.99	12/7/2023	Summer	27.686	17.12		
UKZN Rainfall 175	2.2	-1.91	12/10/2023	Summer	16.51	17.48		
UKZN Rainfall 176	2.8	-2.31	12/11/2023	Summer	0.254	21.28		
UKZN Rainfall 177	-0.1	-2.66	12/16/2023	Summer	31.498	21.18		
UKZN Rainfall 178	7	-1.54	12/19/2023	Summer	16.51	19.32		
UKZN Rainfall 179	-4.5	-1.78	12/24/2023	Summer	1.27	9.74		
UKZN Rainfall 180	-14.8	-3.45	12/25/2023	Summer	6.604	12.8		
UKZN Rainfall 181	4.4	-2.17	12/26/2023	Summer	15.75	21.76		
UKZN Rainfall 182	13.8	-0.96	12/27/2023	Summer	18.54	21.48		
UKZN Rainfall 183	-16.5	-4.01	12/31/2023	Summer	10.16	15.58		
UKZN Rainfall 184	15.3	-1.16	1/1/2024	Summer	5.842	24.58		
UKZN Rainfall 185	12.3	-0.32	1/4/2024	Summer	10.414	14.86		
UKZN Rainfall 186	2	-1.91	1/5/2024	Summer	1.524	17.28		
UKZN Rainfall 187	9.5	-0.56	1/8/2024	Summer	0.254	13.98		

UKZN Rainfall 188	9.2	-0.19	1/9/2024	Summer	2.54	10.72		
UKZN Rainfall 189	-12.3	-3.42	1/10/2024	Summer	32.77	15.06		
UKZN Rainfall 190	-10.5	-3.2	1/11/2024	Summer	0.762	15.1		
UKZN Rainfall 191	-27.1	-5.18	1/12/2024	Summer	4.572	14.34		
UKZN Rainfall 192	-0.5	-1.93	1/15/2024	Summer	34.792	14.94		
UKZN Rainfall 193	4.6	-1.19	1/16/2024	Summer	7.62	14.12	26	27.6
UKZN Rainfall 194	-12	-3.61	1/17/2024	Summer	1.016	16.88	2	17.3
UKZN Rainfall 195	-11.2	-3.18	1/28/2024	Summer	30.228	14.24		
UKZN Rainfall 196	10.5	0.63	2/4/2024	Summer	2.794	5.46		
UKZN Rainfall 197	15.2	0.68	2/5/2024	Summer	0.254	9.76		
UKZN Rainfall 198	3.1	-1.43	2/6/2024	Summer	5.588	14.54	85	28.3

Table 8.2: The stable isotope composition of rainfall from Howick station.

Sample code	δ^2H (‰)	$\delta^{18}O$ (‰)	Date of collection (m/d/y)	Rainfall Amount (mm)	D-excess (‰)	EC
Howick Rainfall 1	-47.3	-7.34	2/23/2023	236.71	11.42	
Howick Rainfall 2	5	-1.47	3/23/2023	97.01	16.76	
Howick Rainfall 3	-9.9	-3.37	5/5/2023	109.74	17.06	29
Howick Rainfall 4	-20.4	-5.02	7/14/2023	113.01	19.76	22
Howick Rainfall 5	5.3	-1.66	8/17/2023	11.68	18.58	86
Howick Rainfall 6	43.3	7.75	9/13/2023	17.26	-18.7	306
Howick Rainfall 7	37.2	6.75	10/13/2023	76.2	-16.8	365
Howick Rainfall 8	-26	-4.81	11/17/2023	176.1	12.48	9
Howick Rainfall 9	4.9	-2.82	12/20/2023	226.84	27.46	
Howick Rainfall 10	-5.9	-2.66	1/16/2024	231.91	15.38	

Table 8.3 Stable isotope composition of rainfall from Durban station.

Sample code	δ^2H (‰)	$\delta^{18}O$ (‰)	Date of collection (m/d/y)	Rainfall Amount (mm)	D-excess (‰)	EC
Durban Rainfall 1	-35.5	-5.7	3/7/2023	148.6	10.1	
Durban Rainfall 2	4.1	-1.15	3/29/2023	56.1	13.3	
Durban Rainfall 3	-0.8	-2.28	5/5/2023	112.6	17.44	445
Durban Rainfall 4	-9.8	-3.6	6/29/2023	158.2	19	1124
Durban Rainfall 5	4.8	-2	8/25/2023	19.6	20.8	
Durban Rainfall 6	14.1	0.76	10/13/2023	20.8	8.02	1647
Durban Rainfall 7	-16.4	-3.68	11/3/2023	155.4	13.04	436
Durban Rainfall 8	12.5	-0.49	12/8/2023	103.6	16.42	292
Durban Rainfall 9	-8.2	-2.84	1/16/2024	288.2	14.52	122

Table 8.4 Stable isotope composition of groundwater (Springs and boreholes) wet season.

Sample code	Water Type	Longitude	Latitude	Elevation (m)	Collection date (m/d/y)	$\delta^{18}O$	δ^2H	EC	Temperature
Umgeni river Spring 1	Spring	30.8641	-29.716	165	3/7/2023	-2.91	-9.6	535	25.1
Umgeni River Spring 2	Spring	30.8515	-29.706	236	3/7/2023	-2.79	-9.1	425	25.4
Umgeni River Spring 3	Spring	30.7238	-29.652	404	3/7/2023	-1.42	-4.1	186	27.2
Umgeni River Spring 4	Spring	30.7198	-29.656	367	3/7/2023	-2.68	-9.1	95	24.1
Umgeni River Spring 5 A	Spring	30.713	-29.659	363	3/7/2023	-2.66	-9.1	125	25
Karkloof River Spring 1	Spring	30.3314	-29.311	1150	3/14/2023	-3.3	-9.3	90	18.4
Umgeni river spring 5 B	Spring	29.8972	-29.487	1445	3/30/2023	-3.69	-12.6	55	16.5
Umgeni river spring 6	Spring	29.8814	-29.474	1534	3/30/2023	-3.67	-12.9	38	13.9
Umgeni river spring 7	Spring	29.8743	-29.467	1748	3/30/2023	-3.77	-12.4	29	15.6

Umgeni River Spring 8	Spring	29.9058	-29.491	1403	3/30/2023	-3.29	-11	30	16.4
Ukulinga Spring	Spring	30.403	-29.661	776	4/4/2023	-2.35	-7.4	1012	20.66
Ukulinga Borehole 1	Borehole	30.4028	-29.661	777	2/27/2023	-2.19	-7.1	928	20.15
Umgeni River Borehole	Borehole	29.902	-29.498	1480	3/30/2023	-3.55	-13.6	96	17.99
Ukzn borehole 1	Borehole	30.4035	-29.628	672	4/19/2023	-2.71	-9.1	128	22.9
Ukzn borehole 2	Borehole	30.4035	-29.628	672	4/20/2023	-2.74	-8.5	153	22.37
Ukzn borehole 3	Borehole	30.4035	-29.628	672	4/21/2023	-2.74	-7.4	183	22.7
Ukzn borehole 4	Borehole	30.4035	-29.628	672	4/24/2023	-2.6	-8.5	177	24.2
Ukzn borehole 5	Borehole	30.4035	-29.628	672	4/26/2023	-2.57	-8.3	204	23.1

Table 8.5: Stable isotope compositions, EC and temperature of surface waters in the wet season.

Sample code	Water Type	Longitude	Latitude	Elevation (m)	Collection Date (m/d/y)	$\delta^{18}O$	$\delta^{2}H$	EC	Temp
Umgeni River Point 1	Stream	31.0183	-29.809	10	3/7/2023	-2.15	-6	95	28.0
Umgeni River Point 2	Stream	30.9803	-29.803	12	3/7/2023	-2.34	-6.9	187	25.0
Umgeni River point 3	Stream	30.8688	-29.716	102	3/7/2023	-2.32	-7	155	26.0
Umgeni River Point 4	Stream	30.797	-29.649	171	3/7/2023	-2.3	-6.4	174	26.0
Umgeni River point 5	Stream	30.7447	-29.648	180	3/7/2023	-2.26	-6.3	164	27.0
Umgeni River point 6	Stream	30.6837	-29.651	259	3/7/2023	-2.38	-6.6	154	26.9
Umgeni River Point 7	Stream	30.328	-29.441	683	3/13/2023	-2.77	-9	93	21.5
Umgeni River Point 8	Stream	30.3438	-29.437	706	3/13/2023	-2.6	-5.3	77	20.0
Umgeni River Point 9	Stream	30.373	-29.374	692	3/13/2023	-2.96	-6.7	96	20.1
Karkloof River Point 1-1	Stream	30.2791	-29.378	1071	3/13/2023	-3.12	-9.2	72	21,4
Karkloof River Point 2	Stream	30.2743	-29.366	1071	3/13/2023	-1.92	-5.7	53	29,6
Karkloof River Point 3-1	Stream	30.2722	-29.34	1078	3/13/2023	-3.28	-10	87	21,25
Karkloof River Point 4	Stream	30.2579	-29.375	1080	3/13/2023	-2.75	-8.6	70	24,8

Karkloof River Point 5	Stream	30.2289	-29.353	1107	3/13/2023	-2.58	-7.6	62	25,2
Karkloof River Point 6-1	Stream	30.1996	-29.333	1118	3/13/2023	-3.48	-12.7	96	20,9
Karkloof River Point 7	Stream	30.2623	-29.323	1165	3/14/2023	-3.83	-11.7	39	17,1
Lions River Point 1	Stream	30.3054	-29.193	1346	3/14/2023	-1.75	-6.4	310	21.0
Umgeni River Point 10	Stream	30.0744	-29.492	1162	3/14/2023	-2.77	-8	91	21,76
Umgeni River Point 11	Stream	29.9499	-29.455	1418	3/14/2023	-3.29	-10.1	95	25,75
Lions River Point 2	Stream	29.936	-29.444	1418	3/14/2023	-2.92	-10.6	110	23,3
Lions River Point 3	Stream	29.9344	-29.437	1418	3/14/2023	-2.87	-10.3	70	23,8
Lions River Point 4	Stream	29.9279	-29.417	1456	3/14/2023	-3.56	-12.3	55	21,36
Lions River Point 5	Stream	29.9424	-29.577	1472	3/14/2023	-3.38	-11	55	18,52
Lions River Point 6	Stream	29.959	-29.397	1472	3/14/2023	-3.09	-9.6	93	22,45
Lions River Point 7	Stream	30.0199	-29.442	1347	3/14/2023	-2.94	-9.2	78	23,96
Lions River Point 8	Stream	30.2018	-29.5	1029	3/14/2023	-2.65	-8.5	80	23,6
Karkloof River Point 9	Stream	30.2757	-29.364	1069	3/23/2023	-3.27	-8.7	80	22,4
Karkloof River Point 10	Stream	30.2767	-29.363	1071	3/23/2023	-2.72	-7.9	75	22,2
Karkloof River Point 11	Stream	30.279	-29.359	1071	3/23/2023	-3.3	-10.1	81	22,4
Karkloof River Point 12	Stream	30.2836	-29.356	1072	3/23/2023	-3.21	-10.1	74	21,6
Karkloof River Point 13	Stream	30.1886	-29.327	1157	3/23/2023	-3.49	-12.5	93	20,1
Karkloof River Point 14	Stream	30.169	-29.319	1173	3/23/2023	-3.29	-12.3	99	20,33
Karkloof River Point 15	Stream	30.148	-29.3	1235	3/23/2023	-3.6	-13.9	101	21,16
Karkloof River Point 16	Stream	30.136	-29.293	1238	3/23/2023	-3.86	-13.2	92	24,44
Karkloof River Point 3-2	Stream	30.2722	-29.34	1077	3/23/2023	-1.14	9.3	88	21,26
Karkloof River Point 6-2	Stream	30.1996	-29.333	1106	3/23/2023	-3.6	-13.5	93	20,77
Karkloof River Point 8-2	stream	30.3238	-29.31	1127	3/23/2023	-3.52	-11.1	60	21,57
Lions River Point 9	Stream	30.152	-29.463	1055	3/30/2023	-2.57	-7.7	95	18,5
Umgeni River Point 12	Stream	29.988	-29.495	1304	3/30/2023	-3.07	-11.2	53	17,5
Umgeni River point 13	Stream	29.8875	-29.477	1478	3/30/2023	-3.18	-12.1	30	15,61
Umgeni River point 14	Stream	29.887	-29.485	1492	3/30/2023	-3.17	-10.7	45	15,56
Umgeni river point 15	Stream	29.9042	-29.49	1406	3/30/2023	-3.57	-11.7	32	16,61
Lions River Point 10	Stream	30.1585	-29.436	1066	3/30/2023	-2.55	-8	84	17,95

Bisley stream	Stream	30.3887	-29.659	709	4/4/2023	-2.46	-8.3	617	20,5
Umgeni River below albert falls	Stream	30.4739	-29.472	599	4/6/2023	-2.41	-7.3	128	22,9
Umgeni River Lake 1	Wetland	30.3529	-29.429	692	3/13/2023	-1.75	-2.8	88	26,8
Lions River Wetland	Wetland	29.9161	-29.421	1467	3/14/2023	-3.27	-11	20	22,05
Lions Riner Wetland 2	Wetland	29.9933	-29.38	1472	3/14/2023	-2.78	-7.9	51	21,15
Karkloof River Wetland	Wetland	30.275	-29.364	1067	3/23/2023	-2.35	-7.1	84	24,7
Umgeni river lake	Weland	29.8682	-29.474	1798	3/30/2023	-3.15	-10.1	33	17,11
Umgeni River Wetland	Wetland	29.8317	-29.479	1824	3/30/2023	-3.36	-11.9	29	15,28
Umgeni River wetland 2	Wetland	29.864	-29.474	1790	3/30/2023	-3.33	-9.7	18	15,06
Bisley wetland	Wetland	30.3887	-29.658	708	4/4/2023	-2.41	-8.3	612	21,6

Table 8.6: The stable isotope composition of groundwater (Springs and boreholes) dry season

Sample code	Water Type	Longitude	Latitude	Elevation (m)	Collection date (m/d/y)	$\delta^{18}O$ (‰)	$\delta^{2}H$ (‰)	EC	Temperature
Ukzn borehole 6	Borehole	30.4035	-29.628	675	5/2/2023	-2.55	-8.2	174	23,17
Ukzn borehole 7	Borehole	30.4035	-29.628	675	5/3/2023	-2.56	-8.2	184	21,7
Ukzn borehole 8	Borehole	30.4035	-29.628	675	5/4/2023	-2.54	-8.1	174	22,7
Ukzn borehole 9	Borehole	30.4035	-29.628	675	5/5/2023	-2.51	-8.3	143	22,4
Ukzn borehole 10	Borehole	30.4035	-29.628	675	5/8/2023	-2.51	-8.1	180	22,9
Ukzn borehole 11	Borehole	30.4035	-29.628	675	5/9/2023	-2.6	-8.6	134	22,3
Ukzn borehole 12	Borehole	30.4035	-29.628	675	5/10/2023	-2.57	-8.2	154	21,5
Ukzn borehole 13	Borehole	30.4035	-29.628	675	5/11/2023	-2.6	-8.5	183	22,6
Ukzn borehole 14	Borehole	30.4035	-29.628	675	5/12/2023	-2.5	-8.3	123	22,8
Ukzn borehole 16	Borehole	30.4035	-29.628	675	5/15/2023	-2.33	-8.4	157	157
Ukzn borehole 17	Borehole	30.4035	-29.628	675	5/16/2023	-2.32	-8.2	128	22,1
Ukzn borehole 18	Borehole	30.4035	-29.628	675	5/17/2023	-2.28	-8.3	119	22,3

Ukzn borehole 19	Borehole	30.4035	-29.628	675	5/19/2023	-2.75	-10	145	21,4
Ukzn borehole 20	Borehole	30.4035	-29.628	675	5/26/2023	-2.34	-7.8	121	19,5
Ukzn borehole 21	Borehole	30.4035	-29.628	675	6/3/2023	-2.42	-8	114	20,4
Ukzn borehole 22	Borehole	30.4035	-29.628	675	6/30/2023	-2.36	-9.1	678	22
Westfalia Spring	Spring	30.262	-29.45	1194	8/17/2023	-2.52	-8.2	68	17.9
Umgeni River Spring 1	Spring	29.8814	-29.474	1473	8/18/2023	-3.2	-12.4	38	18.2
Umgeni River Spring 2	Spring	29.872	-29.469	1762	8/18/2023	-3.34	-11.5	52	14.9
Umgeni River Spring 3	Spring	29.88	-29.474	1553	8/18/2023	-3.31	-12.5	115	14.1
Umgeni River Spring 4	Spring	30.8641	-29.716	176	8/29/2023	-1.95	-4.3	625	17.9
Umgeni River Spring 5	Spring	30.8515	-29.706	238	8/29/2023	-0.35	-1.6	374	25.3
Umgeni spring 6	Spring	30.7198	-29.656	400	8/29/2023	-1.45	-1.6	177	16.9
Karkloof river spring 1	Spring	30.2884	-29.354	1086	9/11/2023	-3.08	-11.3	68	16.6
Westfalia Fruit Borehole	Borehole	30.2646	-29.451	1133	8/17/2023	-2.74	-7.8	112	18.9
Ukzn Borehole	Borehole	30.4035	-29.628	675	8/24/2023	-2.61	-9	553	22.1
Ukulinga Borehole	Borehole	30.4028	-29.661	780	8/30/2023	-1.8	-7.2	813	20
Umgeni Borehole UCL Farm	Borehole	30.329	-29.363	1073	8/31/2023	-3.18	-8.5	166	19.2
Umgeni Borehole Khayalami	Borehole	30.3768	-29.419	696	8/31/2023	-2.33	-8.1	522	20.8
Umgeni Borehole Sinkle farm	Borehole	30.0575	-29.492	1180	9/6/2023	-2.29	-9.1	162	17.8
Lions river borehole Johnson/ Sardan Farm 1	Borehole	30.0206	-29.442	1336	9/6/2023	-3.3	-14	153	19.6
Karkloof borehole by wetland	Borehole	30.2791	-29.355	1075	9/11/2023	-2.33	-7.9	113	18.8
Howick Borehole	Borehole	30.2646	-29.451	1133	9/13/2023	-2.88	-9.3	207	15.6
Borehole Sinkle Farm 2	Borehole	30.0575	-29.492	1180	9/13/2023	-1.95	-8.9	164	18.8
Ukzn Borehole	Borehole	30.4035	-29.628	675	9/14/2023	-2.3	-6	379	18

Borehole KwaNdlovu	Borehole	30.2299	-29.349	1116	9/15/2023	-3.63	-14.8	204	17.8
Borehole Thanon Farm	Borehole	30.2237	-29.347	1115	9/15/2023	-2.36	-8	526	21
Ukzn Borehole	Borehole	30.4035	-29.628	675	10/2/2023	-2.48	-7.8	485	23.1
Ukzn Borehole	Borehole	30.4035	-29.628	675	10/9/2023	-2.51	-9.1	500	21.6
Durban DUT Borehole	Borehole	31.0059	-29.852	21	10/13/2023	-2.06	-5.1	561	24.1
Umgeni Vlei borehole	Borehole	29.8974	-29.488	1469	10/13/2023	-3.58	-13.7	222	18.5

Table 8.7: Stable isotope composition, EC and temperature of surface waters in the dry season.

Sample code	Water Type	Longitude	Latitude	Elevation (m)	Collection Date (m/d/y)	$\delta^{18}O$ (‰)	$\delta^{2}H$ (‰)	EC	Temp
Karkloof point 1 below wetland	Stream	30.27914	-29.378	1069	8/17/2023	-2.79	-8.9	108	16.5
Karkloof point 3	Stream	30.27	-29.365	1069	8/17/2023	-2.25	-7.1	104	17.3
Karkloof point 4	Stream	30.2763	-29.363	1070	8/17/2023	-1.74	-6.2	110	17.2
Karkloof point 5	Stream	30.27	-29.359	1069	8/17/2023	-2.85	-10.5	120	16.5
Umgeni River Point 1	Stream	29.9148	-29.416	1473	8/18/2023	-3.45	-11.6	70	12.5
Umgeni Point 2 Mouth	Stream	31.01828	-29.809	1	8/29/2023	-1.62	-4.5	4000	20.9
Umgeni Point 3 Mine	Stream	30.98029	-29.803	36	8/29/2023	-1.1	-4.3	380	20.8
Inanda Outlet	Stream	30.8688	-29.716	104	8/29/2023	-1.79	-6	250	19.1
Umgeni river Inanda inlet	Stream	30.797	-29.649	167	8/29/2023	-2.06	-6.2	365	19.2
Umgeni river point 8	Stream	30.7447	-29.648	165	8/29/2023	-1.84	-5.5	383	22.9
Umgeni River point 9 Last bridge	Stream	30.6837	-29.651	270	8/29/2023	-0.97	-2.6	365	18.8
Ukulinga Stream	Stream	30.403	-29.661	772	8/30/2023	-1.53	-4.9	243	21.3
Bisley stream	Stream	30.38873	-29.659	711	8/30/2023	-1.91	-6.6	634	19
Umgeni river point 10	Stream	30.4739	-29.472	600	8/31/2023	-1.99	-6.4	168	16.4
Umgeni River Point 11 Albrt falls Outlet	Stream	30.43238	-29.433	623	8/31/2023	-2.16	-6.7	103	15.9
Umgeni river point 12	Stream	30.3736	-29.374	751	8/31/2023	-2.51	-5.5	129	16
Umgeni River point 13	Stream	30.427	-29.35	729	8/31/2023	-2.37	-6.5	109	16.3
Umgeni River point 14	Stream	30.338132	-29.437	684	8/31/2023	-2.63	-5.8	82	16.7

Umgeni River Point 15	Stream	30.33	-29.44	685	8/31/2023	-1.44	-2.9	101	15.9
Umgeni River Point 16	Stream	30.33	-29.441	673	8/31/2023	-1.57	-4.6	138	17.3
Midmar dam outlet	Stream	30.20227	-29.493	1026	9/6/2023	-2.48	-6.6	94	13.7
Umgeni river Point 17	Stream	30.0744	-29.492	1164	9/6/2023	-2.4	-6.3	128	14.4
Umgeni River point 18	Stream	29.9499	-29.455	1420	9/6/2023	-2.81	-9.9	94	12.8
Lions River point 1	Stream	29.936	-29.444	1420	9/6/2023	-1.61	-3.8	113	14
Lions River point 2	Stream	29.9344	-29.437	1438	9/6/2023	-1.25	-3.2	82	14.1
Lions River Point 3	Stream	29.9279	-29.417	1456	9/6/2023	-2.62	-7.9	65	15
Lions River Point 4	Stream	29.959	-29.397	1432	9/6/2023	-2.39	-8.8	69	15.5
Lions River point 5	Stream	30.0199	-29.442	1336	9/6/2023	-1.8	-5.5	106	15.8
Lions River Point 6	Stream	30.15846	-29.436	1066	9/7/2023	-1.13	-3.9	126	18.3
Lions River Point 7	Stream	30.0459	-29.405	1282	9/7/2023	-2.01	-6.1	125	20.74
Lions River Point 8	Stream	30.0459	-29.405	1282	9/7/2023	-3	-10.7	81	16.2
Umgeni River Point 19	Stream	29.94178	-29.451	1417	9/7/2023	-1.79	-5.2	133	19.1
Umgeni River Point 20	Stream	29.95048	-29.455	1421	9/7/2023	-2.53	-10.1	94	17.7
Umgeni River Point 21	Stream	30.05357	-29.489	1187	9/7/2023	-1.91	-5.8	110	18.4
Umgeni point 22 (Karkloof)	Stream	30.2756	-29.364	1071	9/11/2023	-1.02	-3.2	130	17.1
Umgeni point 23 (Karkloof)	Stream	30.2832	-29.356	1069	9/11/2023	-2.35	-7.2	106	17.9
Karkloof point 6 (Yarrow joining Karkloof)	Stream	30.28623	-29.348	1074	9/11/2023	-2.37	-7.8	101	17.9
Karkloof point 7	Stream	30.27744	-29.362	1070	9/11/2023	-1.51	-3.4	117	18.5
Karkloof point 8 before tribute	Stream	30.27744	-29.362	1070	9/12/2023	-1.3	-3.7	123	12.7
Karkloof point 9	Stream	30.26256	-29.326	1083	9/12/2023	-3.33	-10.7	50	11.5
Karkloof point 10	Stream	30.26794	-29.328	1103	9/12/2023	-3.51	-10.7	70	12
Karkloof point 11	Stream	30.27001	-29.331	1110	9/12/2023	-2.94	-9.2	54	13.6
Karkloof point 12	Stream	30.27122	-29.334	1092	9/12/2023	-2.02	-4.1	95	13.1
Karkloof point 14	Stream	30.3369	-29.31	1168	9/12/2023	-3.02	-10	179	12.9
Karkloof point 15	Stream	30.32347	-29.31	1129	9/13/2023	-2.45	-10.7	80	14
Karkloof fort Nottingham Nature Reserve	Stream	29.9148	-29.416	1472	9/13/2023	-3.29	-11.6	74	13.1
Lions river	Stream	30.1585	-29.436	1066	9/13/2023	-3.14	-13.2	129	18.1
Karkloof point 16	Stream	30.22879	-29.383	1109	9/15/2023	-2.58	-8.9	86	19.5
Karkloof point 18	Stream	30.11996	-29.333	1424	9/16/2023	-3.02	-10.9	140	20.3

Karkloof Point 19	Stream	30.1886	-29.328	1137	9/16/2023	-1.72	-6	143	19.1
Karkloof Point 20	Stream	30.1748	-29.3	1365	9/16/2023	-2.35	-9.9	125	17.1
Karkloof Point 21	Stream	30.169	-29.333	1391	9/16/2023	-2.95	-11.9	139	16.3
Karkloof Point 22	Stream	30.136627	-29.328	1384	9/16/2023	-1.67	-6.7	188	19.9
Karkloof Point 16 (Repeat) KwaNdlovu Stream	Stream	30.2299	-29.349	1115	10/13/2023	-1.92	-6.3	70	18.5
Umgeni River Point 23	Stream	29.88751	-29.477	1478	10/13/2023	-0.78	-0.7	45	16.25
Karkloof pool	Wetland	30.27	-29.37	1075	8/17/2023	-1.58	-2.6	107	18.84
Umgeni River Wetland 2	Wetland	29.864	-29.474	1790	8/18/2023	-0.81	1.8	30	13
Umgeni Wetland 1	Wetland	29.83172	-29.479	1827	8/18/2023	-3.34	-11.1	37	12
Umgeni River Lake 1	Wetland	29.837	-29.48	1824	8/18/2023	-1.42	-5.4	31	14
Bisley wetland	Wetland	30.38867	-29.658	708	8/30/2023	-1.68	-4.2	639	20.4
Lions River Wetland 2	Wetland	29.9933	-29.383	1469	9/6/2023	-2.44	-9.5	97	14.9
Lions River Wetland 3	Wetland	30.02086	-29.43	1434	9/7/2023	-2.94	-11.3	96	17.7
Lions River Wetland 1	Wetland	29.9161	-29.421	1467	9/6/2023	-2.59	-7.4	39	15.5
Karkloof wetland (Point 15) tribute	Wetland	30.2767	-29.363	1071	9/13/2023	-1.14	-3.4	120	16.2

8.2 Appendix B: Radon

This appendix presents the data from radon measurements of groundwater and surface waters. The primary values are given in the ^{222}Rn in the Air column, with the lowest detected limits labelled +/-. The ^{222}Rn in Water values, obtained after conversions, are provided in a separate column with their corresponding +/-. The temperature values used for these conversions were measured on-site and are presented in Appendix A.

Table 8.8: ^{222}Rn in groundwater and surface waters in the wet season.

Sample Code	Water body	Date (d/m/y)	Longitude	Latitude	^{222}Rn in Air	(±)	^{222}Rn in Water	(±)
Umgeni River Borehole	Borehole	30/3/2023	29.902	-29.4975	32690	770	27570	650
Ukulinga Borehole	Borehole	4/4/2023	30.40279	-29.6611	1640	190	1350	160

Ukzn borehole	Borehole	25/4/2023	30.4035	-29.628	28150	870	22820	710
Karkloof River Point 8	stream	28/2/2023	30.32381	-29.31	240	60	38.7	15
UMngeni River Point 2	Stream	7/3/2023	30.98029	-29.803	3.7	7.5	1.3	1.9
Umgeni River point 3	Stream	7/3/2023	30.8688	-29.7162	11	13	1.5	1.7
Umgeni River point 5	Stream	7/3/2023	30.7447	-29.648	11	13	3.2	3.7
Umgeni River point 6	Stream	7/3/2023	30.6837	-29.6513	0	0	0	0
Umgeni River Point 7	Stream	13/3/2023	30.32796	-29.4414	28	18	12.2	7.7
Umgeni River Point 9	Stream	13/3/2023	30.37298	-29.3739	220	130	176	93
Karkloof River Point 1	Stream	13/3/2023	30.27914	-29.3777	495	87	395	69
Karkloof River Point 4	Stream	13/3/2023	30.25793	-29.3745	500	100	378	81
Karkloof River Point 6	Stream	14/3/2023	30.19961	-29.3329	280	140	200	100
Karkloof River Point 7	Stream	14/3/2023	30.26233	-29.3227	205	55	164	55
Lions River Point 1	Stream	14/3/2023	30.30541	-29.1933	51	24	32	15
Umgeni River Point 10	Stream	14/3/2023	30.0744	-29.492	2700	200	2210	170
Umgeni River Point 11	Stream	14/3/2023	29.94985	-29.4551	1840	170	1450	130
Lions River Point 4	Stream	14/3/2023	29.9279	-29.417	2140	180	1740	150
Lions River Point 7	Stream	14/3/2023	30.01987	-29.4418	100	40	71	28
Lions River Point 8	Stream	14/3/2023	30.2018	-29.4995	0	0	0	0
Karkloof River Point 1	Stream	23/3/2023	30.27914	-29.3777	574	93	442	71
Karkloof River Point 3	Stream	23/3/2023	30.27218	-29.3396	494	67	395	53
Karkloof River Point 6	Stream	23/3/2023	30.19961	-29.3329	304	68	240	53
Karkloof River Point 8	stream	23/3/2023	30.32381	-29.31	182	63	139	48
Lions River Point 9	Stream	30/3/2023	30.152	-29463	145	46	111	36
Umgeni River point 14	Stream	30/3/2023	29.887	-29.485	135	45	106	35
Umgeni River Wetland	Wetland	30/3/2023	29.83172	-29.4788	2240	180	1930	160
Bisley stream	Stream	4/4/2023	30.38873	-29.6589	1970	210	1610	170
Umgeni River Watsburg	Stream	6/4/2023	30.4739	-29.4722	87	45	60	31

Table 8.9: ^{222}Rn in groundwater and surface waters in the dry season.

Sample Code	Water body	Date (m/d/y)	Longitude	Latitude	^{222}Rn in Air	±	^{222}Rn in water	±
Karkloof point 1 below wetland	Stream	8/17/2023	30.27914	-29.3777	9200	470	7800	400
Umgeni Wetland 1	Wetland	8/18/2023	29.83172	-29.4788	19110	690	17180	620
Umgeni River Point 1	Stream	8/18/2023	29.9148	-29.4158	20430	610	18260	540
Umgeni Point 2 Mouth	Stream	8/29/2023	31.01828	-29.8089	11	53	3	33
Umgeni Point 3 Mine	Stream	8/29/2023	30.98029	-29.803	127	38	94	28
Inanda Outlet	Stream	8/29/2023	30.8688	-29.7162	3.7	7.3	1	2
Umgeni river Inanda inlet	Stream	8/29/2023	30.797	-29.649	22	59	8	39
Umgeni river point 8	Stream	8/29/2023	30.7447	-29.648	11	52	3	32
Umgeni River point 9 Last bridge	Stream	8/29/2023	30.6837	-29.6513	11	16	3.3	4.6
Ukulinga Stream	Stream	8/30/2023	30.403	-29.661	89	44	62	31
Bisley wetland	Wetland	8/30/2023	30.38867	-29.6578	310	68	246	54
Umgeni river point 10	Stream	8/31/2023	30.4739	-29.4722	63	38	44	26
Umgeni River Point 16	Stream	8/31/2023	30.33	-29.4414	1330	120	1100	100
Midmar dam outlet	Stream	9/6/2023	30.20227	-29.4931	83	36	63	27
Umgeni river Point 17	Stream	9/6/2023	30.0744	-29.492	700	100	610	89
Lions River Point 7	Stream	9/7/2023	30.0459	-29.4055	482	73	386	59
Lions River Wetland 1	Wetland	9/6/2023	29.9161	-29.4205	8670	320	7490	280
Umgeni River Point 21	Stream	9/7/2023	30.05357	-29.4894	5070	240	4200	200
Umgeni point 22 (Karkloof)	Stream	9/11/2023	30.2756	-29.3645	1000	120	800	100
Umgeni point 23 (Karkloof)	Stream	9/11/2023	30.2832	-29.3563	1530	130	1280	110
Karkloof point 8 before tribute	Stream	9/12/2023	30.27744	-29.362	1800	200	1590	180
Karkloof point 9	Stream	9/12/2023	30.26256	-29.3261	130	54	107	45
Karkloof point 14	Stream	9/12/2023	30.3369	-29.3103	258	76	219	65
Karkloof wetland (Point 15) tribute	Stream	9/13/2023	30.2767	-29.3627	621	84	523	71

Karkloof Nottingham Nature Reserve	Stream	9/13/2023	29.9148	-29.4158	1170	160	1030	140
Karkloof point 16	Stream	9/15/2023	30.22879	-29.3828	6800	400	5620	340
Karkloof Point 22	Stream	9/16/2023	30.13663	-29.3275	2080	330	1720	270
Westfalia Fruit Borehole	Borehole	8/17/2023	30.2646	-29.4506	17910	670	14980	560
Ukulinga Borehole	Borehole	8/30/2023	30.40279	-29.6611	190	120	148	87
Umgeni Borehole UCL Farm	Borehole	8/31/2023	30.329	-29.3629	284	65	227	52
Umgeni Borehole Khayalami	Borehole	8/31/2023	30.37675	-29.4191	7350	420	6040	340
Umgeni Borehole Sinkle farm	Borehole	9/6/2023	30.05748	-29.4919	342500	4800	289500	4100
Lions river borehole Sardan Farm 1	Borehole	9/7/2023	30.02063	-29.4424	15000	500	12440	410
Borehole KwaNdlovu	Borehole	9/15/2023	30.2299	-29.3493	122400	2200	103500	1900
Ukzn Borehole	Borehole	10/9/2023	30.4035	-29.628	17960	490	14700	400
Durban DUT Borehole	Borehole	10/13/2023	31.00592	-29.8525	17360	13920	13920	430
Umgeni Vlei borehole	Borehole	10/13/2023	29.89744	-29.4884	23100	1100	19420	920

8.3 Appendix C: Baseflow Separation

This appendix presents the baseflow results, including the data from DWS (station number, place, catchment area, data range and the coordinate of the station). The calculated N values and all the results, graphs, and statistics generated by the BFI+ software are included for each station.

Table 8.10 River station locations across the catchment and the calculated N values.

Station No	Place	Catchment Area (km^2)	Latitude	Longitude	Data Available (y/m/d)	N	BFI index
U2H001	Mgeni River @	937	-29.487	30.2375	1948-12-01 to 1993-01-05	10	0.77
U2H002	Mgeni River @ Inanda Loc	3949	-29.65	30.7998	1928-03-04 to 1975-05-21	13	0.64
U2H003	Mgeni River @ Kwa-Dabek Howick	4249	-29.759	30.9351	1931-05-22 to 1978-12-31	13	0.88
U2H004	Mgeni River @ Inanda Loc.	2521	-29.585	30.6208	1931-07-08 to 1939-10-31	12	0.67

U2H005	Mgeni River @ Table Mountain	2519	-29.576	30.6026	1950-11-01 to 2024-02-29	12	0.75
U2H006	Karkloof River @ Shafton	339	-29.382	30.2778	1954-01-04 to 2024-02-29	8	0.88
U2H007	Lions River (Mpofana River) @ Weltevreden	358	-29.443	30.1485	1954-07-16 to 2024-02-29	8	0.71
U2H011	Msunduze River @ Henley Dam	176	-29.647	30.2598	1957-12-24 to 2024-02-29	7	0.75
U2H012	Sterk River @ Groothoek	438	-29.423	30.4883	1960-08-11 to 2023-07-25	8	0.68
U2H013	Mgeni River @ Petrus Stroom	299	-29.513	30.0944	1960-08-10 to 2024-02-28	8	0.71
U2H015	Mgeni River @ Inanda Loc.	4023	-29.692	30.822	1971-11-18 to 1987-09-21	13	0.65
U2H021	Crammond Stream @ Crammond	4.3	-29.422	30.4306	1981-08-20 to 2000-06-07	3	0.78
U2H022	Msunduze River @ Inanda Loc.	881	-29.661	30.6362	1983-09-07 to 2024-02-29	10	0.77
U2H041	Msunduze River @ Hamstead Park	534	-29.608	30.4503	1996-01-31 to 2024-02-29	9	0.75
U2H042	Mngeweni River @ Inanda Loc.	29	-29.659	30.6837	1995-07-21 to 2000-08-17	5	0.70
U2H044	Umthinzima River @ Rietvallei	19	-29.553	30.1884	1988-08-16 to 1992-05-15	5	0.42
U2H045	Nguku River @ Grootvlei	30	-29.546	30.1714	1988-08-26 to 1992-06-12	5	0.72
U2H046	Kwagqushi River @ Ashley Grange	69	-29.543	30.1242	1989-05-12 to 1992-06-12	6	0.71
U2H052	Mgeni River @ Inanda Loc.	2535	-29.585	30.625	1993-07-06 to 2023-07-25	12	0.36
U2H055	Mgeni River @ Inanda Loc.	3771	-29.642	30.6886	1989-10-26 to 2023-12-19	13	0.69
U2H057	Slang Spruit @ Pietermaritzburg	48	-29.631	30.3532	1995-06-02 to 2023-06-30	5	0.81
U2H058	Msunduze River @ Masons Mill	327	-29.641	30.3654	1995-04-25 to 2019-04-02	8	0.68
U2H061	Mpofana River	45	-29.392	30.063	2013-02-26 to 2024-02-29	5	0.75

Table 8.11 Minimum, average and maximum values generated in the BFI+ software for station number U2H001.

	Min	Avg	Max
Discharge	0.014	5.1226	926.711
Baseflow	0.01	2.6312	23.28
BFI Index	0	0.7714	24.38

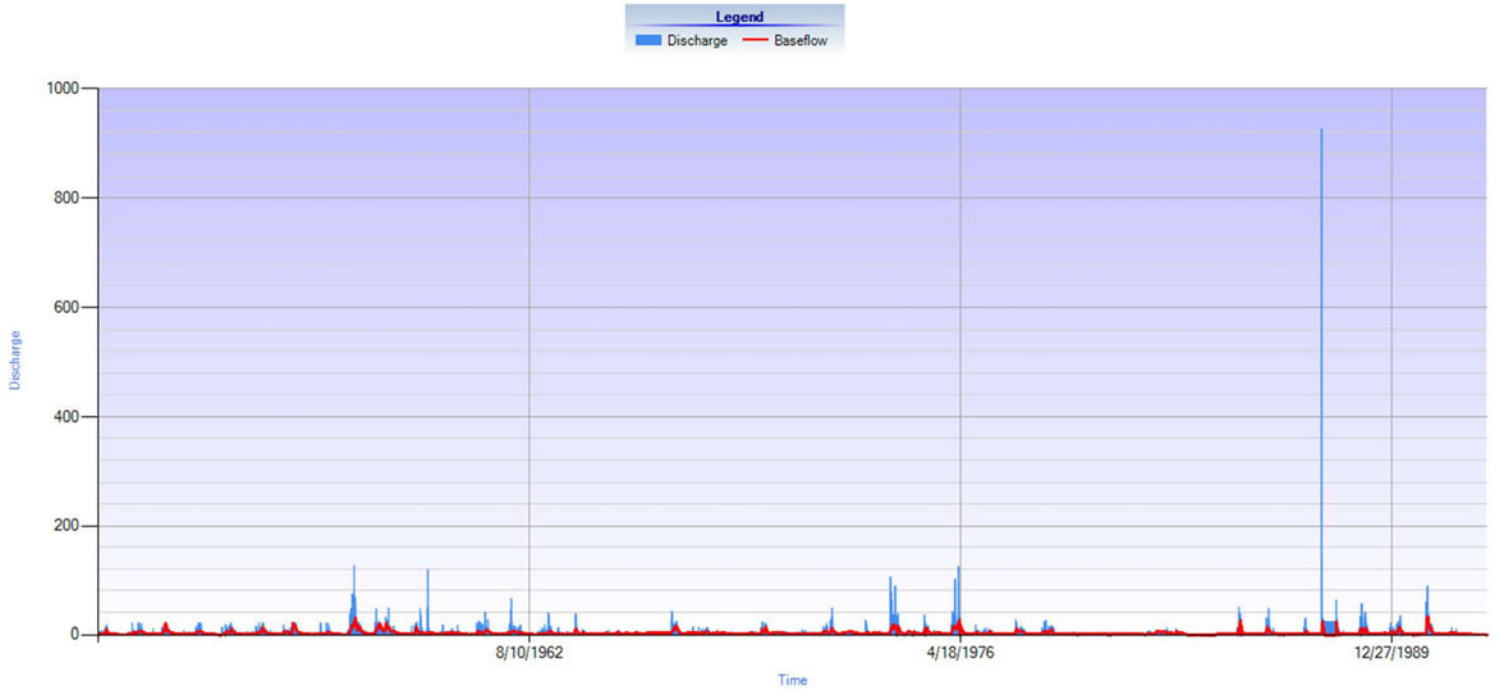

Figure 8.1 Simulated baseflow (red line) and total discharge (blue area) at U2H001 station from 1948 to 1993.

Table 8.12 Minimum, average and maximum values generated in the BFI+ software for station number U2H002.

	Min	Avg	Max
Discharge	0.469	16.1990	536.294
Baseflow	0.469	5.6175	42.99
BFI Index	0.01	0.6385	13.04

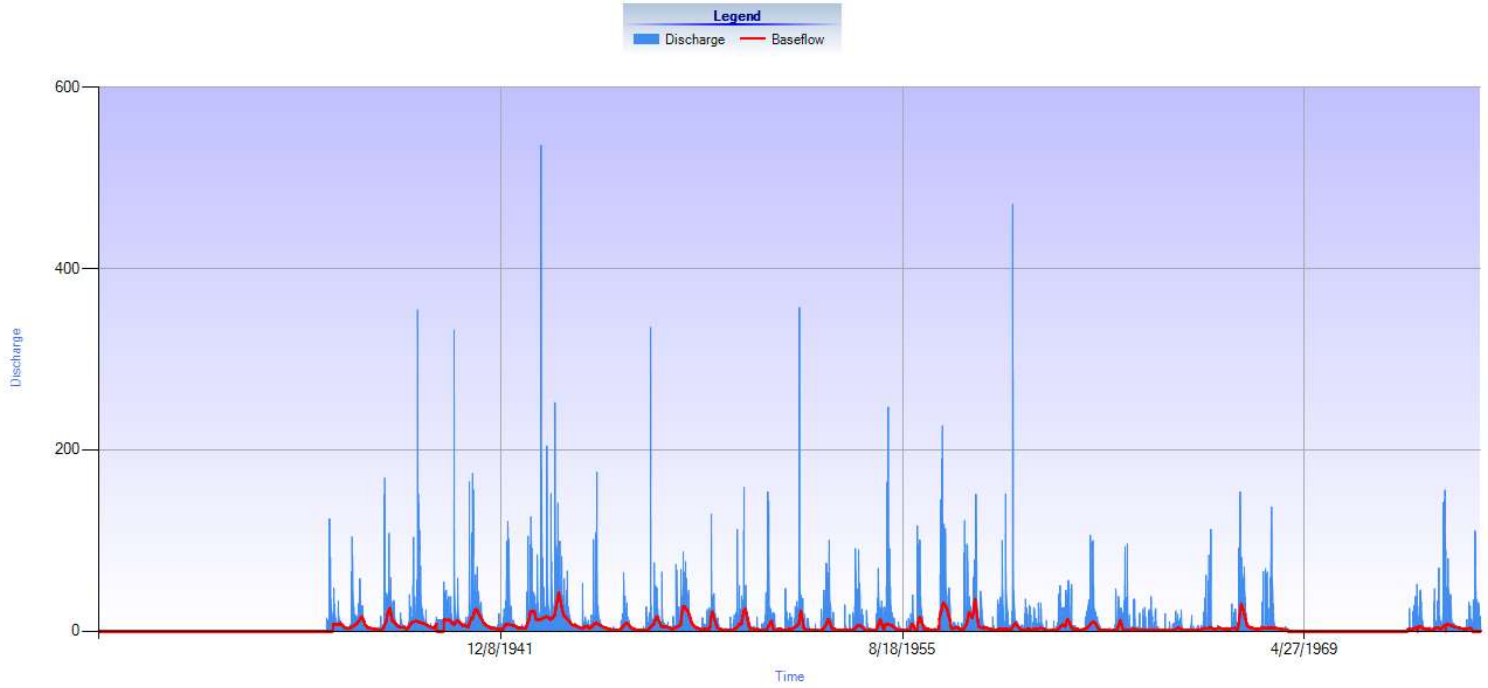

Figure 8.2 Simulated baseflow (red line) and total discharge (blue area) at U2H002 station from 1928 to 1975.

Table 8.13 Minimum, average and maximum values generated in the BFI+ software for station number U2H003.

	Min	Avg	Max
Discharge	0.821	4.1459	5.636
Baseflow	0.82	3.6287	4.96
BFI Index	0.24	0.8771	4.96

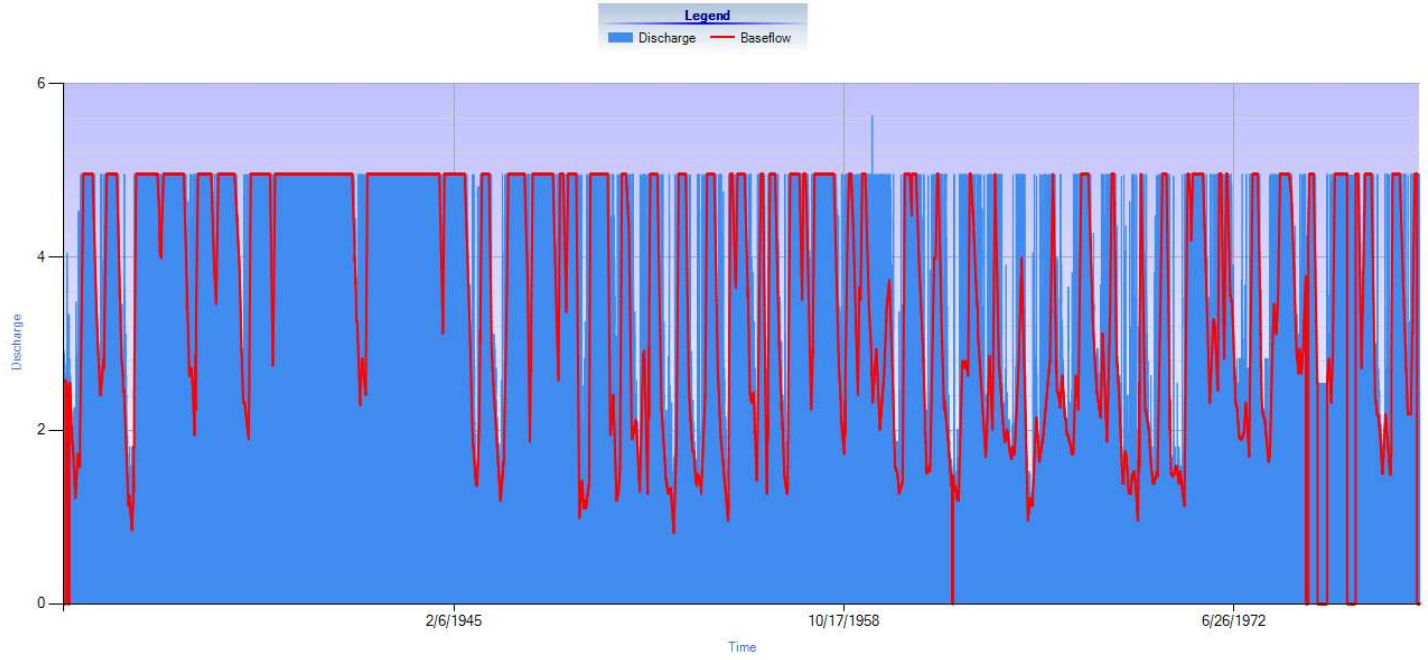

Figure 8.3 Simulated baseflow (red line) and total discharge (blue area) at U2H003 station from 1931 to 1978.

Table 8.14 Minimum, average and maximum values generated in the BFI+ software for station number U2H004.

	Min	Avg	Max
Discharge	0.425	15.6253	366.744
Baseflow	0.42	6.1989	68.99
BFI Index	0.02	0.6737	1

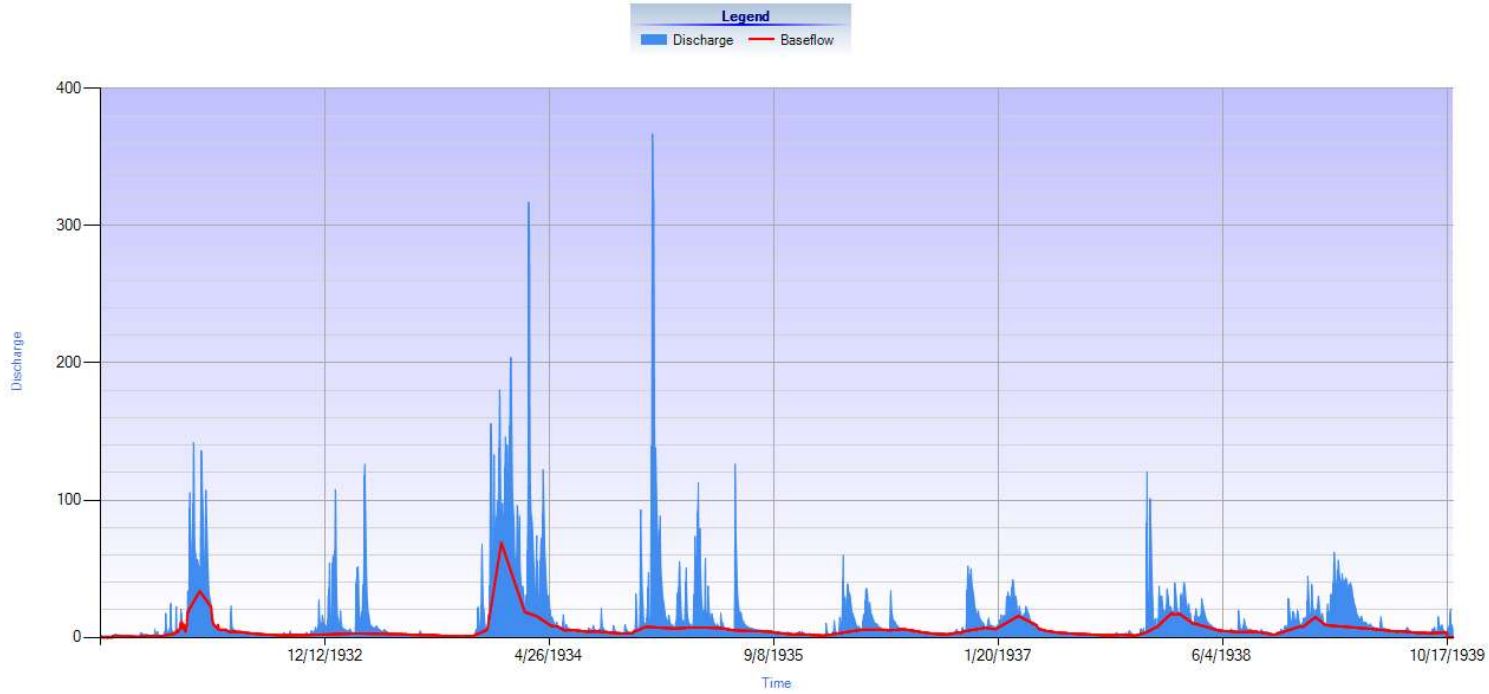

Figure 8.4 Simulated baseflow (red line) and total discharge (blue area) at U2H004 station from 1931 to 1939.

Table 8.15 Minimum, average and maximum values generated in the BFI+ software for station number U2H005.

	Min	Avg	Max
Discharge	0.628	10.2274	760.82
Baseflow	0.63	5.2449	56.08
BFI Index	0.01	0.7460	66.24

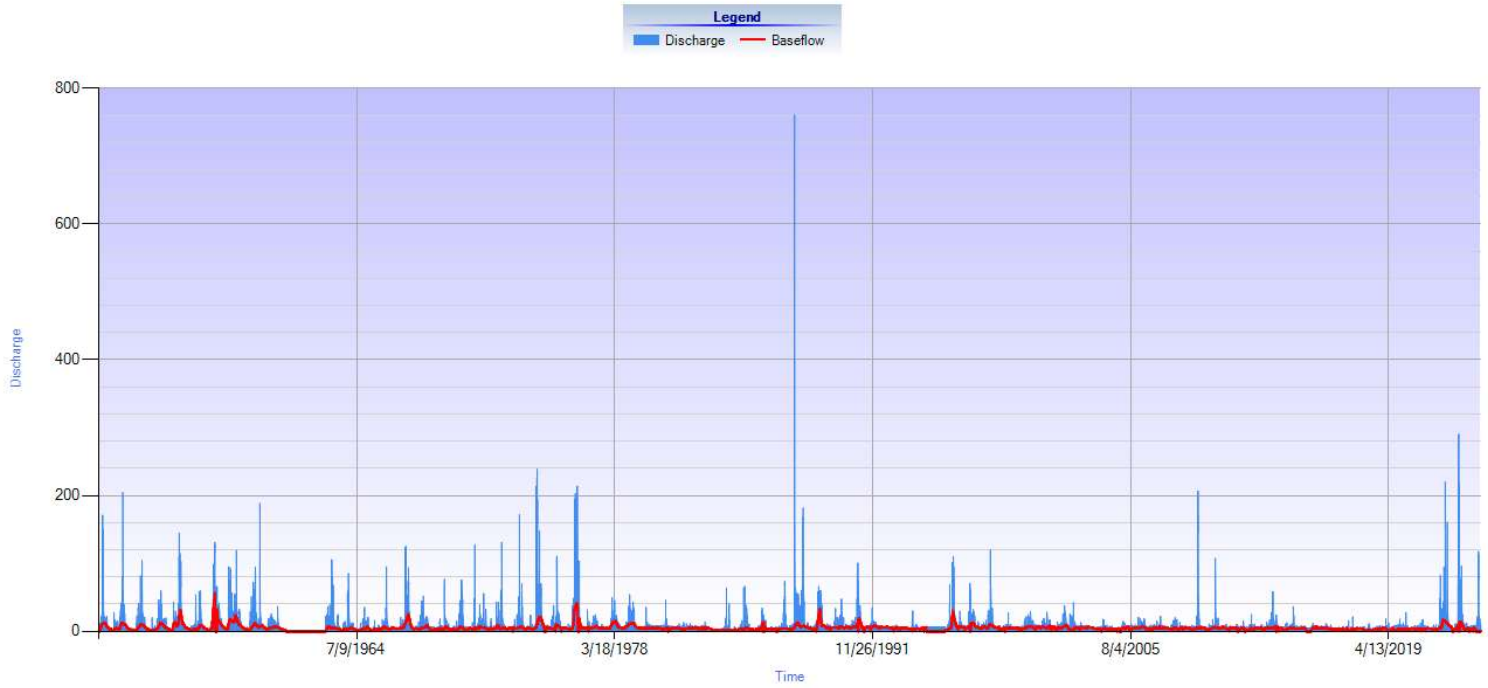

Figure 8.5 Simulated baseflow (red line) and total discharge (blue area) at U2H005 station from 1950 to 2024.

Table 8.16 Minimum, average and maximum values generated in the BFI+ software for station number U2H006.

	Min	Avg	Max
Discharge	0.821	4.1459	5.636
Baseflow	0.82	3.6287	4.96
BFI Index	0.24	0.8771	4.96

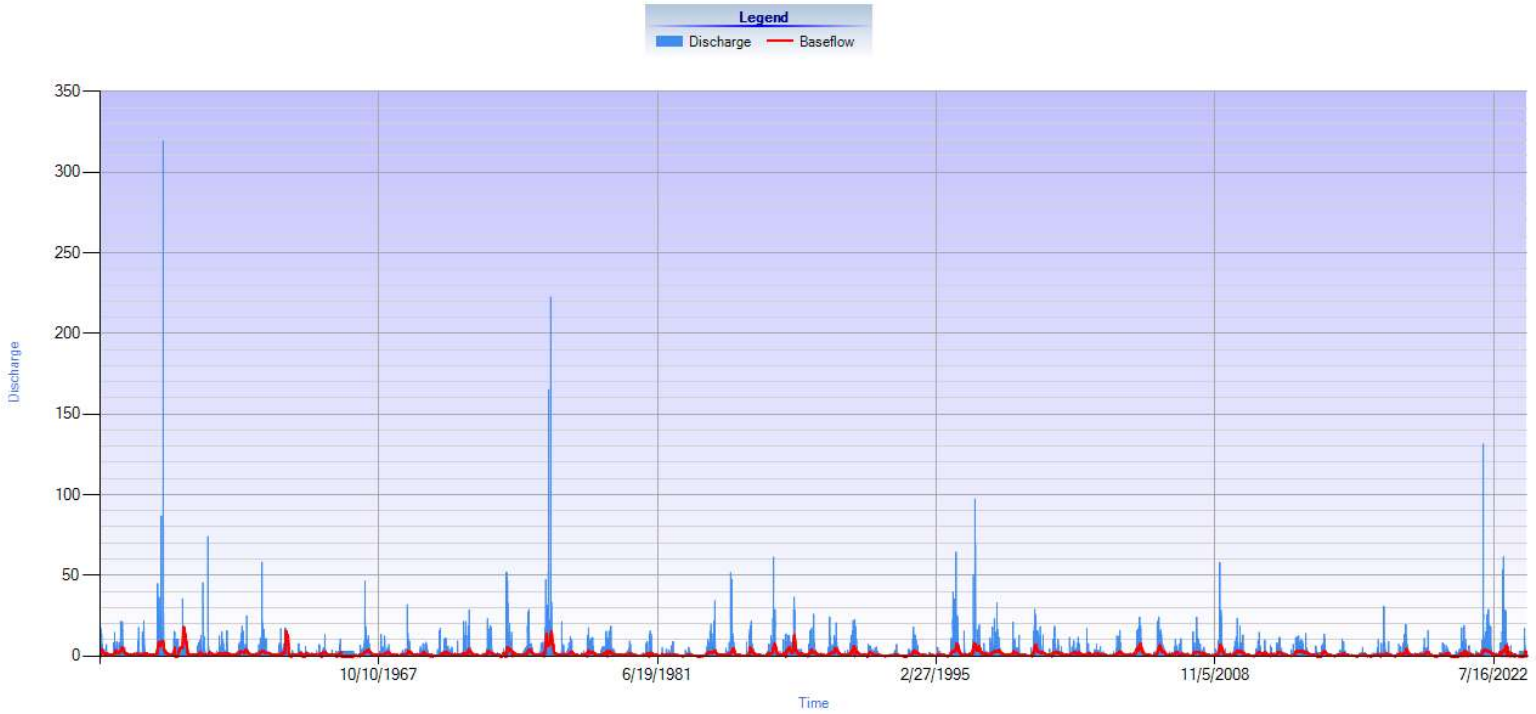

Figure 8.6 Simulated baseflow (red line) and total discharge (blue area) at U2H006 station from 1954 to 2024.

Table 8.17 Minimum, average and maximum values generated in the BFI+ software for station number U2H007.

	Min	Avg	Max
Discharge	0	2.1294	306.52
Baseflow	0.00	1.2421	12.74
BFI Index	0.01	0.7148	5.19

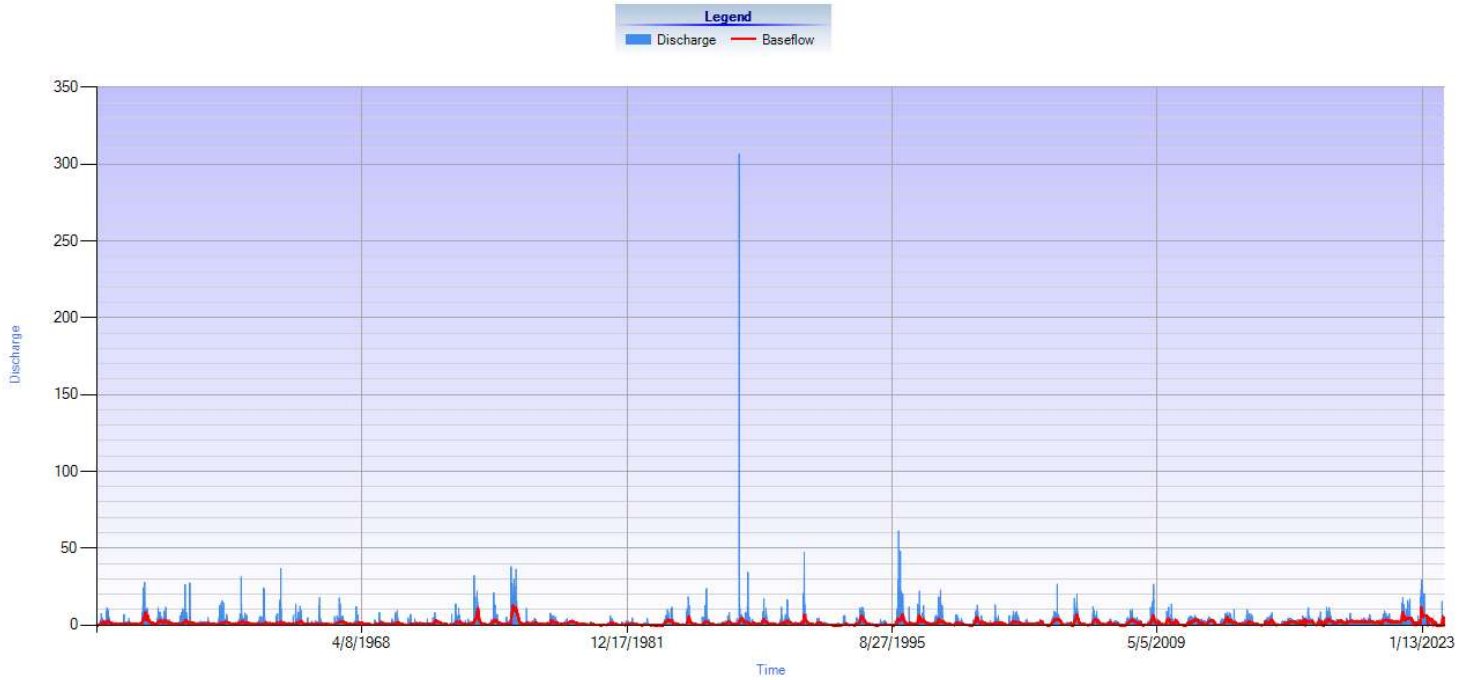

Figure 8.7 Simulated baseflow (red line) and total discharge (blue area) at U2H007 station from 1954 to 2024.

Table 8.18 Minimum, average and maximum values generated in the BFI+ software for station number U2H011.

	Min	Avg	Max
Discharge	0	1.0262	187.388
Baseflow	0.00	0.5292	3.82
BFI Index	0	0.7481	3.91

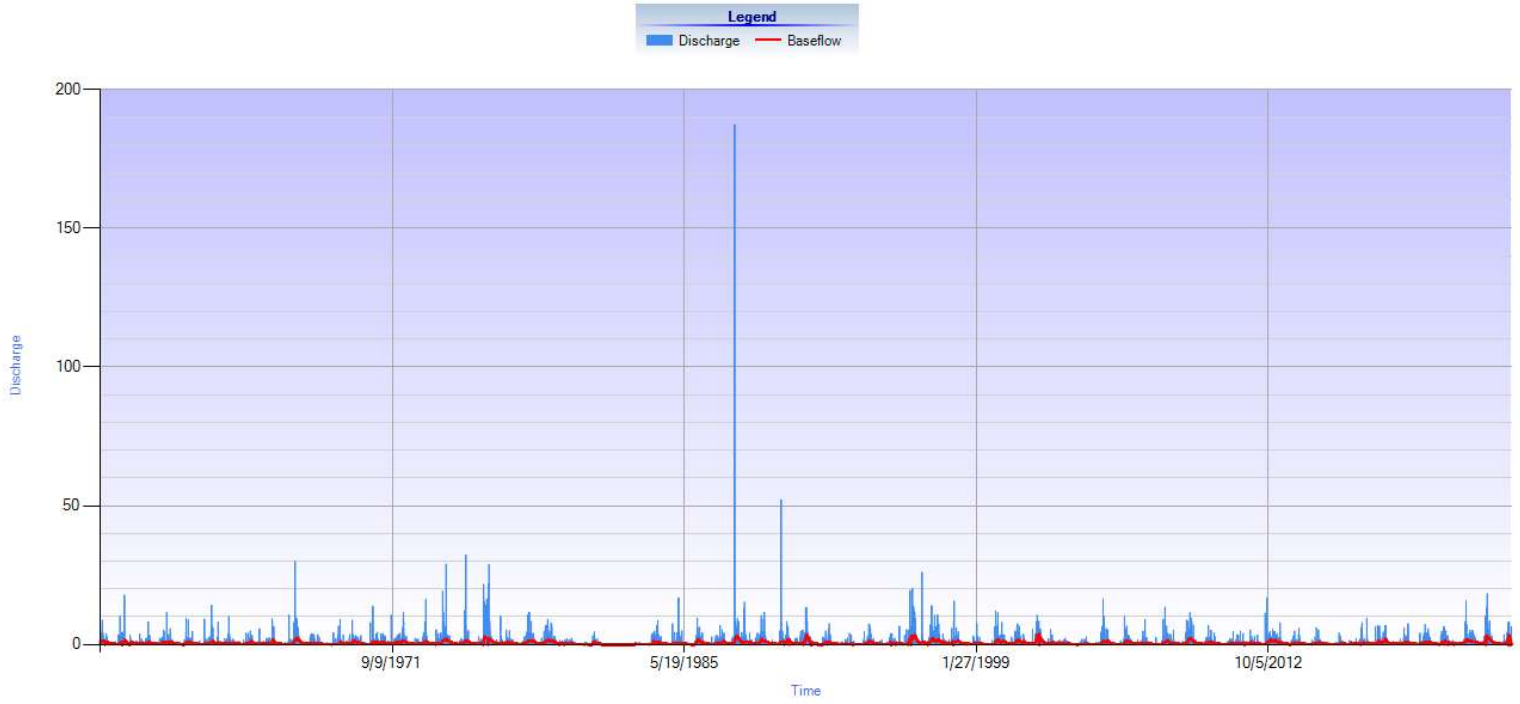

Figure 8.8 Simulated baseflow (red line) and total discharge (blue area) at U2H011 station from 1957 to 2024.

Table 8.19: Minimum, average and maximum values generated in the BFI+ software for station number U2H012.

	Min	Avg	Max
Discharge	0	1.7084	170.395
Baseflow	0	0.8023	13.20
BFI Index	0	0.6817	13.91

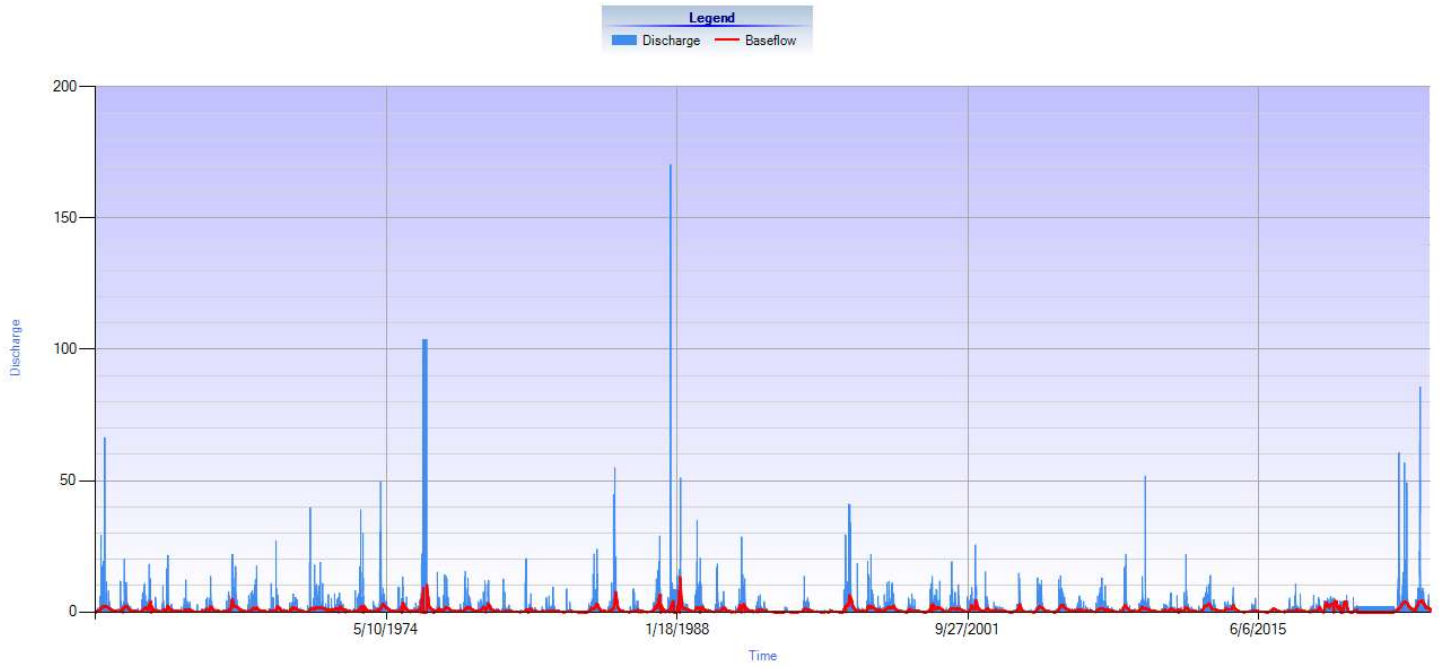

Figure 8.9 Simulated baseflow (red line) and total discharge (blue area) at U2H012 station from 1960 to 2023.

Table 8.20 Minimum, average and maximum values generated in the BFI+ software for station number U2H013.

	Min	Avg	Max
Discharge	0.034	2.4279	262.435
Baseflow	0.03	1.1431	14.78
BFI Index	0.01	0.7086	15.14

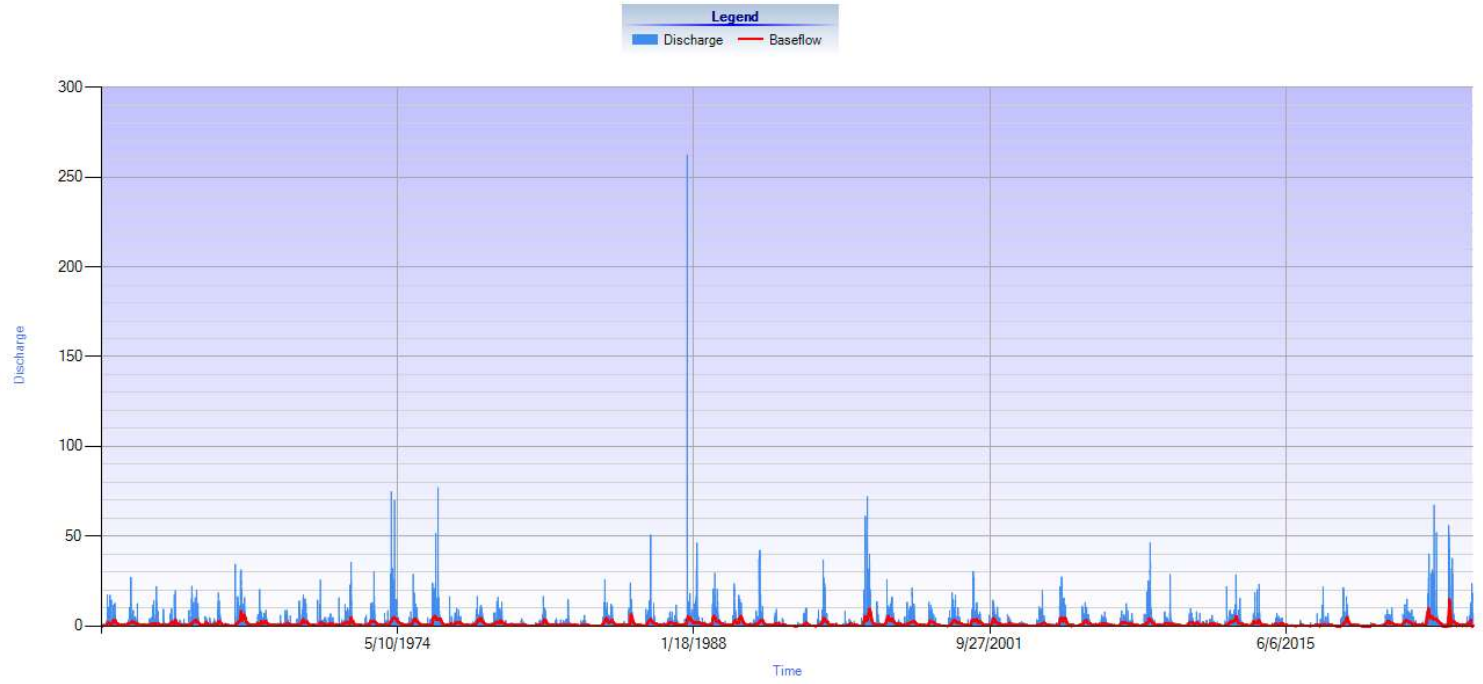

Figure 8.10 Simulated baseflow (red line) and total discharge (blue area) at U2H013 station from 1960 to 2024.

Table 8.21 Minimum, average and maximum values generated in the BFI+ software for station number U2H015.

	Min	Avg	Max
Discharge	0.226	9.2584	97.384
Baseflow	0.23	3.1672	29.59
BFI Index	0.01	0.6471	1

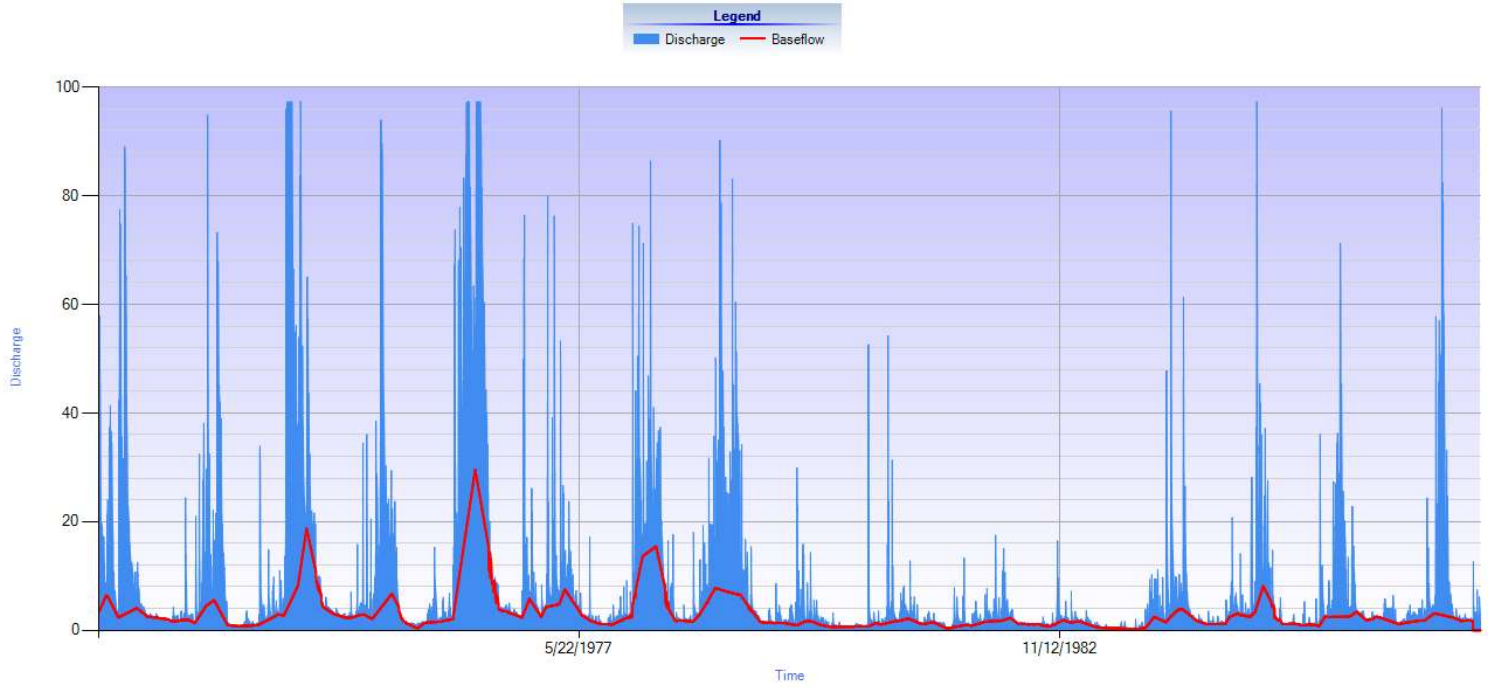

Figure 8.11 Simulated baseflow (red line) and total discharge (blue area) at U2H015 station from 1971 to 1985.

Table 8.22 Minimum, average and maximum values generated in the BFI+ software for station number U2H021.

	Min	Avg	Max
Discharge	0	0.0236	4.392
Baseflow	0.00	0.0122	0.96
BFI Index	0	0.7782	1

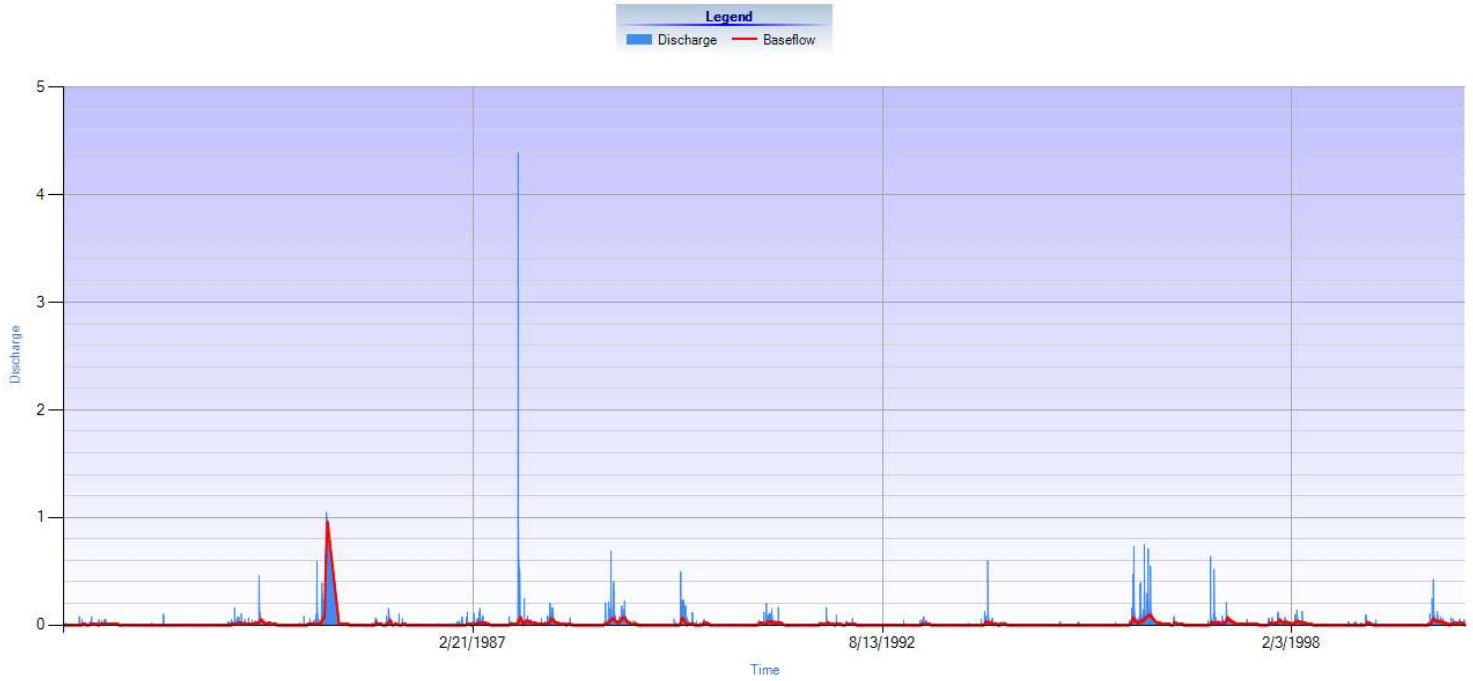

Figure 8.12 Simulated baseflow (red line) and total discharge (blue area) at U2H021 station from 1981 to 2000.

Table 8.23 Minimum, average and maximum values generated in the BFI+ software for station number U2H022.

	Min	Avg	Max
Discharge	0.161	4.2803	136.214
Baseflow	0.16	2.4073	10.86
BFI Index	0.01	0.7669	10.48

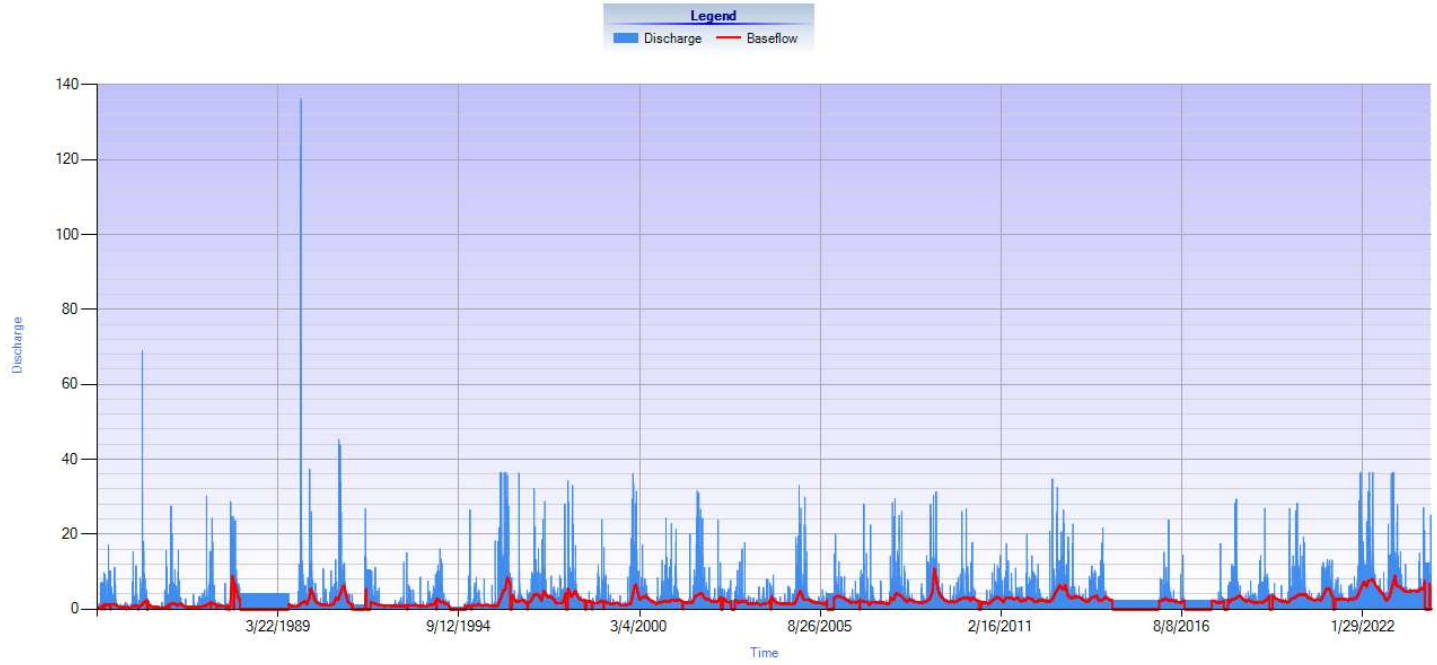

Figure 8.13 Simulated baseflow (red line) and total discharge (blue area) at U2H022 station from 1983 to 2024.

Table 8.24 Minimum, average and maximum values generated in the BFI+ software for station number U2H041.

	Min	Avg	Max
Discharge	0	4.8978	96.866
Baseflow	0	2.3320	18.07
BFI Index	0.01	0.7473	12.34

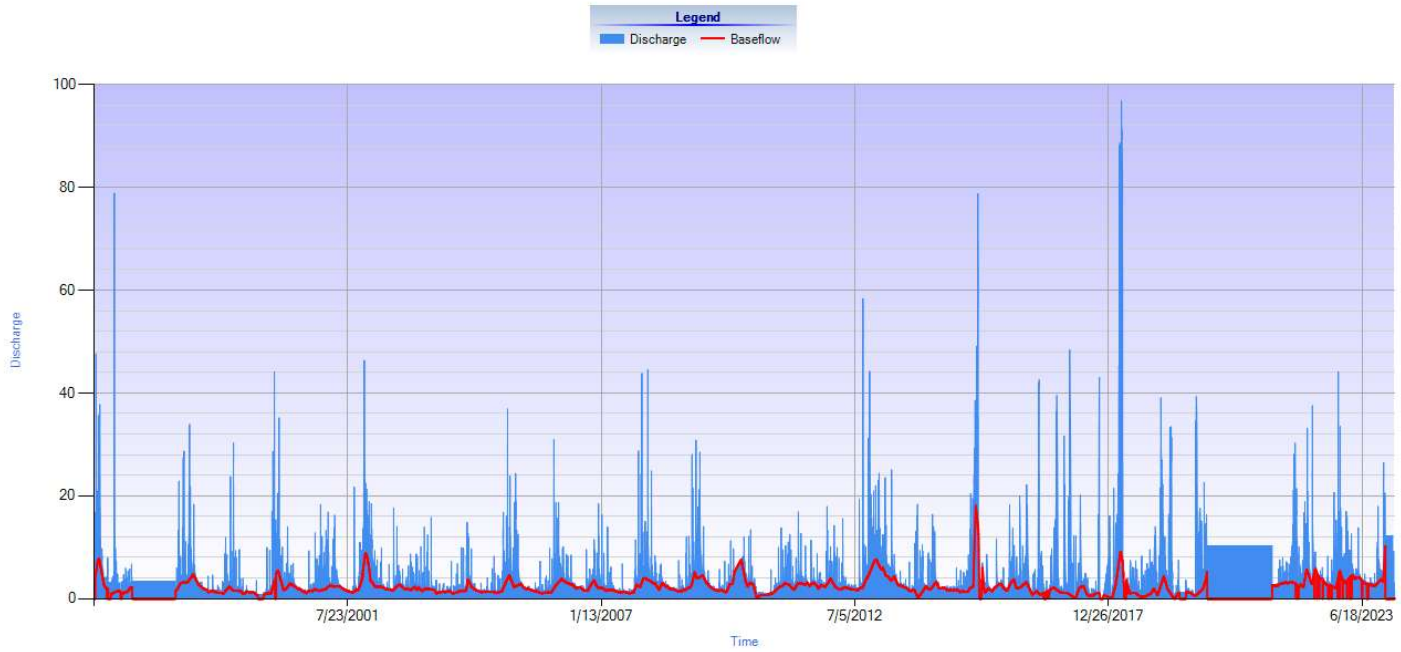

Figure 8.14 Simulated baseflow (red line) and total discharge (blue area) at U2H041 station from 1996 to 2024.

Table 8.25 Minimum, average and maximum values generated in the BFI+ software for station number U2H042.

	Min	Avg	Max
Discharge	0.008	0.0834	1.595
Baseflow	0.01	0.0407	0.23
BFI Index	0.03	0.7000	1

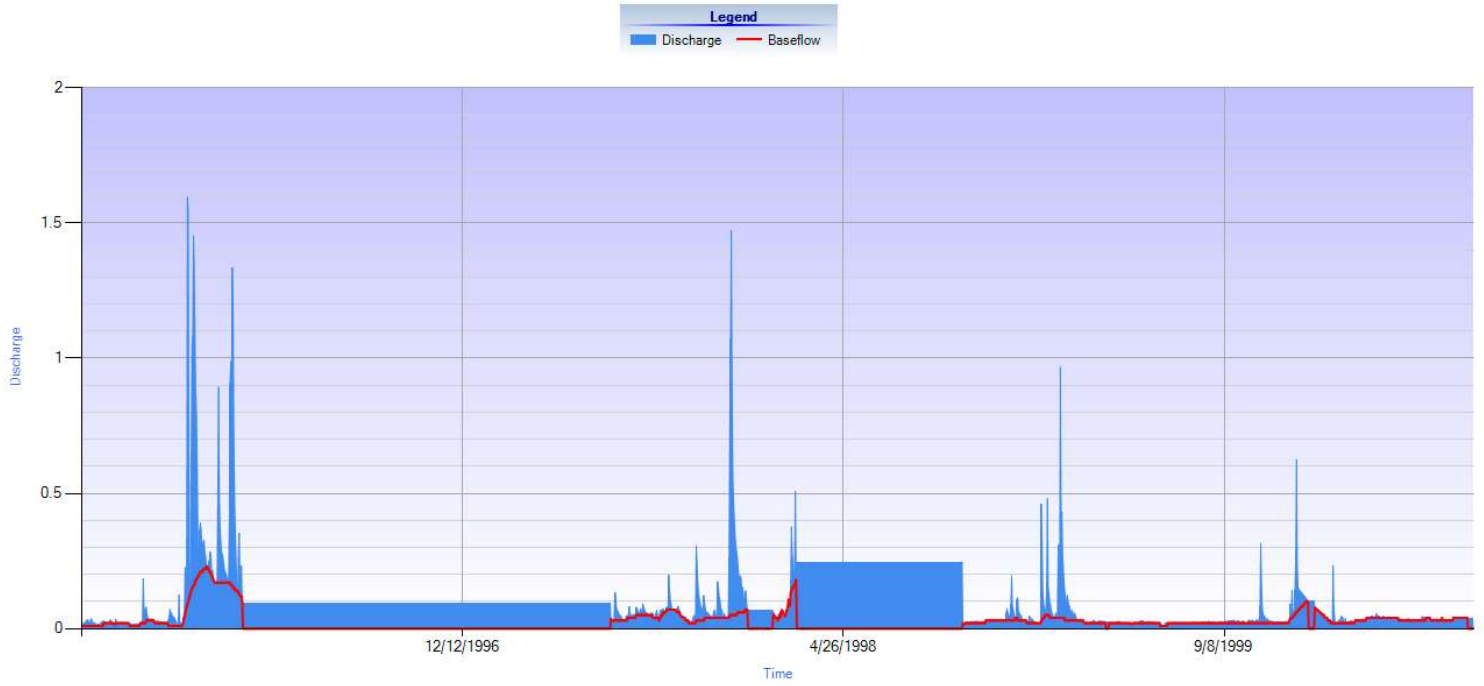

Figure 8.15 Simulated baseflow (red line) and total discharge (blue area) at U2H042 station from 1995 to 2000.

Table 8.26 Minimum, average and maximum values generated in the BFI+ software for station number U2H044.

	Min	Avg	Max
Discharge	0	0.0265	1.467
Baseflow	0	0.0062	0.16
BFI Index	0	0.4197	1

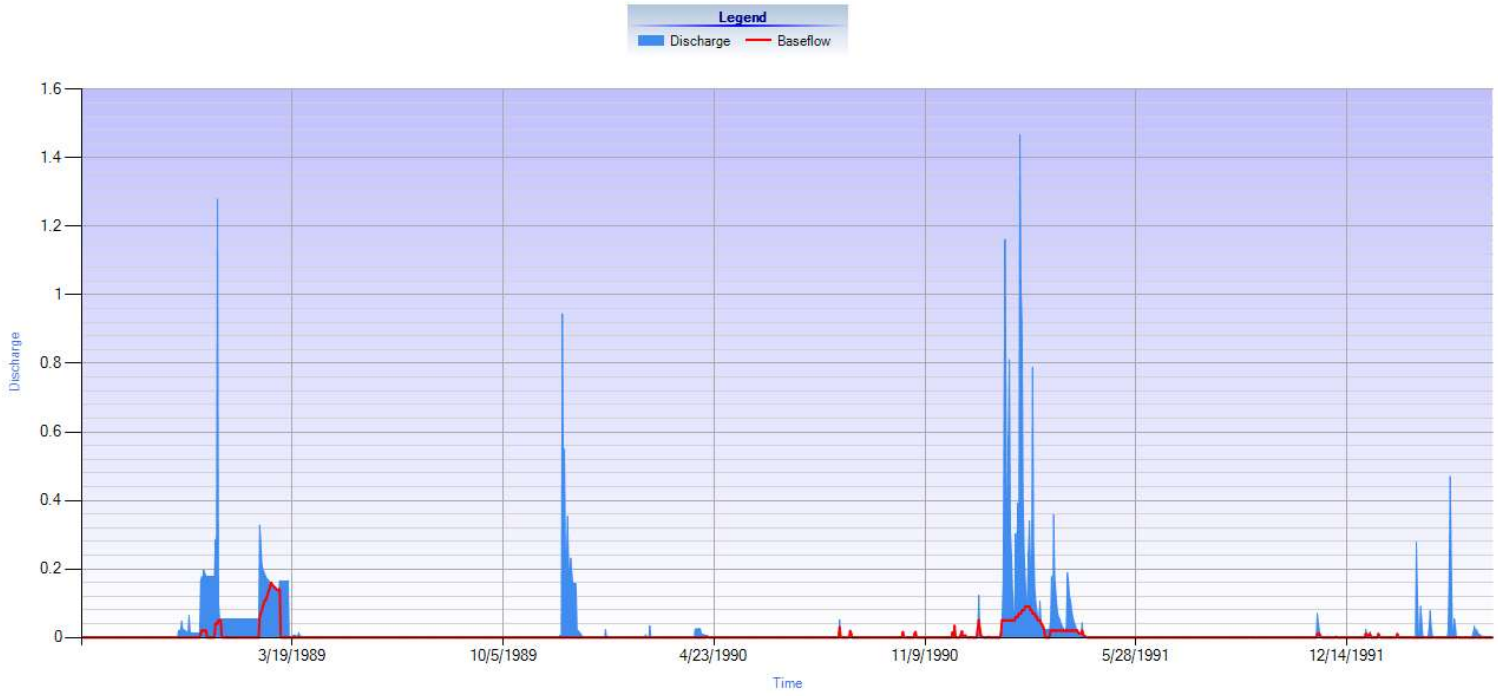

Figure 8.16 Simulated baseflow (red line) and total discharge (blue area) at U2H044 station from 1988 to 1992.

Table 8.27 Minimum, average and maximum values generated in the BFI+ software for station number U2H045.

	Min	Avg	Max
Discharge	0.004	0.1784	1.78
Baseflow	0.00	0.0973	1.02
BFI Index	0.02	0.7198	1.06

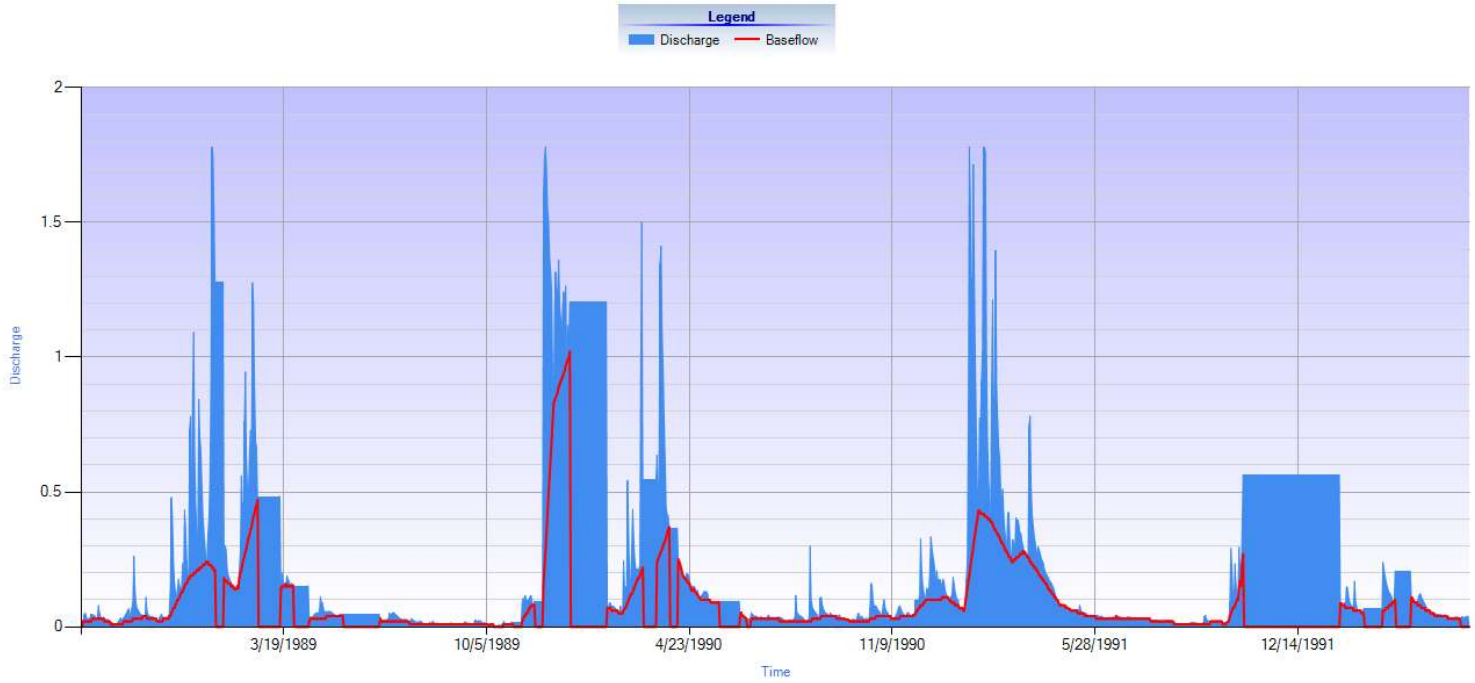

Figure 8.17 Simulated baseflow (red line) and total discharge (blue area) at U2H044 station from 1988 to 1992.

Table 8.28 Minimum, average and maximum values generated in the BFI+ software for station number U2H046.

	Min	Avg	Max
Discharge	0	2.1294	306.52
Baseflow	0.00	1.2421	12.74
BFI Index	0.01	0.7148	5.19

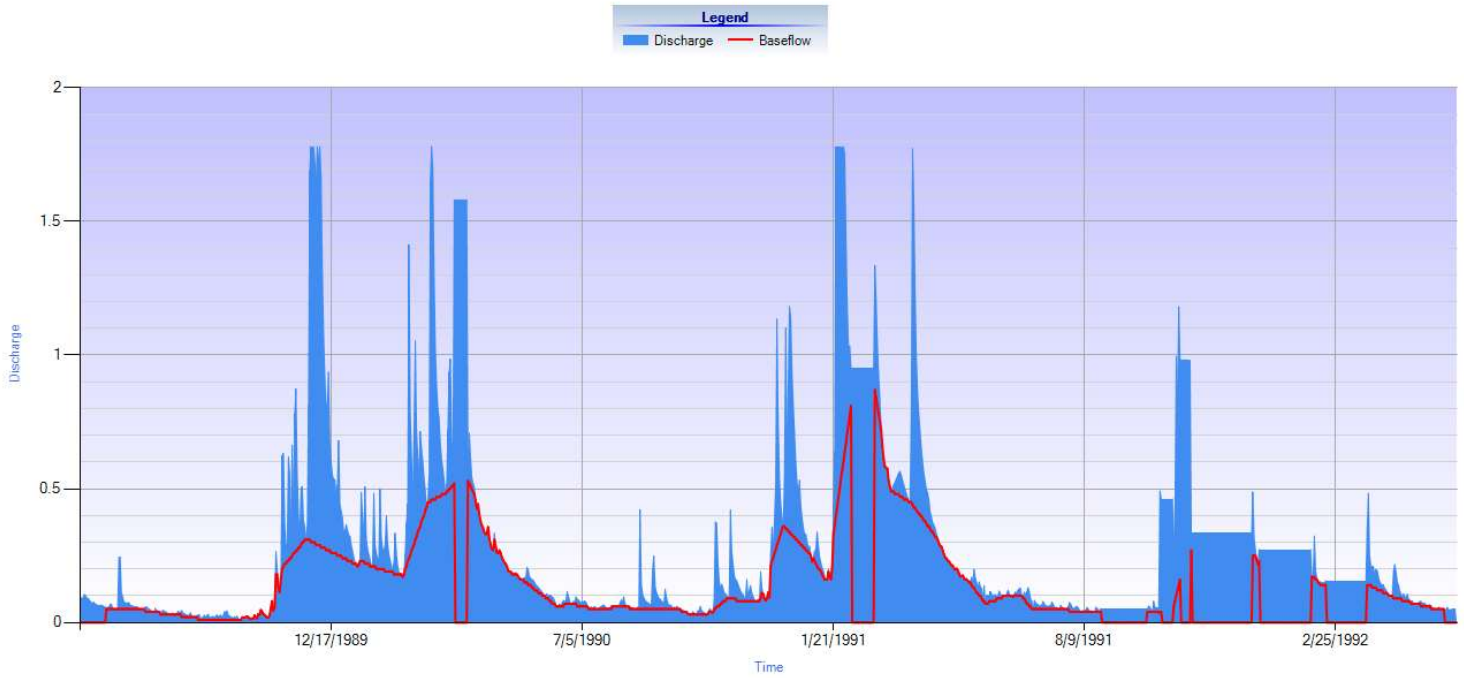

Figure 8.18 Simulated baseflow (red line) and total discharge (blue area) at U2H046 station from 1989 to 1992.

Table 8.29 Minimum, average and maximum values generated in the BFI+ software for station number U2H052.

	Min	Avg	Max
Discharge	0	0.1301	23.906
Baseflow	0	0.0465	2.38
BFI Index	0	0.3595	1

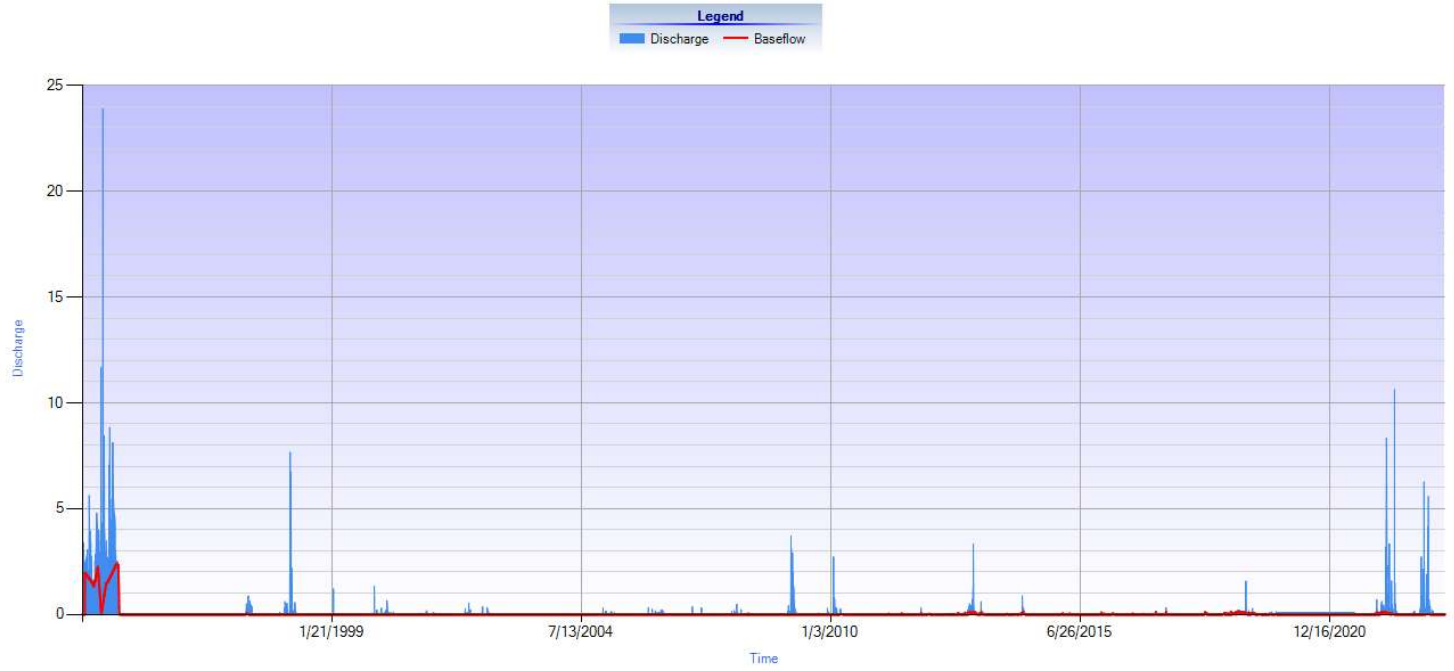

Figure 8.19 Simulated baseflow (red line) and total discharge (blue area) at U2H052 station from 1993 to 2023.

Table 8.30 Minimum, average and maximum values generated in the BFI+ software for station number U2H055.

	Min	Avg	Max
Discharge	0.051	8.4053	465.101
Baseflow	0.05	3.2877	23.69
BFI Index	0.02	0.6886	3.78

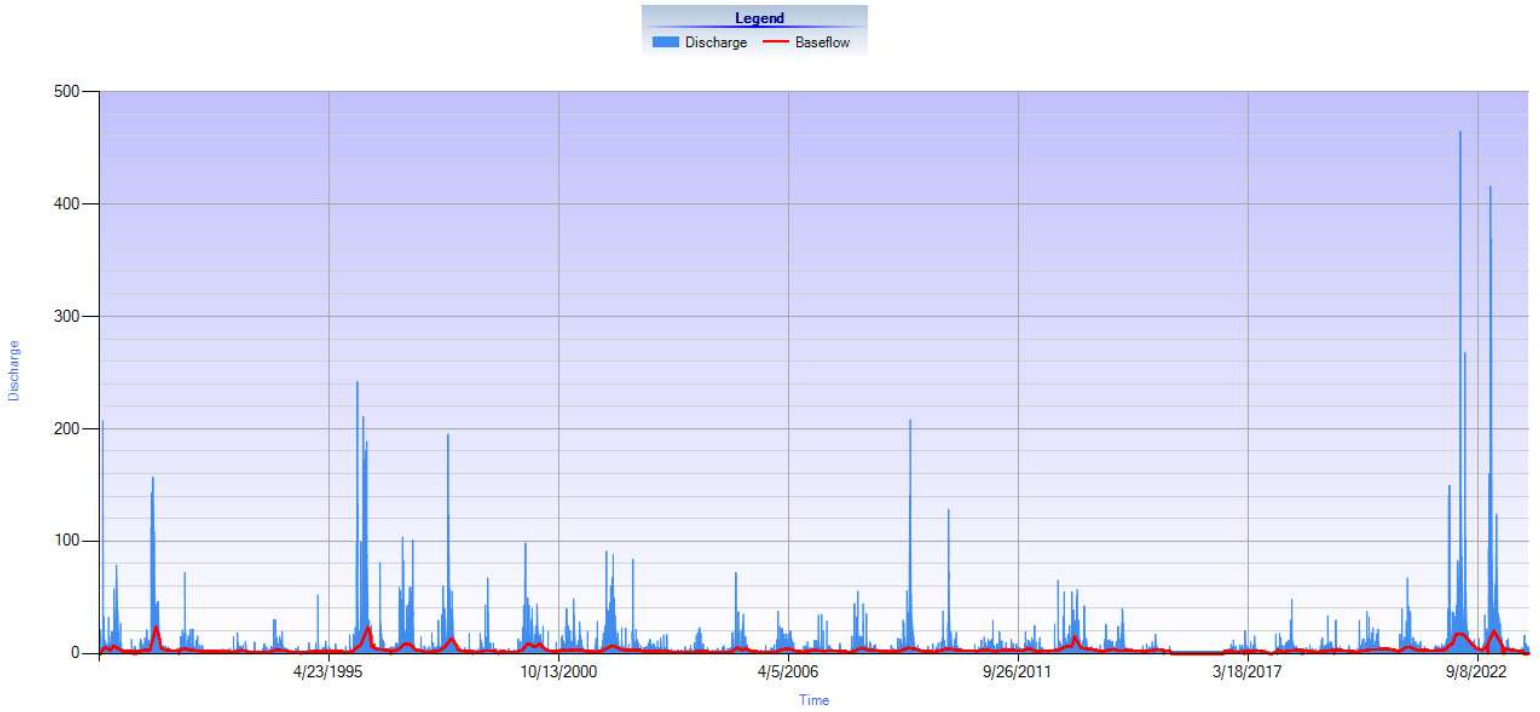

Figure 8.20 Simulated baseflow (red line) and total discharge (blue area) at U2H055 station from 1989 to 2023.

Table 8.31 Minimum, average and maximum values generated in the BFI+ software for station number U2H057.

	Min	Avg	Max
Discharge	0.024	0.3899	17.788
Baseflow	0.02	0.2765	1.42
BFI Index	0.02	0.8097	1

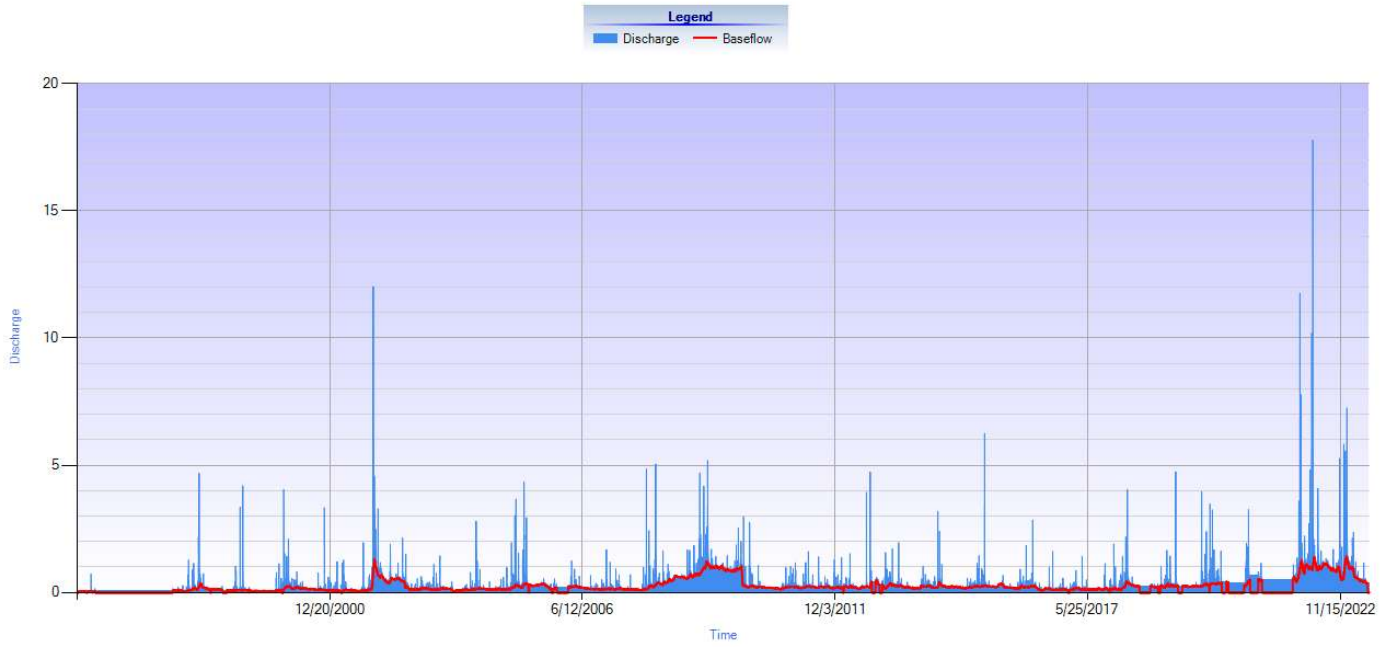

Figure 8.21 Simulated baseflow (red line) and total discharge (blue area) at U2H057 station from 1995 to 2023.

Table 8.32 Minimum, average and maximum values generated in the BFI+ software for station number U2H058.

	Min	Avg	Max
Discharge	0.059	1.9833	68.089
Baseflow	0.06	0.8868	5.79
BFI Index	0.01	0.6758	3.37

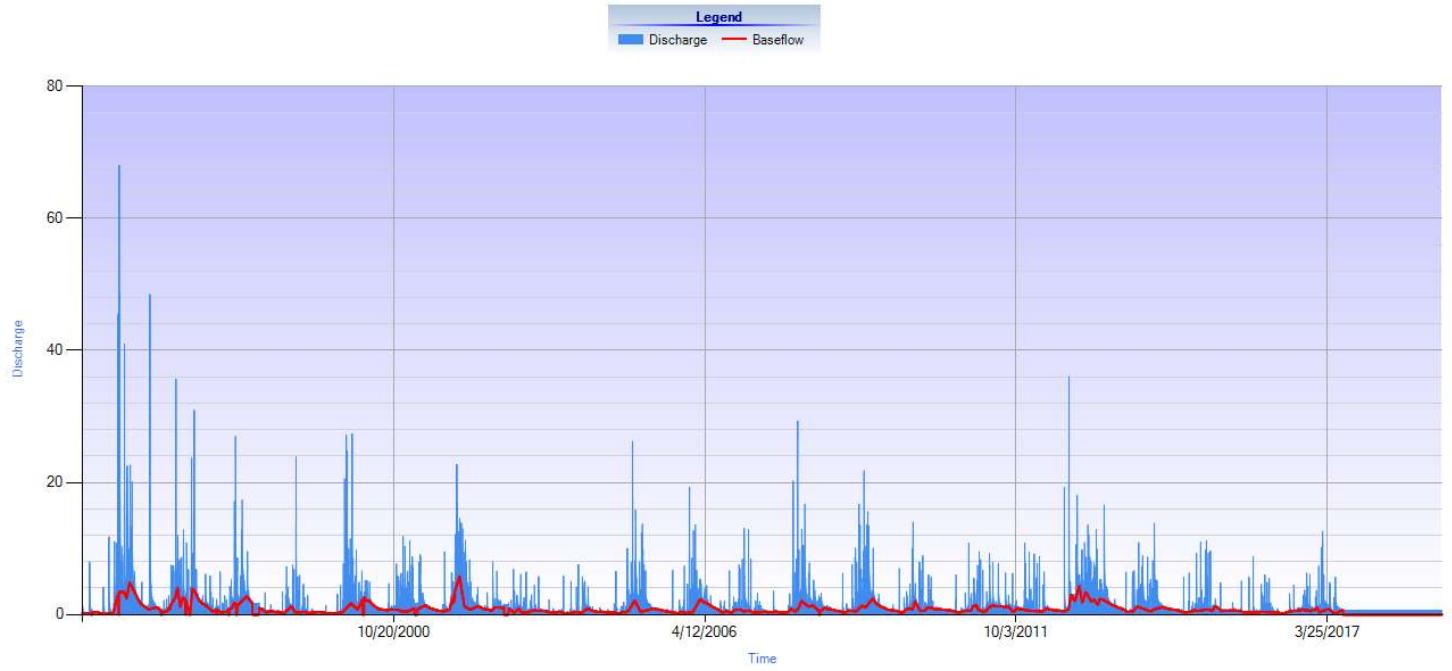

Figure 8.22 Simulated baseflow (red line) and total discharge (blue area) at U2H057 station from 1995 to 2023.

Table 8.33 Minimum, average and maximum values generated in the BFI+ software for station number U2H061.

	Min	Avg	Max
Discharge	0.015	2.5774	5.788
Baseflow	0.02	1.8188	5.06
BFI Index	0.01	0.7461	4.32

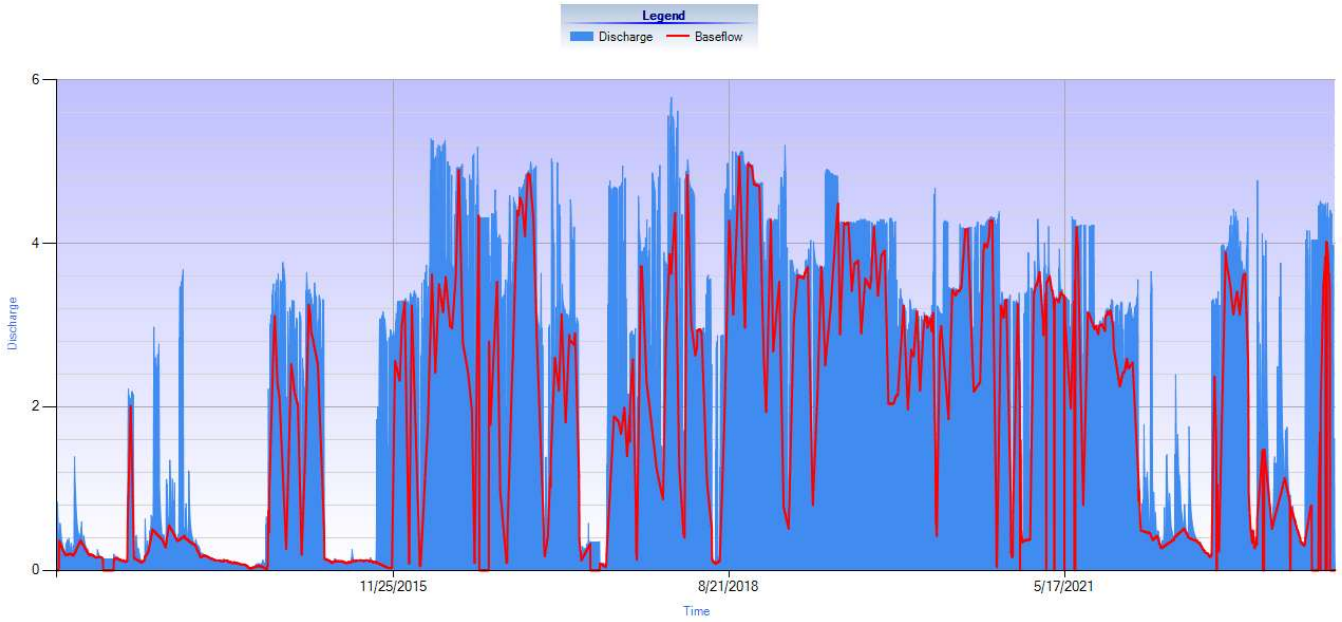

Figure 8.23 Simulated baseflow (red line) and total discharge (blue area) at U2H061 station from 2013 to 2024.